UNIVERSITY OF CALIFORNIA
RIVERSIDE

Vesicular Horizon Distribution, Properties, and Pedogenic Processes in Deserts of the Western United States

A Dissertation submitted in partial satisfaction
of the requirements for the degree of

Doctor of Philosophy

in

Soil and Water Sciences

by

Judith Katherine Turk

March 2012

Dissertation Committee:
Dr. Robert C. Graham, Chairperson
Dr. Christopher Amrhein
Dr. Katherine Kendrick

The Dissertation of Judith Katherine Turk is approved:

_____

_____

_____

Committee Chairperson

University of California, Riverside

ACKNOWLEDGEMENTS

I would like to acknowledge my advisor, Dr. Robert Graham, and committee members, Dr. Christopher Amrhein and Dr. Katherine Kendrick, for their guidance with the project. I am greatly indebted to several friends who helped me in the field, including Shahriar Uddin, Christina Conn, Myles Davis, and Nathan Bailey. I would like to thank Dr. Brenda Buck and Dr. Patrick Drohan for their helpful reviews of my SSSA paper, included here as Chapter 2. I am thankful to Myles Davis, Peter Homyak, and Annie Rossi for many helpful discussions about the work. I'd like to thank Tricia Menchaca for her help interpreting the lithology of the desert pavements and Nicole Pietrasiak for sharing her description of the Clark Mountains soil with me, and for including me in her permit application to work at this site. I would like to thank Woody Smith, who conducted the ICP analysis of the soil extracts, and Dr. Scott Bradford for allowing me to use the laser particle-size analyzer at the USDA Salinity Laboratory. Computed tomography scans were produced by the University of Texas High-Resolution X-Ray Computed Tomography Facility and funding for the CT scanning was provided by the National Science Foundation. Other funding for the project was provided by the USDA-NRCS, and I would especially like to thank Dave Smith, California State Soil Scientist, for his support of this work.

The text of this dissertation, in part or in full, is a reprint of the material as is appears in the *Soil Science Society of America Journal* ["Distribution and properties of vesicular horizons in the western United States", Jul.-Aug. 2011]. The co-author (Robert C. Graham) listed in that publication directed and supervised the research which forms

the basis for this dissertation. This article is reprinted with permission from the Soil Science Society of America.

DEDICATION

This dissertation is dedicated to my husband, Shahriar, I could not have completed work without his support. I would also like to recognize my friends at UCR who have made my graduate school experience a fun one, especially the Broadbent crew: Nathan Bailey, Megs Gendreau, Catherine Gibbons, Tony Ly, and Annie Rossi. Lastly, I would like to thank my parents, Greg and Kathy Turk who first inspired me to take an interest in science.

ABSTRACT OF THE DISSERTATION

Vesicular Horizon Distribution, Properties, and Pedogenic Processes in Deserts of the Western United States

by

Judith Katherine Turk

Doctor of Philosophy, Graduate Program in Soil and Water Sciences
University of California, Riverside, March 2012
Dr. Robert C. Graham, Chairperson

Vesicular horizons are common surface horizons in arid and semi-arid lands and are characterized by the prevalence of nearly spherical, non-interconnected vesicular pores. They regulate surface hydrology in water-limited ecosystems, but are easily disrupted by human land-use. In order to interpret potential changes to vesicular horizon distribution and properties in response to land-use and climatic change, we need to know more about the current distribution of vesicular horizons and how they are formed. The objectives of this dissertation are to: 1) evaluate the distribution and properties of vesicular horizons across the western U.S., 2) determine how disturbance and recovery of vesicular horizons impacts their pore morphology and hydraulic properties, and 3) determine the influence of microbial respiration and thermal expansion of gases on vesicular pore formation. The methods used in this research include analysis of soil databases, examination of vesicular horizon recovery from disturbance in the field, creation of vesicular pores in the lab, and X-ray computed tomography analysis of soil

pores. Our results show that vesicular horizons cover 156,000 km^2 of the western U.S. and are best expressed in the cold deserts (*i.e.,* Central and Northern Basin and Range) relative to the warm deserts (*i.e.,* the Sonoran and Mojave Deserts). We observed that vesicular horizons recover rapidly from disturbance, both in artificially disturbed soils and in tire tracks, and that the rate of recovery is dependent on the frequency of precipitation during the recovery period. Disturbance does not severely alter the hydraulic properties of the vesicular horizon, but leads to a slight reduction in K_{sat} and Gardner's α. In the lab, we found evidence that both biotic and abiotic processes are involved in vesicular pore formation; however, the role of thermal expansion of gases in growth of the vesicular pores was not supported. Through this work we have found that vesicular horizons occur extensively throughout arid and semi-arid regions of the western U.S. Vesicular horizon formation and recovery from disturbance is dependent on climatic conditions (*e.g.*, precipitation frequency, soil temperature), biological factors (*e.g.*, shrub cover, microbial respiration), and their interactions.

TABLE OF CONTENTS

LIST OF TABLES

LIST OF FIGURES

LIST OF EQUATIONS

1. INTRODUCTION

Desert lands cover approximately one-third of the Earth's land surface (USGS, 1997), including 1.3 million km^2 in the western U.S. (USEPA, 2006). Uses of desert land in the western U.S. include off-highway vehicle areas, grazing, agriculture, urban lands, roads, utility corridors, and military training grounds (Lovich and Bainbridge, 1999). In response to societal demands for renewable sources of energy, previously undisturbed desert lands are increasingly being used for the generation of solar and wind power (Associated Press, 2010). Climate change models predict that precipitation will decrease in most arid and semi-arid lands over the next half century, causing increasing water stress in already water-limited ecosystems (Ragab and Prudhomme, 2002).

The surface layers of desert soils are critical to the regulation of runoff and run-on patterns that affect the distribution of water in desert landscapes (Abrahams and Parsons, 1991), but are sensitive to disturbance by human land uses (Lovich and Bainbridge, 1999). Vesicular horizons are a common type of surface horizon in desert soils. These are horizons characterized by the prevalence of non-interconnected, nearly spherical vesicular pores. Vesicular pores are formed by gas bubbles that get trapped in the soil during wetting and then become "frozen" in place as the soil dries (Springer 1958; Hugie and Passey, 1964; Miller, 1971; Evenari et al., 1974). Vesicular horizons are often formed in a silt-rich layer that results from eolian additions to the soil surface (McFadden et al., 1998; Anderson et al., 2002).

Infiltration rates are severely restricted in soils with vesicular horizons (Young et al., 2004), leading to runoff generation during heavy rainfall events (Eckert et al., 1979;

Miller et al., 2009) and restricted leaching of soluble salts (Young et al., 2004; Wood et al., 2005). Because vesicular horizons occur predominantly in the shrub interspace (Eckert et al., 1978), they reinforce patterns of runoff from the bare interspace parts of the landscape and concentrate water as run-on in shrub islands and ephemeral washes, where patches of vegetation are supported (Musick, 1975; Wood et al., 2005).

Vesicular horizons can be considered to be a dynamic soil property, capable of change on human time scales (Tugel et al., 2005). They are often the first pedogenic feature to form in desert soils (Dan et al., 1982; Reheis et al., 1989; McDonald et al., 1995) and vesicular pores can reform quickly (within 1 yr) following disturbance (Yonovitz and Drohan, 2009). Vesicular horizons have been described as a "diagnostic feature" of desert soil pedogensis (Lebedeva et al., 2009). Increasing development or coverage of vesicular horizons may indicate the transition to a more arid ecosystem brought on by land use or climate change. In order to interpret future changes in vesicular horizon occurrence and expression, we need to know more about the current distribution of vesicular horizons and the processes that drive their formation.

To this end, this work examines the distribution of vesicular horizons in the western U.S., their recovery from disturbance, and the mechanisms that promote formation of vesicular pores. Chapter 2 examines the broad-scale distribution of vesicular horizons, specifically addressing the objectives of: 1) using soil database information to characterize the distribution of vesicular horizons and their range of physical and chemical properties, 2) developing a field index for quantifying vesicular horizon expression, and 3) applying the field index to the soil database information in

order to evaluate trends in vesicular horizon expression linked to bioclimatic variability (*i.e.*, desert ecoregions) and other soil properties (*i.e.*, texture, soil order, and temperature regime). Chapter 3 examines the impacts of disturbance and recovery on vesicular horizon pore morphology and hydraulic properties. Specific objectives of Chapter 3 are: 1) to evaluate the recovery of vesicular horizon morphology over one year in artificially disturbed soils and determine the factors that influence their recovery, 2) to analyze the impact of disturbance on vesicular horizon morphology and porosity in disturbed locations (*i.e.*, tire tracks and coppice dunes), and 3) to determine the influence of disturbance on the hydraulic properties of the vesicular horizons. Chapter 4 examines the mechanisms that drive vesicular pore formation and growth in soils by recreating vesicular pores in the lab. Two hypotheses are examined: 1) that CO_2 produced by microbial respiration forms the bubbles that create vesicular pores and 2) that thermal expansion of gases drives the growth of the vesicular pores.

The three chapters each take a different approach to studying the distribution and formation processes in vesicular horizons, including database analysis (Chapter 1), field studies (Chapter 2), and laboratory experiments (Chapter 3). These different approaches allow us to examine vesicular horizon distribution and development at different scales, from broad-scale patterns across the entire western U.S. to local disturbance features at our field sites. Then in the lab, we isolate specific factors that could potentially affect the production and expansion of gas bubbles in soil and examine their impact on vesicular pore formation.

REFERENCES

Abrahams, A.D., and A.J. Parsons. 1991. Relation between infiltration and stone cover on a semiarid hillslope, southern Arizona. J. Hydrol. 122:49-59.

Anderson, K., S. Wells, and R. Graham. 2002. Pedogenesis of vesicular horizons, Cima Volcanic Field, Mojave Desert, California. Soil Sci. Soc. Am. J. 66:878-887.

Associate Press. 2010. Solar showdown in tortoises' home [Online]. Available at <http://www.msnbc.msn.com/id/34659369/ns/us_news-environment/> (accessed 11 Nov 2010). MSNBC.

Dan, J., D.H. Yaalon, R. Moshe, and S. Nissim. 1982. Evolution of reg soils in southern Israel and Sinai. Geoderma 28:173-202.

Eckert, R.E., M.K. Wood, W.H. Blackburn, F.F. Peterson, J.L. Stephens, and M.S. Meurisse. 1978. Effects of surface-soil morphology on improvement and management of some arid and semiarid rangelands. p. 299-301. *In* D.N. Hyder (ed.) Proc. of the First Int. Rangeland Congr., Denver, CO. 14-18 Aug. 1978. Society for Range Mangement, Denver, CO.

Eckert, R.E., M.K. Wood, W.H. Blackburn, and F.F. Peterson. 1979. Impacts of off-road vehicles on infiltration and sediment production of two desert soils. J Range Manage 32:394-397.

Evenari, M., D.H. Yaalon, and Y. Gutterman. 1974. Note on soils with vesicular structure in deserts. Z. Geomorphol. 18:162-172.

Hugie, V.K., and H.B. Passey. 1964. Soil surface patterns of some semiarid soils in northern Utah, southern Idaho, and northeastern Nevada. Soil Sci. Soc. Am. Proc. 28:786-792.

Lebedeva, M.P., D.L. Golovanov, and S.A. Inozemtsev. 2009. Microfabrics of desert soils of Mongolia. Euras. Soil Sci. 42:1204-1217.

Lovich, J.E., and D. Bainbridge. 1999. Anthropogenic degradation of the southern California desert ecosystem and prospects for natural recovery and restoration. Environ. Manag. 24:309-326.

McDonald, E.V., L.D. McFadden, and S.G. Wells. 1995. The relative influences of climate change, desert dust, and lithologic control on soil-geomorphic processes on alluvial fans, Mojave Desert, California: Summary of results p. 35-42, *In* R. E. Reynolds and J. Reynolds (eds.) Ancient surfaces of the East Mojave Desert : a volume and field trip guide prepared in conjunction with the 1995 Desert

Research Symposium. Quarterly of the San Bernardino County Museum Association Ser. 42. San Bernardino County Museum Association, Redlands, CA.

McFadden, L.D., E.V. McDonald, S.G. Wells, K. Anderson, J. Quade, and S.L. Forman. 1998. The vesicular layer and carbonate collars of desert soils and pavements: formation, age and relation to climate change. Geomorphology 24:101-145.

Miller, D.E. 1971. Formation of vesicular structure in soil. Soil Sci. Soc. Am. Proc. 35:635-637.

Miller, D.M., D.R. Bedford, D.L. Hughson, E.V. McDonald, S.E. Robinson, and K.M. Schmidt. 2009. Mapping Mojave Desert ecosystem properties with surficial geology., p. 225-251. *In* R. H. Webb, et al. (eds.) The Mojave Desert: Ecosystem Processes and Sustainability. University of Nevada Press, Reno, NV.

Musick. 1975. Barrenness of desert pavement in Yuma County, Arizona. J. Arizona Acad. Sci. 10:24-28.

Ragab, R., and C. Prudhomme. 2002. Climate change and water resources management in arid and semi-arid regions: Prospective and challenges for the 21st century. Biosyst. Eng. 81:3-34.

Reheis, M.C., J.W. Harden, L.D. McFadden, and R.R. Shroba. 1989. Development rates of late quaternary soils, Silver Lake Playa, California. Soil Sci. Soc. Am. J. 53:1127-1140.

Springer, M.E. 1958. Desert pavement and vesicular layer of some soils of the desert of the Lahontan Basin, Nevada. Soil Sci. Soc. Am. Proc. 22:63-66.

Tugel, A.J., J.E. Herrick, J.R. Brown, M.J. Mausbach, W. Puckett, and K. Hipple. 2005. Soil change, soil survey, and natural resources decision making: A blueprint for action. Soil Sci. Soc. Am. J. 69:738-747.

USEPA. 2006. Ecological regions of North America [Online]. Available by USEPA < http://www.epa.gov/wed/pages/ecoregions/na_eco.htm> (verified 9 Mar. 2011).

USGS, 1997. Distribution of Non-Polar Arid Lands [Online]. Available by USGS <http://pubs.usgs.gov/gip/deserts/what/world.html> (verified 25 Jan. 2011).

Wood, Y.A., R.C. Graham, and S.G. Wells. 2005. Surface control of desert pavement pedologic process and landscape function, Cima Volcanic field, Mojave Desert, California. Catena 59:205-230.

Yonovitz, M., and P.J. Drohan. 2009. Pore morphology characteristics of vesicular horizons in undisturbed and disturbed arid soils; implications for arid land management. Soil. Use. Manage. 25:293-302.

Young, M.H., E.V. McDonald, T.G. Caldwell, S.G. Benner, and D.G. Meadows. 2004. Hydraulic properties of a desert soil chronosequence in the Mojave Desert, USA. Vadose Zone J 3:956-963.

2. DISTRIBUTION AND PROPERTIES OF VESICULAR HORIZONS IN THE WESTERN UNITED STATES

ABSTRACT

Vesicular horizons are thin (usually <10 cm) surface or near-surface horizons characterized by the predominance of vesicular porosity. They are widespread in arid and semi-arid lands, occurring on every continent and covering 156,000 km^2 of the western United States. Vesicular horizons have critical implications for management due to their role in controlling surface hydrology and dust mobilization. This study evaluates the distribution and variation in expression of vesicular horizons across the western United States using the soil databases available from the USDA. A vesicular horizon index (VHI) that incorporates vesicular horizon thickness and the size and quantity of vesicular pores was developed using soil descriptions from a published chronosequence study. The VHI was applied to descriptions from the soil survey databases in order to evaluate vesicular horizon expression across the western United States. Vesicular horizons were better expressed (higher VHI) in the Central and Northern Basin and Range compared to the Mojave and Sonoran Basin and Range. This may be due to differences in temperature regime or to larger areas of playas in the Central and Northern Basin and Range that serve as sources of dust that forms the parent material for vesicular horizons. The median VHI was highest in the Aridisols and Mollisols compared to other soil orders. No significant relationship was found between VHI and soil textures. Vesicular horizons are widely distributed in western United States and occur across a wide range of soil types and soil-forming environments.

INTRODUCTION

The vesicular horizon is a surface or near-surface horizon characterized by the predominance of bubble-like vesicular pores (Fig. 2.1). They are a common feature of soils in arid and semi-arid lands and play an important role in controlling the surface hydrology (Young et al., 2004) and dust emissions (Goossens and Buck, 2009) in the landscapes where they occur. Vesicular horizons are common in extremely arid, arid, and semi-arid lands around the world (Fig. 2.2), and have been reported in salt flats in a sub-humid setting as well (Fig. 2.2 reference 3). The expression of vesicular horizons is heterogeneous on multiple scales. For example, in an alluvial fan or bajada landscape (Peterson, 1981), the vesicular horizons vary with the age of the geomorphic surface on which they occur (McDonald, 1994), while within a single geomorphic surface vesicular horizons are well expressed in the shrub interspace, with limited or no occurrence in the shrub islands (Eckert et al., 1978; Shafer et al., 2007). Vesicular horizons are associated with certain types of surface cover, including physical and biological surface crusts, as well as desert pavement (Eckert et al., 1978).

It has consistently been observed that parts of the landscape with vesicular horizons have much lower infiltration rates compared to those without vesicular horizons (Table 2.1). As a result, runnoff and ponding are more common on parts of the landscape with vesicular horizons (Eckert et al., 1978; Brown and Dunkerley, 1996). The low infiltration rates can be attributed primarily to the development of the vesicular horizon, rather than any underlying horizon, since infiltration rates increase dramatically when the vesicular horizon is removed (Young et al., 2004). Negative correlations have been

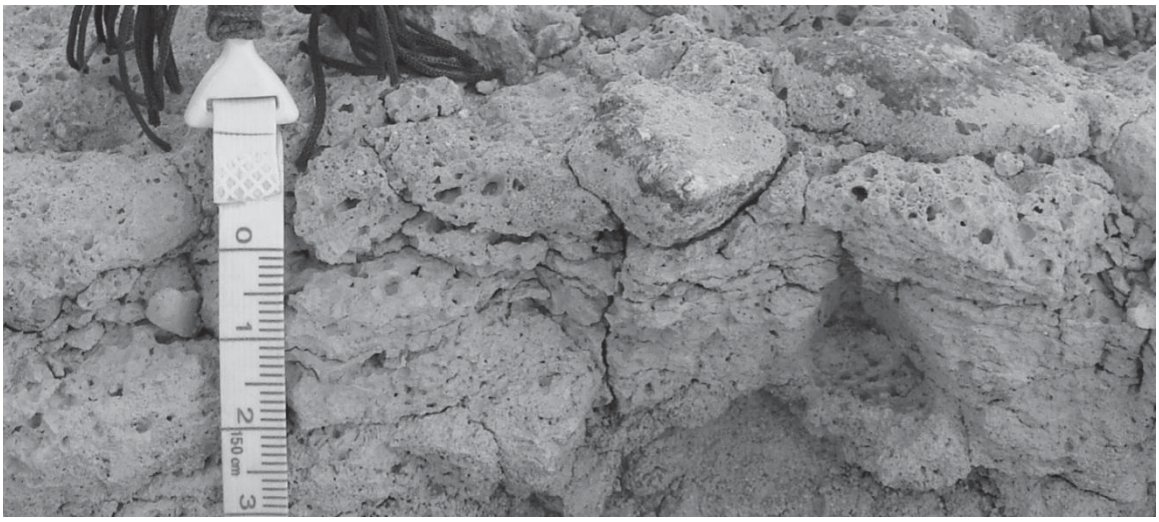

Fig. 2.1. Photograph of vesicular horizon with platy structure (Dixie Valley, NV).

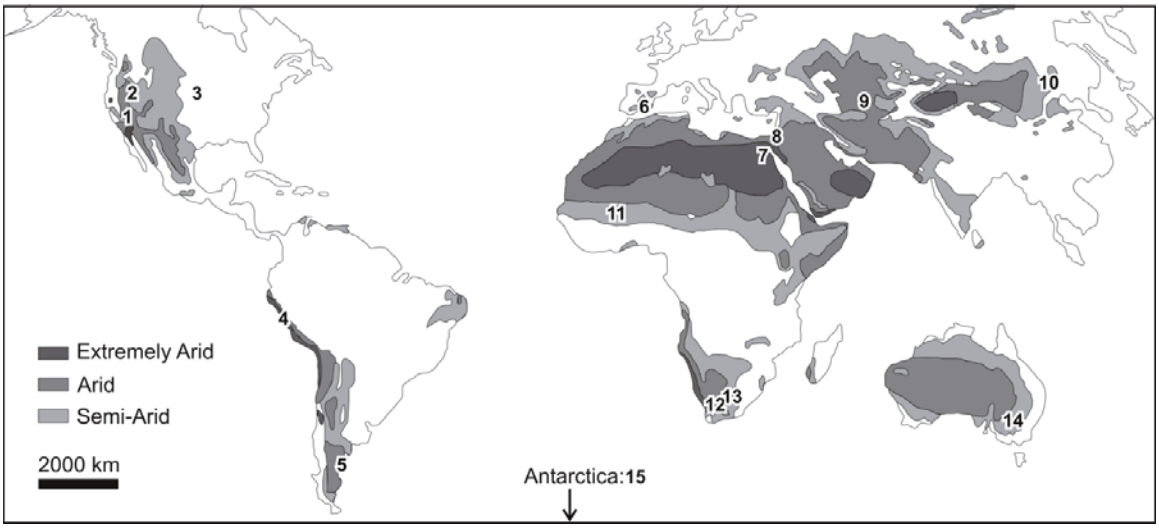

Fig. 2.2. Examples of studies recognizing vesicular horizons around the world, in relation to the global distribution of extremely arid, arid, and semi-arid lands (USGS, 1997). References: (1) McDonald, 1994, (2) Blackburn, 1975, (3) Joeckel and Clement, 1999, (4) Noller, 1993, (5) Bouza et al., 1993, (6) Cantón et al., 2003; (7) Adelsberer and Smith, 2009; (8) Amit and Gerson, 1986; (9) Paletskaya et al., 1958; (10) Lebedeva et al., 2009; (11) Valentin, 1994; (12) Ellis, 1990; (13) Henning and Kellner, 1994; (14) Brown and Dunkerley, 1996; (15) Bockheim, 2010.

Table 2.1. Summary of studies finding lower infiltration rates in soils with vesicular horizons compared to soils without vesicular horizons in the same landscape. Regions are designated as SON = Sonoran Basin and Range, MOJ = Mojave Basin and Range, CBR = Central Basin and Range.

Region	**Dominant Vegetation**	**Infiltration Rate ($cm\ hr^{-1}$)**		**Reference**
		Vesicular	**Non-vesicular**	
SON	*Larrea divaricata*, *Ambrosia dumosa*	0.8	6.0-9.6	Musick, 1975
MOJ	*Larrea tridentata*, *Ambrosia dumosa*, *Yucca* spp.	0.3-0.8	6.8-15	Young et al., 2004
MOJ	*Larrea tridentata*	1.3-4.6	8.9	Miller et al., 2009
MOJ/CBR	*Coleogyne ramosissima*, *Ephedra nevadensis*, *Atriplex canescens*	1.2-4.5	5.5-17	Shafer et al., 2007
MOJ/CBR	*Larrea tridentata*, *Coleogyne ramosissima*	0.4-1.4	3.1-3.2	Eckert et al., 1979
CBR	*Artemisia* spp.	1.7-3.2	5.8-7.2	Blackburn, 1975

observed between the abundance of vesicular pores in the surface horizon and infiltration rates (Blackburn, 1975; Valentin, 1994; Lebedeva et al., 2009), further suggesting that the vesicular horizon is a critical regulator of infiltration. Soil development in deserts, including vesicular horizon formation, tends to reduce the plant water supply, leading to lower shrub densities (McAuliffe, 1994) and more drought-adapted species (Hamerlynck et al., 2002) on older surfaces. Desert landscapes are characterized by clusters of plants in "islands of fertility" separated by barren shrub interspaces (Schlesinger et al., 1990). This pattern is reinforced by stronger expression of vesicular horizons, and resulting in runoff of water from shrub interspace and concentration of runon in the "islands of fertility," where infiltration rates are higher (Shafer et al., 2007). Vesicular horizons are better expressed under increasingly arid conditions, which may create a positive feedback that promotes desertification in semi-arid lands by reinforcing hydrologic and ecological patterns characteristic of desert shrublands (Lebedeva et al., 2009).

Vesicular horizons are often best expressed on geomorphic surfaces that trap dust, especially surfaces that are mantled by desert pavement, a monolayer of interlocking clasts that occurs at the surface of many desert soils (Wood et al., 2005). The primary mechanism of desert pavement formation is through vertical inflation by eolian materials trapped beneath the surface clasts (McFadden et al., 1987; Wells et al., 1995). This process causes a smoothing of the original surface topography and the accumulation of an eolian mantle that favors the formation of vesicular horizons and other pedogenic features. Relatively weak expression of vesicular horizons has been observed on landforms with smooth microtopography (*e.g.*, sandy beach ridges) compared to those

with initially rough microtopography that favors dust entrapment and desert pavement formation (*e.g.*, gravelly piedmont and lava flows) (McFadden et al., 1992). The eolian origin of vesicular horizons has been supported in settings where the suite of minerals contributed by dust is distinct from the underlying parent material (Well et al., 1985; Ugolini et al., 2008). The vesicular horizon is often formed predominantly in eolian parent materials, even when the underlying soil horizons are formed in another parent material, such as alluvium (McDonald, 1994) or glacial till (Rossi, 2009).

As a consequence of their eolian origins, soils with vesicular horizons are prone to high dust emission when they are disturbed by human activities, such as off-road driving (Goossens and Buck, 2009). Dust released from soil disturbance can have adverse effects on human health (Smith and Lee, 2003) and far-reaching ecological impacts. Desert dust deposited on alpine snow packs reduces their albedo, thereby increasing their melting rate and altering the hydrology of major river systems (Painter et al., 2010).

Vesicular horizons occur at or near the soil surface and are commonly thin (<10 cm) (Anderson et al., 2002). The morphological feature that distinguishes vesicular horizons from other surface horizons is the predominance of isolated, nearly spherical vesicular pores. Columnar or prismatic structure that parts to platy structure is a common, but not universal, feature of vesicular horizons. The pedogenic processes that form vesicular horizons include: 1) the additions of eolian material to the soil surface, 2) the development of a surface seal in the form of an embedded gravel layer or a physical or biological crust, and 3) wetting and drying cycles that cause the growth of vesicular pores and their collapse to form platy structure (Fig. 2.3). The role of wetting and drying

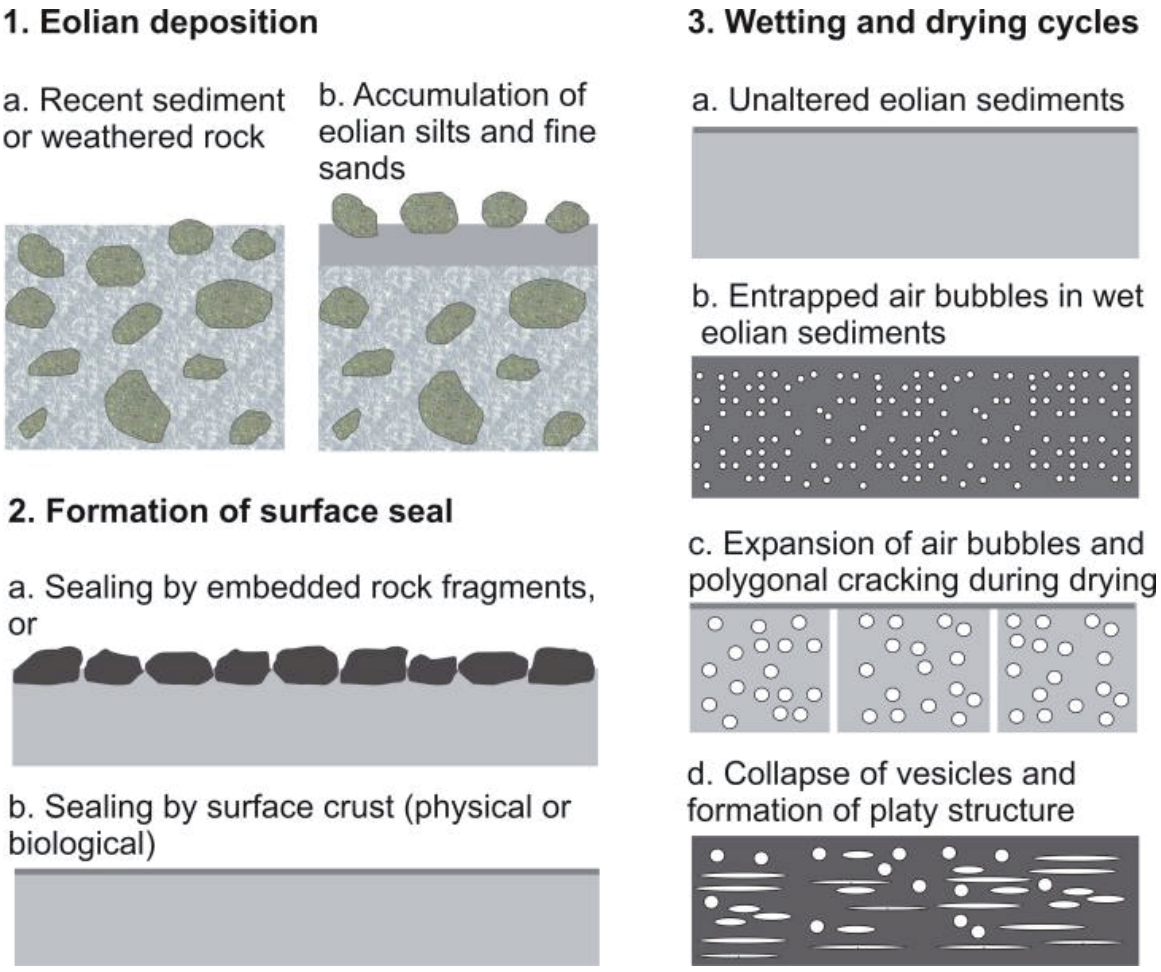

Fig. 2.3. Summary of processes central to vesicular horizon formation.

cycles in the formation of vesicular pores has been observed in laboratory studies in which vesicular pores are regenerated through the wetting and drying of crushed soils (Springer, 1958, Miller, 1971, Evenari et al., 1974; Figueira and Stoops, 1983). Wetting and drying cycles also cause polygonal cracking and the formation of prismatic or columnar structure in the vesicular horizons. The vesicular pores are believed to be formed by air that is trapped as bubbles during the wetting of an initially dry soil. The presence of a gravel layer or a physical or biological crust prevents the trapped air from escaping at the soil surface (Evenari et al., 1974). Vesicular pores are more common under embedded surface rock fragments compared to non-embedded rock fragments, due to the more effective surface sealing (Valentin, 1994). The formation of vesicular pores has been associated with silt-rich soil materials (Miller, 1971). The addition of eolian materials to the surface of desert soils helps to create conditions for vesicular pore formation by enriching the soil surface in silt-sized particles. The process of eolian additions may continue even in well-developed vesicular horizons. This material may be carried into the vesicular horizon with infiltrating water, resulting in a progressive thickening of the vesicular horizon and the formation of ped surface features that may help to stabilize the vesicular pores and platy peds (*e.g.*, argillans and calcite coating) (Sullivan and Koppi, 1991; Anderson et al., 2002; Lebedeva et al., 2009).

The process of vesicular pore formation can occur rapidly. In the lab, vesicular pores are observed to form in disturbed soil material collected from vesicular horizons over four to 25 wetting and drying cycles (Miller, 1971; Figueira and Stoops, 1983). In the field, vesicular pores were observed to reform in disturbed soils after only four

months (Yonovitz and Drohan, 2009). Thin vesicular horizons (<1 cm) have been observed on very young (<100 yrs) geomorphic surfaces (Gile and Hawley, 1968) and surfaces subject to active sediment transport (Peterson, 1980). Chronosequence studies in the Mojave Desert have suggested that vesicular horizons are the first indicators of soil development (McFadden et al., 1986; McFadden, 1988). The rapid formation of vesicular pores indicates that they are a dynamic soil property. However, the eolian surface horizon, containing material that is conducive to vesicular pore formation, may be considered a stable feature, unless physical disturbance (Goossens and Buck, 2009) or a change in hydrologic conditions (Wells et al., 1985) causes erosion of the surface material.

A wealth of pedon descriptions, using a consistent terminology for describing key features of the vesicular horizon (*e.g.*, the size and quantity of vesicular pores) is available through the USDA databases of Official Soils Descriptions (OSDs) (Soil Survey Staff, 2009a) and National Soil Survey Characterization Data (Soil Survey Staff, 2009b). We used these databases to study the distribution and properties of vesicular horizons across the western United States. Our objectives were to 1) use soil database information to characterize the distribution of vesicular horizons and their range of physical and chemical properties, 2) to develop a field index for quantifying vesicular horizon expression, and 3) to apply the developed field index to the soil database information, in order to evaluate trends in vesicular horizon expression across different ecoregions (*i.e.,* warm and cold deserts) and among soils with varying properties (*i.e.,* soil temperature regimes, soil orders, and textures). This broad evaluation of vesicular

horizon distribution and variability in expression is intended to reveal the extent of this feature, as well as to examine patterns that may help us unravel the mechanisms involved in vesicular horizon formation. The vesicular horizon's near-surface position, its control of surface hydrology (Young et al., 2004), and its sensitivity to dust mobilization (Goossens and Buck, 2009), as well as the dynamic nature of vesicular porosity (Yonovitz and Drohan, 2009) make it an important feature to be recognized in land-use planning and studies of ecological change in arid and semi-arid lands.

MATERIALS AND METHODS

Analysis of soil databases

Soil series with vesicular horizons were found by searching all OSDs (Soil Survey Staff, 2009a) in the 11 western states for the term "vesicular" and checking each description for vesicular pores in a horizon that starts within the upper 10 cm of the soil surface. Only those descriptions in which the vesicular pores had a higher quantity class than all other pore types were included in the dataset. These criteria were used to limit the dataset to those horizons that are similar to vesicular horizons described in the literature that restrict infiltration rates (Table 2.1) because they are close to the surface and are dominated by non-interconnected porosity. The area of soil series with vesicular horizons mapped in the Soil Survey Geographic (SSURGO) dataset was determined using the Soil Extent Mapping Tool (Soil Survey Staff, 2007). This evaluation represents a minimum estimate of the area of vesicular horizons, since areas mapped after 2007, including many soil survey areas in arid and semiarid regions, are not yet entered into the

Soil Extent Mapping Tool. The distribution of soils with vesicular horizons was also evaluated using the State Soil Geographic data set (STATSGO) (USDA-NRCS, 2006), by selecting all map units in which one or more major components is a soil series with a vesicular horizon in the OSD. This data set lacks the resolution and accuracy of the SSURGO data, but offers a complete, broad-scale depiction of vesicular horizon occurrence in the western United States.

The names of the soil series with vesicular horizons were used to query the National Soil Survey Characterization Data (Soil Survey Staff, 2009b) for lab data and National Soil Information System (NASIS) pedon descriptions of soils with vesicular horizons. Using both OSDs and NASIS pedon descriptions creates potential for duplication of data points, because some OSDs are also in NASIS. To avoid this problem, all OSDs that had the same location description as a NASIS pedon descriptions were removed from our dataset. The location of each pedon description with a vesicular horizon (type location for the OSDs) was plotted using ArcMap 9.3 (ESRI, 2008). Locations recorded using the Public Land Survey System were converted to an approximate latitude and longitude using Graphical Locator (Gustafson, 2003).

Development and application of the vesicular horizon index

The methods for developing a field index for the vesicular horizon were based on those used by Harden (1982) to evaluate the soil development index (SDI). The index was evaluated using pedon descriptions from a published chronosequence study in the Mojave Desert (McDonald, 1994), according to the most recent evaluations of surface

age at the site (McDonald, 2008). This chronosequence study, located on a series of alluvial fan deposits of the Providence Mountains in California, was selected because it includes a high level of replication (5-15 pedon descriptions per surface age) and a wide range of surface ages (750-135,000 yrs).

The VHI was then applied to our dataset of pedon descriptions with vesicular horizons derived from the USDA databases and used to analyze variability in the vesicular horizon expression across the western United States. The pedon description locations were overlaid with Level III Ecoregions (USEPA, 2006a) in order to group the points in a way that reflects spatial variability in climate and biotic factors. The VHI was compared among soils grouped by ecoregions of the Basin and Range Province, including the Sonoran Basin and Range (SON), Mojave Basin and Range (MOJ), Central Basin and Range (CBR), and Northern Basin and Range (NBR) ecoregions. The Basin and Range Province was selected for analysis because vesicular horizons are frequently described in this region (see Fig. 2.4a) and the ecoregions represent a gradient of climatic and biotic influences. The SON and MOJ ecoregions are considered warm deserts, while the CBR and NBR are considered cold deserts (USEPA, 2006b). The VHI was also used to compare vesicular horizon expression among different soil orders, soil temperature regimes, and vesicular horizon textures.

Due to the non-normal distribution of VHI, all statistical tests were performed using non-parametric analyses, including the Kruskal-Wallis test (Sheskin, 2007) for comparison among all groups and the Mann-Whitney test (Sheskin, 2007) and Bonferonni correction (Abdi, 2007) for comparisons between specific groups. All

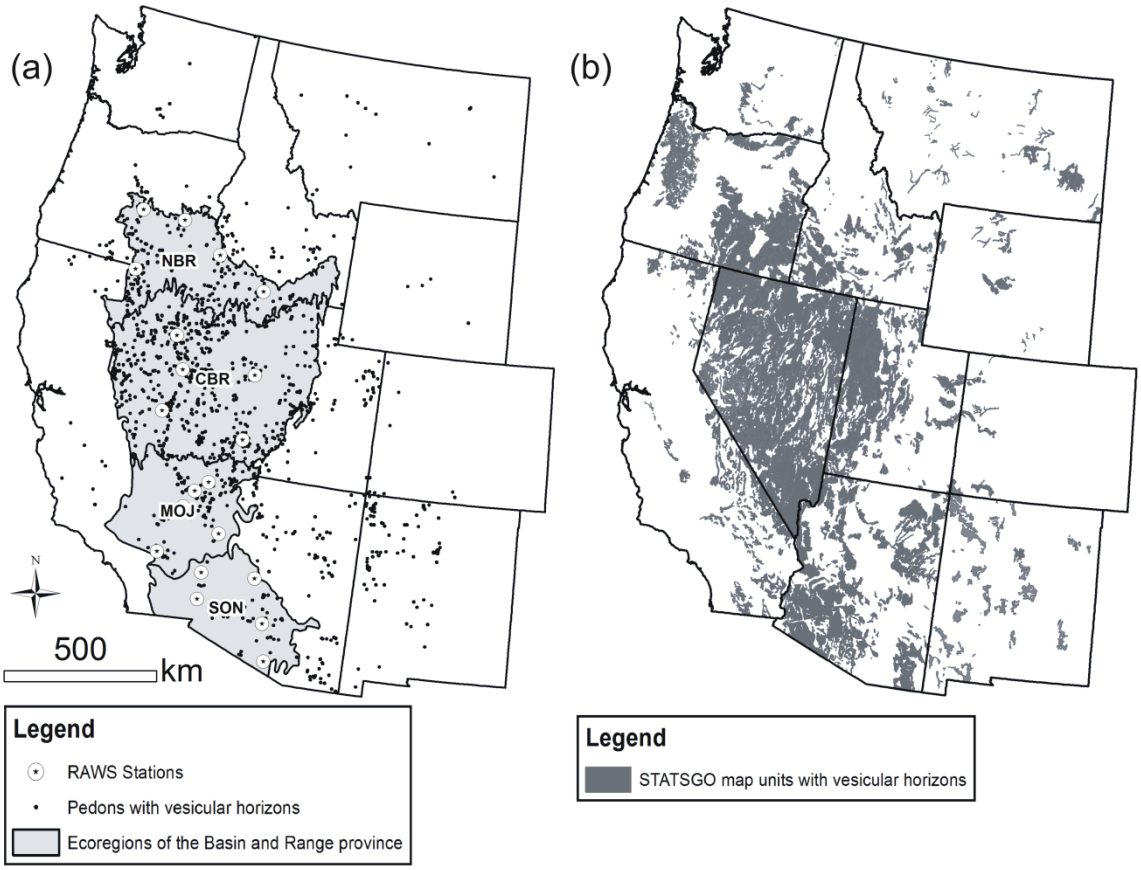

Fig. 2.4. Spatial distribution of soils with vesicular horizons indicated by: (a) Soil descriptions with vesicular horizons, including Official Series Descriptions (OSDs) and National Soils Information System (NASIS) pedon descriptions and the location of Remote Automated Weather Stations (RAWS) used in climate analysis and (b) State Soil Geographic data set (STATSGO) map units in which one or more major components are soil series with a vesicular horizon in the OSD. Shaded areas in (a) indicate the ecoregions of the Basin and Range Province, SON = Sonoran Basin and Range, MOJ = Mojave Basin and Range, CBR = Central Basin and Range, NBR = Northern Basin and Range.

nonparametric analyses were performed using MINITAB 15 (Mintab, 2007) and the Bonferonni correction was calculated by hand.

Analysis of weather records

In order to consider the relationship of VHI to modern climate conditions, weather records were analyzed at 20 Remote Automated Weather Stations (RAWS) (Western Regional Climate Center, 2011), including five stations in each of the ecoregions discussed above (SON, MOJ, CBR, and NBR). The stations were selected based on proximity to database pedon descriptions with vesicular horizons (Fig. 2.4a). Two climatic variables were extracted: 1) the average number of precipitation events per year and 2) the average increase in temperature during the drying period following a precipitation event (ΔT). These variables are considered the most significant in terms of understanding the relation of climate to vesicular pore formation. The amount of time required for the vesicular horizon to dry following a precipitation event, hereafter called the drying period, is a critical assumption that influences the analysis of both of these variables. The drying period was used to define the split between successive precipitation events, under the assumption that the soil will not trap air and form vesicular pores if it has not dried first, thus introducing more air to be trapped. The ΔT was defined as the difference between the maximum temperature during the drying period and the temperature at the time of initial precipitation. Air temperatures were used for this analysis, rather than soil temperatures, because these data were readily available and because the vesicular horizons typically occur at the soil surface, where temperature

fluctuations are most directly influenced by aboveground weather conditions. Vesicular pores only form and expand when the soil is wet (Springer, 1958; Miller, 1971; Figueira and Stoops, 1983), presumably because vesicular horizons have a weak structural consistence when they are wet (Bouza et al., 1993).

The actual drying period depends on current weather conditions (*e.g.*, air temperature, relative humidity), the water retention characteristics of the vesicular horizons, the relationship between water content and consistence of the vesicular horizon, and drainage conditions of the soil. Our analysis assumed a drying period of one day during the summer (Jun.-Aug.), five days during the winter (Dec.-Feb.), and three days at other times of the year. These assumptions were based on casual observations of vesicular horizon behavior in the field. Thorough verification of these assumptions was beyond the scope of this study, but we did consider the sensitivity of our analysis to the assumption of drying period (Table 2.2). Assumption of a longer drying period results in calculation of fewer precipitation events per year and a greater ΔT. Using a longer drying period resulted in fewer precipitation events because the drying period was used to define the separation of successive precipitation events, therefore using a longer drying period causes more precipitation to be lumped into a single event. The impact of this assumption was similar at climate stations located in each of the ecoregions and therefore is not presumed to introduce any bias to our comparison between ecoregions. Precipitation events of less than five mm were not included in the analysis, as small events are unlikely to be effective at trapping air and forming vesicular pores. Our analysis included between five and 10 years of weather records at each RAWS site. The

Table 2.2. Influence of assumed drying period on calculation of ΔT and the frequency of precipitation events.

RAWS Site (Ecoregion)[†]	ΔT[‡]			Annual Precipitation Events		
	DP[§]=1d	DP=3d	DP=5d	DP=1d	DP=3d	DP=5d
Haley Hills, AZ (SON)	7.5±0.6[¶]	11.2±0.6	12.8±0.7	8.1±1.2	7.5±1.0	7.0±1.0
Horse Thief Spgs, CA (MOJ)	5.9±0.4	9.7±0.5	11.6±0.5	10±0.9	8.3±0.6	7.4±0.6
Austin, NV (CBR)	7.4±0.5	11.3±0.6	13.6±0.7	10.8±0.9	9.8±0.8	7.9±0.5
Triangle, ID (NBR)	6.1±0.4	9.2±0.5	11.3±0.6	13.6±1.2	11.1±0.9	10±0.7

[†]Ecoregions: SON=Sonoran Basin and Range, MOJ = Mojave Basin and Range, CBR = Central Basin and Range, NBR = Northern Basin and Range
[‡]ΔT = Increase in air temperature during vesicular horizon drying after a precipitation event
[§]DP = Drying period used to define the time required for vesicular horizon drying after a precipitation event
[¶]Mean ± 1 Standard Error

annual number of precipitation events and ΔT were compared between the ecoregions according to analysis of variance (ANOVA) and multiple comparisons using Tukey's test (Sheskin, 2007). Statistical analysis was performed using MINITAB 15 (Minitab, 2007).

RESULTS AND DISCUSSION

Distribution and range of properties

The analysis of soil databases produced 1092 OSDs and 295 NASIS pedon descriptions with vesicular horizons. Soils with vesicular horizons occur throughout the western United States, but have been described most frequently in the Basin and Range Province, particularly in the NBR and CBR (Fig. 2.4a). This distribution may be biased by differences in the intensity of sampling across different soil survey areas and the scarcity of points in areas where soil surveys have not been completed (*e.g.*, the Mojave Desert region of California). The distribution of soil series with vesicular horizons derived from the STATSGO dataset (Fig. 2.4b) may provide a better depiction of the overall distribution of vesicular horizons. These data also show that vesicular horizons are extensive throughout the western United States, but are especially common in the Basin and Range Province. The total area of soil series with vesicular horizons mapped in SSURGO is 156,000 km^2 (as of 2007). Based on SSURGO, the vesicular horizons cover about 5% of the western United States and 21% of the Basin and Range Province.

The distribution of vesicular horizons in the western United States (Fig. 2.4), as well as the worldwide distribution of research sites where vesicular horizons have been described (Fig. 2.2), show that they mainly occur in arid and semiarid regions. Vesicular

porosity is also better expressed under the more arid conditions across a climatic gradient in Mongolia (Lebedeva et al., 2009). The soils with vesicular horizons in our dataset derived from the USDA databases are mostly soils with aridic moisture regimes (72%). The association of vesicular horizons with arid ecoregions and soils with aridic moisture regimes can be attributed to a few factors: 1) high rates of dust deposition which create a surface layer that is conducive to vesicular pore formation (McFadden, 1988; McFadden et al., 1998), 2) periodic drying and re-wetting of the soil surface, which drives vesicular pore formation (Springer, 1958; Miller, 1971; Figueira and Stoops, 1983), and 3) low vegetative cover, which allows surface crusting and air entrapment in the soil (Evenari et al., 1971).

The vesicular horizons in the soil databases occurred in a range of soil orders and were present across all temperature regimes. The soils included in the data set are mostly Aridisols (65%), but also include Mollisols (14%), Entisols (13%), Alfisols (5%), Inceptisols (3%), and a few Andisols and Vertisols (<1% each). The common occurrence of vesicular horizons in Aridisols reflects the association of vesicular horizons with arid environments. The temperature regimes of the soils with vesicular horizons were hyperthermic (4%), thermic (13%), mesic (64%), frigid (18%), and cryic (1%). Mesic and frigid temperature regimes were most common because many of the pedons with vesicular horizons were described in the cold deserts (*i.e.*, CBR and NBR ecoregions) (Fig. 2.4a).

The most common field-determined texture of the vesicular horizons was loam (35%), followed by sandy loam (18%), silt loam (15%), fine sandy loam (13%), very fine

sandy loam (6%), clay loam (4%), silty clay loam (3%), loamy sand (1%), coarse sandy loam (1%), and loamy fine sand (1%). Other textures (sand, silty clay, loamy coarse sand, clay, and coarse sand) each occurred in <1% of the vesicular horizons. Peterson (1980) observed a similar distribution of textures in the vesicular horizons of the Panamint Valley, California, which ranged from loamy sand to clay loam, but were most commonly sandy loam, loam, and silt loam. Laboratory-determined textures, available for 279 of the vesicular horizons, show a similar range of textures, but with stronger concentration of textures in the high-silt corner of the textural triangle (Fig. 2.5).

The geomorphic settings described in the NASIS pedon descriptions, grouped based on the classification of landforms by Peterson (1981), indicate that vesicular horizons are most common on piedmont landforms (alluvial fans, bajadas, fan remnants, fan skirts, fan terraces, and pediments) (72%), but also occur in mountains (mountainslopes, hillslopes, and structural benches) (13%) and basin floors (alluvial flats, alluvial plains, barrier flats, beach plains, lake terraces, playas, and sand sheets) (16%). Slopes reported in the NASIS pedon descriptions indicate that soils with vesicular horizons are generally on low slope gradients, with a median of 2% slope and an interquartile range from 1 to 5%, but can occur on slopes up to 45%. These findings are consistent with soil morphological descriptions made across an arid landscape in the Mojave Desert, in which vesicular horizons were observed to occur on landforms of the piedmont, mountains, and basin floor, but within the mountains, were more common on gently sloping landforms (e.g., mountainflat) compared to steep landforms (e.g., mountainflank) (Hirmas and Graham, 2011). Along a single hillslope in Australia,

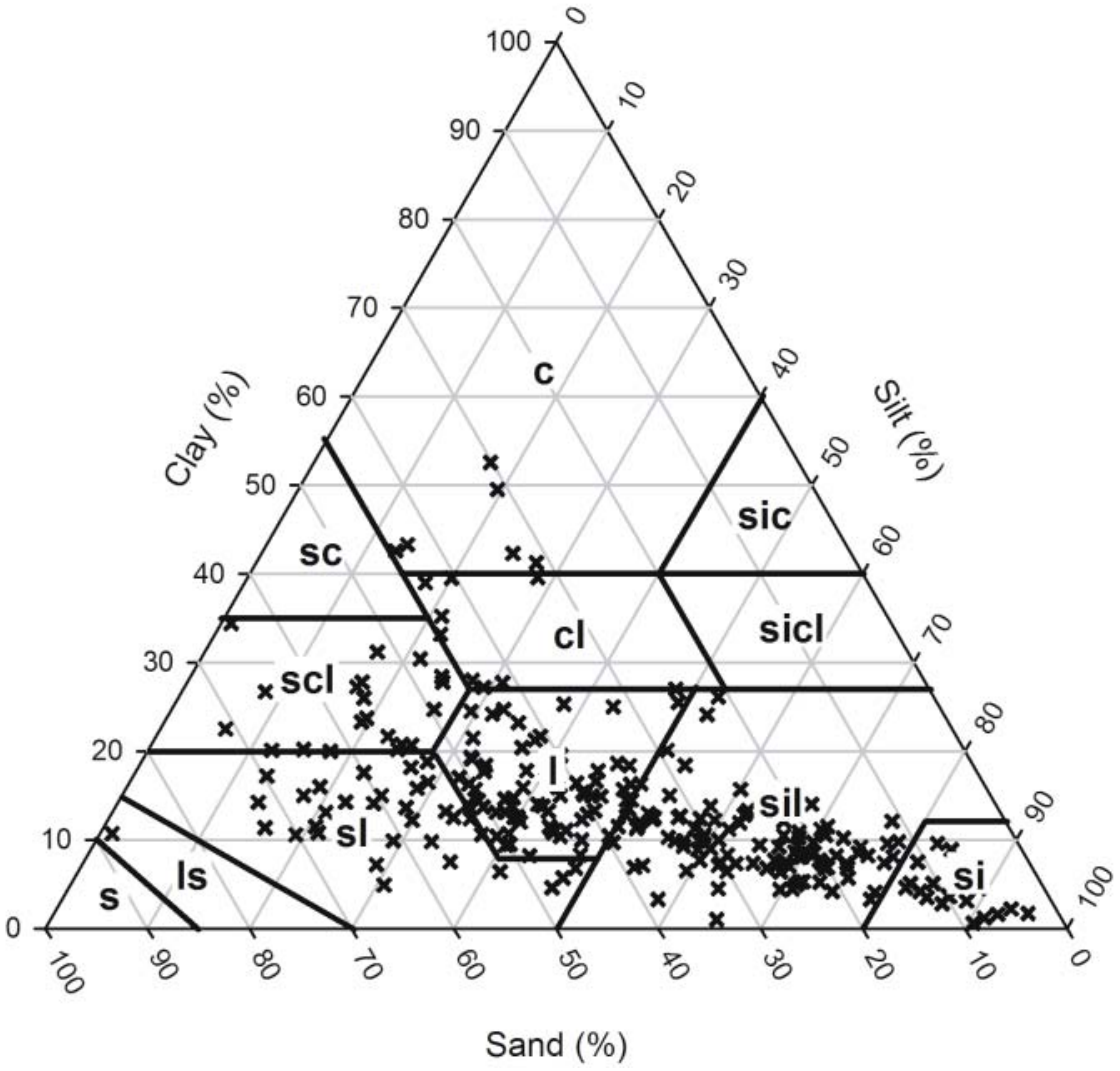

Fig. 2.5. Laboratory-determined textures of vesicular horizons plotted on the soil textural triangle.

vesicular horizons were most common on low slope gradients as well (Brown and Dunkerley, 1996).

Vesicular horizons in the western United States occur across several ecoregions, which represent different climatic and biological influences, and are formed in various geomorphic settings, which represent differences in surface age, parent material, and relief. Thus, it is not surprising that the chemical properties of the vesicular horizon, including organic C, $CaCO_3$, pH, electrical conductivity, and exchangeable sodium percentage (ESP), vary widely (Table 2.3). Although some studies have suggested that low organic C (Wood et al., 1978), high $CaCO_3$ (Evenari et al., 1974), and high exchangeable Na percentage (Bouza et al., 1993) promote vesicular pore formation, none of these can be considered an essential prerequisite for vesicular horizon development. Of the soils analyzed, 68% contained measureable $CaCO_3$ and only 11% were sodic soils (ESP>15; U.S. Regional Salinity Laboratory, 1954).

Vesicular horizon index

The vesicular horizon index (VHI) was developed as a way to quantify vesicular horizon expression based on standard information recorded in field descriptions. Vesicular horizon expression is defined here according to the abundance of vesicular pores (more pores = better expression), the size of vesicular pores (larger pores = better expression), and the horizon thickness (thicker horizon = better expression). Previous studies have used similar rating systems for the purpose of comparing vesicular horizon expression within their study areas, based on the grade of platy and prismatic structure

Table 2.3. Chemical properties of vesicular horizons based on lab data for National Soils Information System pedon descriptions with vesicular horizons.

Property	Median	Inter-quartile Range	Total Range	N
Organic C (%)	0.7	0.4-1.2	0-5.3	269
Electrical Conductivity (dS m^{-1})	1.2	0.8-2.3	0.1-218	187
Exchangeable Na (%)	2	1-6	0-96	256
pH	8.0	7.3-8.4	5-10.7	263
$CaCO_3$ (%)	4	0-12	0-49	205

and the quantity class of vesicular pores (Blackburn, 1975; McDonald, 1994). Neither of these rating systems was suitable for application to the soil databases because they are not inclusive of all combinations of structure and porosity.

In order to develop an index that is inclusive of all possible ranges and combinations of properties that occur in vesicular horizons, the VHI was modeled after the soil development index (SDI) (Harden, 1982). In the SDI, the thickness of the soil horizons is multiplied by terms that quantify individual soil properties. The SDI does not include a term for vesicular porosity, therefore the first step in developing the VHI was to determine a suitable method for assigning a numerical value based on the description of vesicular pores. The standard method for describing vesicular pores includes the assignment of both a quantity class (Q) and size class (S) (Soil Survey Division Staff, 1993; Schoeneberger et al., 2002). Point values were assigned to Q (few = 10, common = 20, many = 30) and S (very fine = 10, fine = 20, medium = 30, coarse = 40, very coarse = 50) using intervals of ten to be consistent with points assignments used in the SDI (Harden, 1982). Several possible combinations of Q and S were compared by calculating each of the candidate terms for soil descriptions from a chronosequence study in the Mojave Desert (McDonald, 1994) (Fig. 2.6). Two of the terms fit equally well to the chronosequence data ($r^2 = 0.89$, $p=0.005$): 1) the term calculated by summing Q + S for all size classes included in the description and (Fig. 2.6b) and 2) the term calculated by summing the product of Q × S for all size classes included in the description (Fig. 2.6d). The term calculated by summing Q + S for all size classes included in the description (Fig. 2.6b) was selected for use in the VHI because summation of soil property

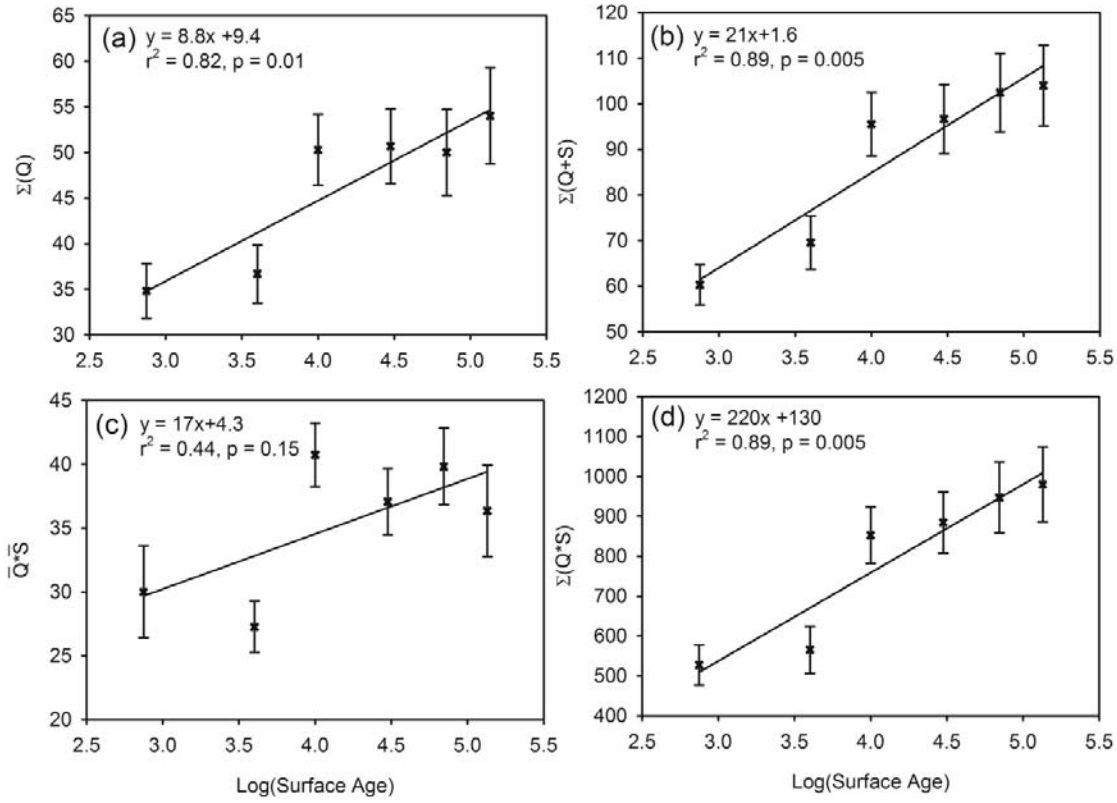

Fig. 2.6. Comparison of terms for the quantification of vesicular pore descriptions, applied to soils of increasing age on a chronosequence of alluvial fans in the Mojave Desert (McDonald, 1994): (a) ΣQ, (b) Σ(Q+S), (c) $\overline{Q} \times \overline{S}$, (d) Σ(Q×S), where Q = quantity class (few = 10, common = 20, many = 30) and S = size class (very fine = 10, fine = 20, medium = 30, coarse = 40, very coarse = 50). Error bars indicate one standard error.

descriptors is more consistent with the calculations applied in the SDI (Harden, 1982). Following the notation used by Harden (1982), the vesicular pore term is denoted as X_{ve}. As in the SDI, X_{ve} is then set to a scale from 0 to 1 (X_{ven}) by dividing by the highest value of the term. The highest value for X_{ve} encountered in the soil databases was 220, this would represent a vesicular horizon with many very fine, many fine, many medium, and many coarse vesicular pores. Very coarse vesicular pores are rarely described and therefore not included in the calculation of the maximum X_{ve}. Finally, VHI is calculated by multiplying vesicular horizon thickness by X_{ven}. If more than one vesicular horizon is present in the soil profile, the VHI is calculated for each horizon and then summed. An outline and example of VHI calculation is provided in Fig. 2.7.

The resulting index shows a strong relationship with the log of surface age (r^2=0.94) for the surfaces under 100,000 yrs old (Fig. 2.8). These data demonstrate that although vesicular pores may be subject to collapse and reformation on a short time-scale (Fig. 2.3; Yonovitz and Drohan, 2009) there are also long term trends in vesicular horizon expression. This may be related to the addition of eolian materials to the vesicular horizon. Eolian additions cause the vesicular horizon to grow thicker. With age, the vesicular pores may also become stabilized by calcitans and argillans, which are formed by the transport of eolian-derived $CaCO_3$ and clay into the vesicular horizon with infiltrating water (Anderson et al., 2002). The decrease in VHI at the oldest site in the chronosequence (Fig. 2.8) can be attributed to dissection and erosion of this surface (Meadows et al., 2008). Although the VHI (which includes horizon thickness) decreases on the oldest surface, the X_{ve} increases (Fig. 2.6b). This suggests that X_{ve} alone may be a

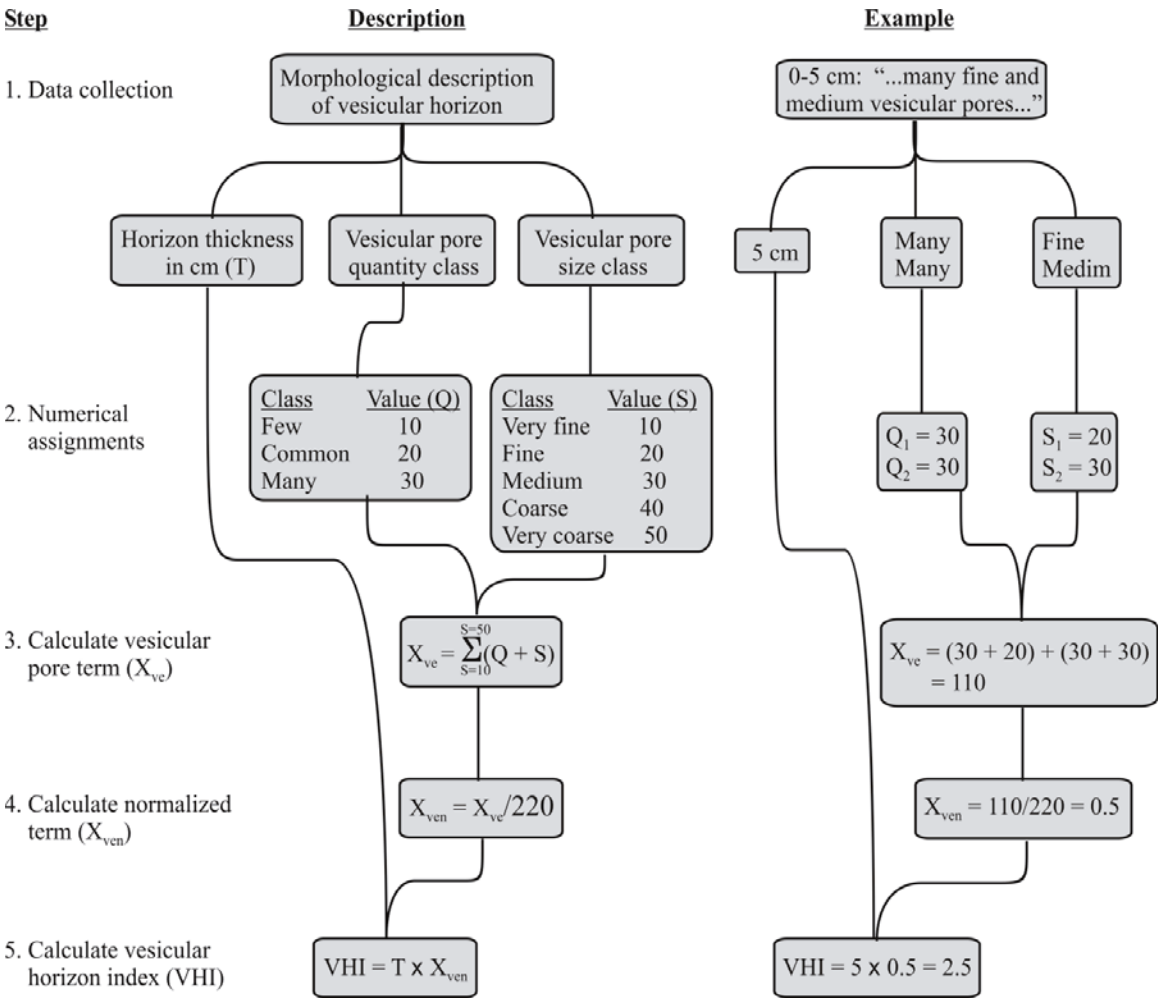

Fig. 2.7. Outline, description, and example of steps involved in calculation of the vesicular horizon index.

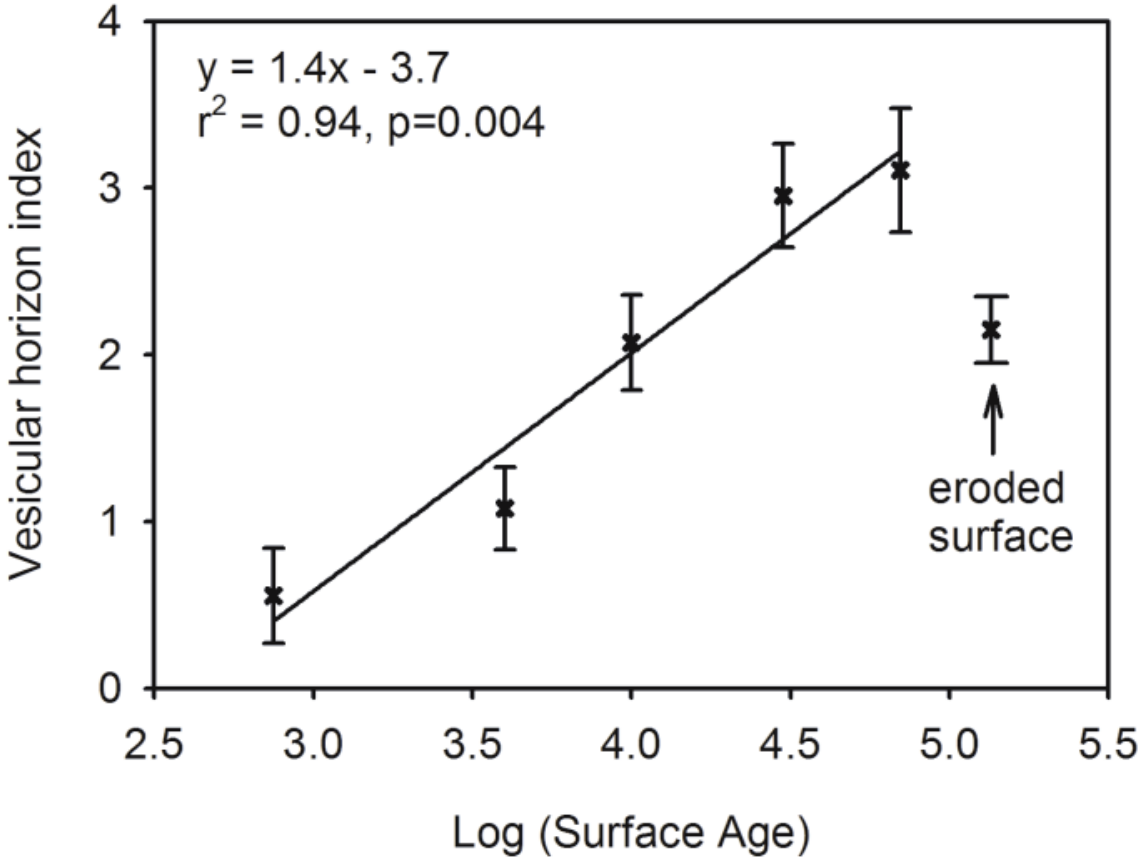

Fig. 2.8. Vesicular horizon index as a function of soil age on a chronosequence of alluvial fans in the Mojave Desert (McDonald, 1994). Error bars indicate one standard error.

better indicator of surface age on dissected surfaces where the vesicular horizon has been partially eroded. However, this would only be true in cases where erosion has been relatively minor. Severe erosion of well-developed desert soils has been described in chronosequence studies and attributed to a pedogenic threshold, in which reduced permeability due to soil development leads to runoff, dissection, and degradation of the surface (Wells et al., 1985). Under these circumstances the entire vesicular horizon would be removed and neither X_{ve} nor VHI would be reflective of the soil age.

The VHI is developed here for analyzing trends in vesicular horizon expression using soil databases, but it may be otherwise useful. The heterogeneity of vesicular horizons across desert landscapes could be used as an indicator of complex hydrologic patterns. Previous work has shown the infiltration rate of soils with vesicular horizons is negatively correlated with the quantity of vesicular pores described in the field (Blackburn, 1975; Valentin, 1994), as well as with the total porosity calculated from bulk density (Lebedeva et al., 2009). This suggests that VHI should also be negatively correlated with infiltration rate, although VHI is slightly different from the vesicular horizon rating systems used in the correlations described above, because it includes horizon thickness as well as vesicular porosity. Analysis of chronosequence data in arid and semi-arid environments may also be aided by use of either the VHI or by including the X_{ve} term in the calculation of the SDI. Harden (1982) suggested that other terms could be added as the SDI is applied to chronosequences in various environmental settings, undergoing different pedogenic processes.

VHI relation to ecoregions of the Basin and Range Province

A broad-scale trend across the Basin and Range Province is revealed when soil descriptions are grouped by Level III Ecoregions (USEPA, 2006a) (Fig. 2.9). The VHI is higher in the cold deserts (*i.e.*, NBR and CBR) compared to the warm deserts (*i.e.*, MOJ and SON). Possible regulators of vesicular horizon expression at this broad scale include paleoclimatic events, modern climatic conditions, and biotic factors.

The drying of pluvial lakes during interpluvial climatic periods exposed fine-grained sediments to wind erosion, producing vast areas that acted as dust sources. Episodic dust deposition from these events is an important driver of soil formation processes in both the warm (McFadden et al., 1986; McFadden, 1988) and cold deserts (Chadwick and Davis, 1990). The formation of vesicular horizons has been linked to these periods of abundant dust deposition (McFadden et al., 1998; Anderson et al., 2002). The distribution of pluvial lakes is one possible explanation for the difference in vesicular horizon expression between the cold and warm deserts of the Basin and Range Province. Pleistocene pluvial lakes occupied 27% of the area of cold deserts, but only 5% of the area of the warm deserts in the United States (extracted from map by Dutch, 1999). Consequently, sources of the dust that drives vesicular horizon formation are much more extensive in the cold deserts.

The dynamic nature of vesicular horizons, as observed by some authors (Springer, 1958; Yonovitz and Drohan, 2009), suggests that some destruction and reformation of vesicular pores is likely to have occurred under modern climatic conditions. Vesicular porosity has been observed to increase with increasing number of wetting and drying

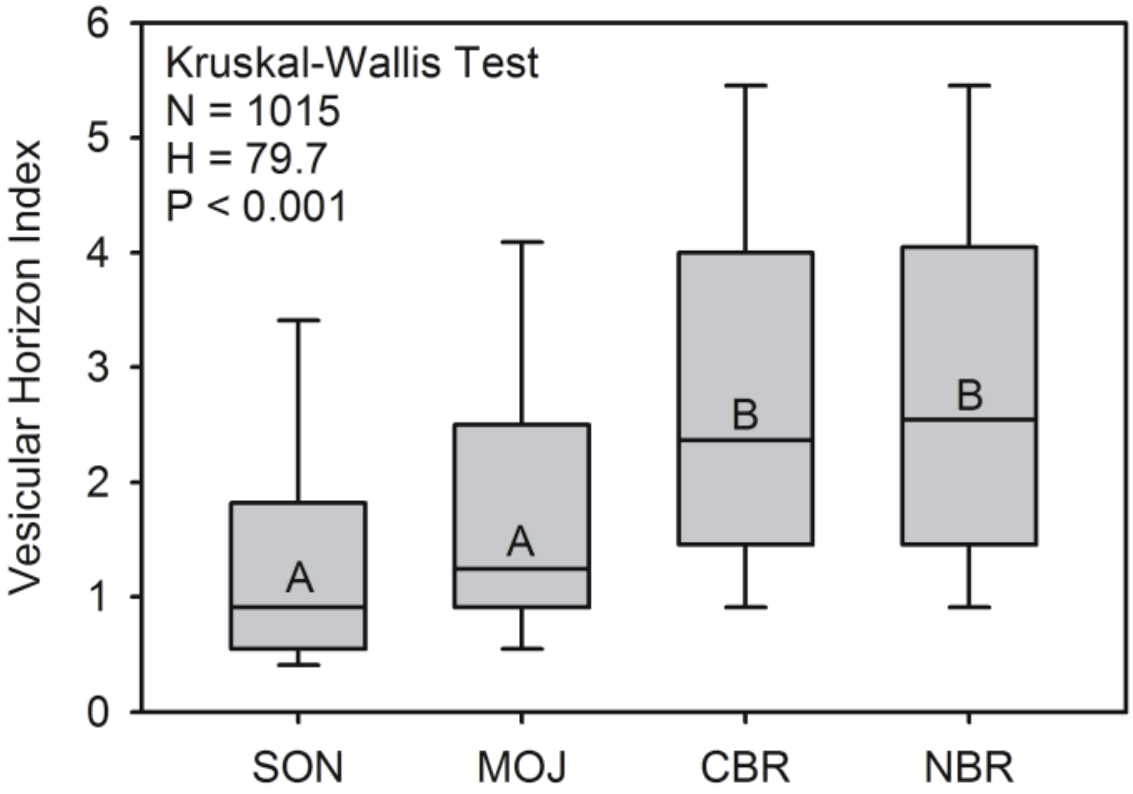

Fig. 2.9. Box plots of vesicular horizon index by Level III ecoregions (USEPA, 2006a): SON = Sonoran Basin and Range, MOJ = Mojave Basin and Range, CBR = Central Basin and Range, NBR = Northern Basin and Range. Boxes labeled with the same letter indicate a non-significant difference between groups, according to the Mann-Whitney test with a Bonferonni correction for multiple comparisons (per family $\alpha = 0.05$, per test $\alpha = 0.008$). Outliers are not shown.

cycles (Miller; 1971; Figueira and Stoops; 1983) and expansion of vesicular pores is commonly hypothesized to be driven by thermal expansion (Paletskaya et al., 1958; Evenari et al., 1974; Bouza et al., 1993; Henning and Kellner, 1994; Brown and Dunkerley, 1996; McFadden et al., 1998). With these mechanisms in mind, climatic records were analyzed to derive the annual number of wetting and drying cycles, as well as the average increase in temperature during drying. The frequency of wetting and drying cycles was found to increase along the gradient of ecoregions from the SON to the NBR (Fig. 2.10a), however high variability within each of the ecoregions means that the difference between the ecoregions was not significant according to ANOVA ($p=0.07$). The modern climate may lead to greater vesicular horizon expression in the cold deserts due to the more frequent precipitation events, which offer more opportunities for vesicular pore formation and growth, but the high variability of precipitation frequency clouds the importance of this trend relative to observed differences in VHI between the ecoregions. Average temperature increase during drying was actually lowest in the NBR and highest in the CBR, with intermediate expression in the SON and MOJ (Fig. 2.10b); therefore difference in thermal expansion does not likely explain the trend in vesicular horizon expression.

Biotic influences on vesicular horizon distribution include past and present vegetation types, burrowing animals, and biological soil crusts. Vesicular horizons are usually not observed, or are weakly expressed, in the undercanopy environment because of the increased activity of burrowing animals (Shafer et al., 2007) and protective canopy cover that prevent surface sealing required for vesicular horizons formation (Evenari et

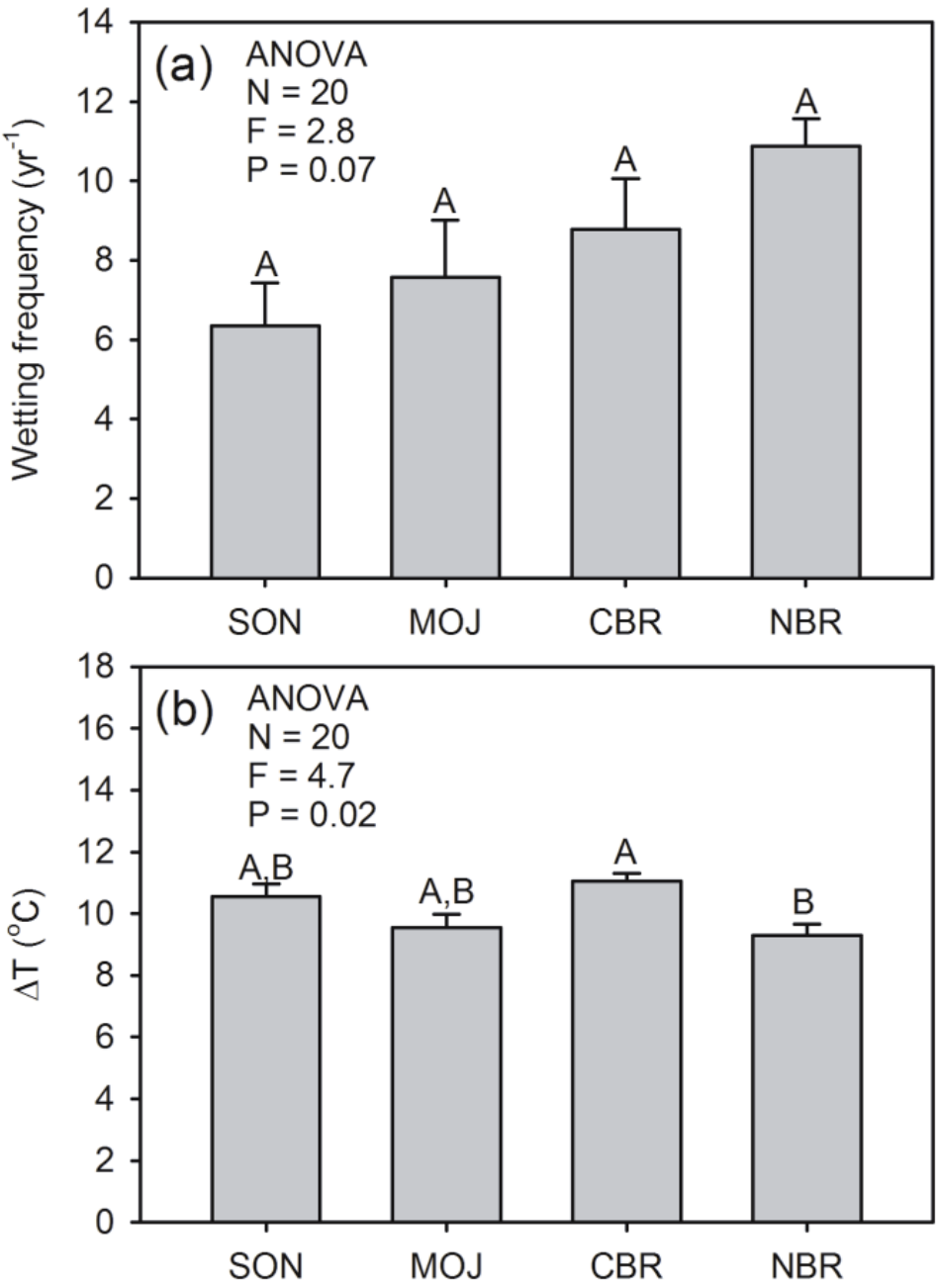

Fig. 2.10. Results of climate analysis grouped by ecoregion (SON = Sonoran Basin and Range, MOJ = Mojave Basin and Range, CBR = Central Basin and Range, NBR = Northern Basin and Range): (a) frequency of precipitation events resulting in wetting of the vesicular horizon and (b) increase in temperature during drying of the vesicular horizon (ΔT). Bars labeled with the same letter indicate a non-significant difference according to Tukey's test.

al., 1974). Bare or clast-covered interspace soils that allow the formation of vesicular horizons are characteristic of desert scrub communities in both the warm and cold deserts (Eckert et al., 1978). In the Mojave Desert vesicular horizons occur in three vegetation communities that occur with increasing elevation: creosote (840 m), blackbush (1400 m), and pinyon-juniper (1750 m), but do not occur in the higher elevation fir-pine forests (Amundson et al., 1989). Contrary to our findings, weaker expression of vesicular horizons was observed in the Great Basin steppe community that occurs at high elevations in the Mojave Desert (Quade, 2001). In that study, the weak expression of vesicular horizons in the high elevation zones was attributed to the disruption of desert pavement by vegetation advances during the last glacial maximum. However, subsequent studies in the Mojave Desert have suggested that desert pavements recover rapidly from disruption due to vegetation advances (Valentine and Harrington, 2006; Pelletier et al., 2007). Considering the rapid formation of vesicular pores under favorable conditions (Yonovitz and Drohan, 2009), it is also likely that vesicular horizons were only temporarily affected by past vegetation advances. Vesicular horizons have been observed to reform in plant scars, which are microtopographic features left by the death of long-lived perennial vegetation, even though these areas were mixed by burrowing animals that inhabited the undercanopy environment during the life of the plant (McAuliffe and McDonald, 2006). Given these considerations, differences in past or modern vegetation are unlikely to explain differences in vesicular horizon expression among the deserts of the Basin and Range Province. Vesicular horizons are observed across a range of plant communities, as long as bare interspace is present, and are

unlikely to be significantly impacted by past vegetation advances that may have decreased or eliminated the bare interspace.

Biological soil crusts are a biotic factor that may have more direct influence on vesicular horizons. Biological soil crusts have been observed growing directly on vesicular horizons (Danin et al., 1998; Joeckel and Clement, 1999; Cantón et al., 2003). Moss-lichen crust can promote vesicular horizon formation by trapping dust (Williams et al., 2010). Biological soil crusts of the hot and cold desert display differences in morphology; having a prominent pinnacled microtopography in the cold deserts and a smooth microtopography and cryptic appearance in the hot deserts (Belnap et al., 2001). This difference in microtopography suggests a stronger dust-trapping capacity by the biological soil crusts in the cold desert, which could impact vesicular horizon formation.

VHI relation to other soil properties

The median VHI was lowest in soils with hyperthermic temperature regimes, higher in thermic soils, and highest in mesic and frigid soils (Fig. 2.11a). Due to the smaller number of cryic soils, the median VHI was not significantly different from the other temperature regimes, except for the hyperthermic soils. The reason for the relationship between VHI and soil temperature regime cannot be evaluated from the purely observational data presented here. This relationship is difficult to separate from that described above between VHI and ecoregions of the Basin and Range Province. While both relationships suggest that vesicular horizons are better expressed in soils of colder environments, the relationship may be an artifact of another factor that influences

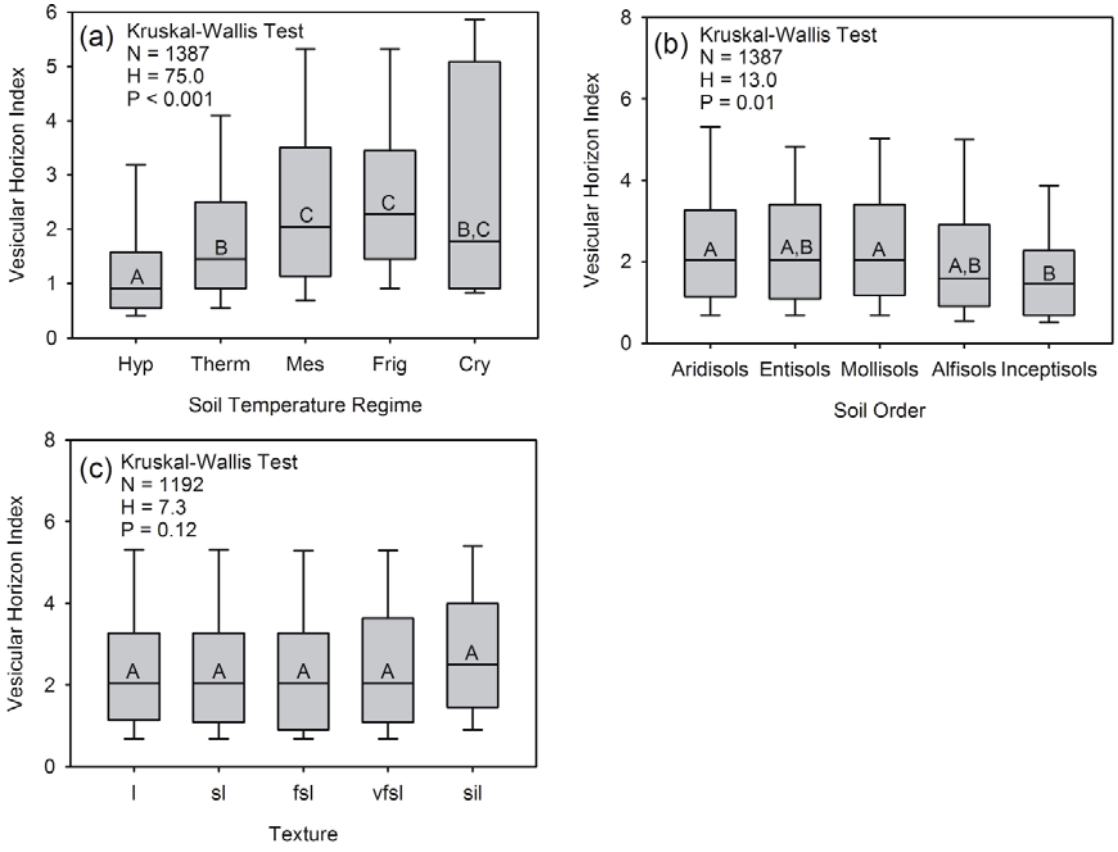

Fig. 2.11. Box plots of vesicular horizon index in soils grouped by: (a) soil temperature regime (Hyp = hyperthermic, Therm = thermic, Mes = mesic, Frig = frigid, Cry = cryic), (b) soil order, and (c) vesicular horizon texture (l = loam, sl = sandy loam, fsl = fine sandy loam, vfsl = very fine sandy loam, sil = silt loam). Boxes in the same graph labeled with the same letter indicate a non-significant difference between groups, according to the Mann-Whitney test with a Bonferonni correction for multiple comparisons (per family $\alpha = 0.05$, per test $\alpha = 0.005$). Outliers are not shown.

vesicular horizon formation, such as the prevalence of pluvial dry lakes that act as dust sources in those areas.

Analysis of VHI by soil order shows that VHI is significantly higher in Aridisols and Mollisols compared to Inceptisols (Fig. 2.11b). The aridic moisture regime of the Aridisols, and most of the Entisols in the dataset, may explain why soils in these orders tend to have high VHIs. Vesicular horizons are better expressed in arid soils because of greater rates of dust deposition (McFadden, 1988; McFadden et al., 1998), exposure to cyclic wetting and drying (Springer, 1958; Miller, 1971; Evenari et al., 1974; Figueira and Stoops, 1983), and sparse vegetation cover, which allows more extensive surface sealing (Evenari et al, 1974). The high VHI of the Mollisols is contrary to the common perception that vesicular horizons are associated with low organic matter soils (Blackburn, 1975). The median organic carbon content of Mollisols in our data set is 1.5%, more than double the median organic carbon content for all of the soil orders in the dataset together (0.7%). The organic carbon content of the Mollisols with vesicular horizons is apparently not sufficient to stabilize aggregates and prevent formation of vesicular pores.

The median VHI is not significantly different among any of the most common vesicular horizon textures (Fig. 2.11c). The median VHI was slightly higher in soils with silt loam textures, but was not significantly different from the other commonly observed textures according to the statistical analysis. This result suggests that all of the most common textures observed in vesicular horizons (loam, sandy loam, fine sandy loam, very fine sandy loam, and silt loam) are equally conducive to vesicular horizon

formation. Previous studies have demonstrated that vesicular porosity can form across a similar range of soil textures (Peterson; 1980; Yonovitz and Drohan, 2009). Coarser textures (*e.g.*, sands and loamy sands) and finer textures (*e.g.*, clay loams) are much less common in vesicular horizons (Fig. 2.6). Thus, coarse-textured parent material may require substantial alteration, typically through eolian additions, to allow vesicular horizon formation. On the other hand, extensive weathering and clay accumulation may lead to textures that are too clay-rich to support vesicular pore formation. This is thought to occur in some settings where eolian deposition allows the formation of a new vesicular horizon at the surface, while the buried vesicular horizon becomes increasingly enriched in clay and is transformed to a B horizon (McFadden, 1988).

SUMMARY AND CONCLUSIONS

Soil databases were used to analyze a large dataset, including 1387 soils with vesicular horizons, spanning the western half of the United States. We estimate that there are 156,000 km^2 of soils with vesicular horizons in the western United States, mostly within the arid Basin and Range Province. Vesicular horizons have highly variable chemical properties (organic C, electrical conductivity, ESP, pH, $CaCO_3$), reflecting the diversity of soil-forming environments in which they occur. The VHI, calculated from horizon thickness and size and quantity of vesicular pores, was developed and used to quantify vesicular horizon expression. Application of the VHI using the soil databases revealed that the strongest expression of the vesicular horizon occurs in the cold deserts (*i.e.*, NBR and CBR ecoregions) and in soils with mesic and frigid temperature regimes.

The association of strongly-developed vesicular horizons with cold soils may be due to a confounding factor, such as the large extent of pluvial dry lake beds that act as sources of dust in the cold deserts of the Basin and Range Province. Only weak associations were found between soil order and VHI, with the highest VHI occurring in the Aridsols and Mollisols. There was no significant difference in VHI among vesicular horizons with different textures (loam, sandy loam, fine sandy loam, very fine sandy loam, and silt loam). Other textures are rarely observed in the vesicular horizon. The cause of the trends presented here cannot be evaluated based on the observational methods used in this study, however, the results suggest hypotheses that may be tested experimentally in future studies.

REFERENCES

Abdi, H. The Bonferroni and Šidák corrections for multiple comparisons. p. 103-106. *In* N. Salkind and K. Rasmussen (eds). Encyclopedia of Measurement and Statistics. SAGE Publications, Thousand Oaks, CA.

Adelsberger, K.A., and J.R. Smith. 2009. Desert pavement development and landscape stability on the Eastern Libyan Plateau, Egypt. Geomorphology 107:178-194.

Amit, R., and R. Gerson. 1986. The evolution of Holocene reg (gravelly) soils in deserts - an example from the Dead Sea region. Catena 13:59-79.

Amundson, R.G., O.A. Chadwick, J.M. Sowers, and H.E. Doner. 1989. Soil evolution along an altitudinal transect in the eastern Mojave Desert of Nevada, USA. Geoderma 43:349-371.

Anderson, K., S. Wells, and R. Graham. 2002. Pedogenesis of vesicular horizons, Cima Volcanic Field, Mojave Desert, California. Soil Sci. Soc. Am. J. 66:878-887.

Belnap, J., R. Rosentreter, S. Leonard, J.H. Kaltenecker, J. Williams, and D. Eldridge. 2001. Biological soil crusts: Ecology and management. USDI-BLM Printed Materials Distribution Center, Denver, CO.

Blackburn, W.H. 1975. Factors influencing infiltration and sediment production of semiarid rangelands in Nevada. Water Resour. Res. 11:929-937.

Bockheim, J.G. 2010. Evolution of desert pavements and the vesicular layer in soils of the Transantarctic Mountains. Geomorphology 118:433-443.

Bouza, P., H.F. Delvalle, and P.A. Imbellone. 1993. Micromorphological, physical, and chemical characteristics of soil crust types of the central Patagonia region, Argentina. Arid Soil Res. and Rehabilitation 7:355-368.

Brown, K.J., and D.L. Dunkerley. 1996. The influence of hillslope gradient, regolith texture, stone size and stone position on the presence of a vesicular layer and related aspects of hillslope hydrologic processes: A case study from the Australian arid zone. Catena 26:71-84.

Cantón, Y., A. Solé-Benet, and R. Lázaro. 2003. Soil-geomorphology relations in gypsiferous materials of the Tabernas Desert (Almeria, SE spain). Geoderma 115:193-222.

Chadwick, O.A., and J.O. Davis. 1990. Soil-forming intervals caused by eolian sediment pulses in the Lahontan basin, northwestern Nevada. Geology 18:243-246.

Danin, A., I. Dor, A. Sandler, and R. Amit. 1998. Desert crust morphology and its relations to microbiotic succession at Mt. Sedom, Israel. J. Arid. Environ. 38:161-174.

Dutch, S. 1999. Pleistocene glaciers and geography [Online]. Available by University of Wisconsin - Green Bay. <http://www.uwgb.edu/dutchs/earthsc202notes/glacgeog.htm> (verified 22 Feb. 2011).

Eckert, R.E., M.K. Wood, W.H. Blackburn, F.F. Peterson, J.L. Stephens, and M.S. Meurisse. 1978. Effects of surface-soil morphology on improvement and management of some arid and semiarid rangelands, p. 299-301. Proceedings of the First International Rangeland Congress. Society for Range Management, Denver, CO.

Eckert, R.E., M.K. Wood, W.H. Blackburn, and F.F. Peterson. 1979. Impacts of off-road vehicles on infiltration and sediment production of two desert soils. J. Range Manage. 32:394-397.

Ellis, F. 1990. Note on soils with vesicular structure and other micromorphological features in Karoo soils., pp. 326-336. 16th Congress of the Soil Science Society of South Africa, Pretoria.

ESRI. 2008. ArcGIS 9.3. Esri, Redlands, CA.

Evenari, M., D.H. Yaalon, and Y. Gutterman. 1974. Note on soils with vesicular structure in deserts. Z. Geomorphol. 18:162-172.

Figueira, H., and G. Stoops. 1983. Application of micromorphometric techniques to the experimental study of vesicular layer formation. Pedologie 33:77-89.

Gile, L.H., and J.W. Hawley. 1968. Age and comparative development of desert soils at Gardner Spring radiocarbon site, New Mexico. Soil Sci. Soc. Am. Proc. 32:709-716.

Goossens, D., and B. Buck. 2009. Dust emission by off-road driving: Experiments on 17 arid soil types, Nevada, USA. Geomorphology 107:118-138.

Gustafson, D.L. 2003. Web interface and graphical locator. [Online]. Available by Montana State University <http://www.esg.montana.edu/gl/trs-data.html> (verified Sept. 14, 2010).

Hamerlynck, E.P., J.R. McAuliffe, E.V. McDonald, and S.D. Smith. 2002. Ecological responses of two Mojave Desert shrubs to soil horizon development and soil water dynamics. Ecology 83:768-779.

Harden, J.W. 1982. A quantitative index of soil development from field descriptions: Examples from a chronosequence in central California. Geoderma 28:1-28.

Henning, J.A.G., and K. Kellner. 1994. Degradation of a soil (Aridosol) and vegetation in the semiarid grasslands of southern Africa. Bot. Bull. Acad. Sin. 35:195-199.

Hirmas, D.R., and R.C. Graham. 2011. Pedogenesis and soil-geomorphic relationships in an arid mountain range, Mojave Desert, California. Soil Sci. Soc. Am. J. 75:192-206.

Joeckel, R.M., and B.A. Clement. 1999. Surface features of the Salt Basin of Lancaster County, Nebraska. Catena 34:243-275.

Lebedeva, M.P., D.L. Golovanov, and S.A. Inozemtsev. 2009. Microfabrics of desert soils of Mongolia. Euras. Soil Sci. 42:1204-1217.

McAuliffe, J.R. 1994. Landscape evolution, soil formation, and ecological patterns and processes in Sonoran Desert bajadas. Ecological Monogr. 64:111-148.

McAuliffe, J.R., and E.V. McDonald. 2006. Holocene environmental change and vegetation contraction in the Sonoran Desert. Quat. Res. 65:204-215.

McDonald, E.V. 1994. The relative influences of climatic change, desert dust, and lithologic control on soil-geomorphic processes and soil hydrology of calcic soils formed on quaternary alluvial-fan deposits in the Mojave Desert, California. Ph.D. Dissertation, The University of New Mexico, Albuquerque, NM.

McDonald, E.V. 2008. Soil formation in the Mojave Desert: New TCN information suggests rates of soil formation may exceed previously established rates. GSA-SSSA-ASA-CSA-GCAGS-HGS Joint Annual Meeting, Houston, TX.

McFadden, L.D., S.G. Wells, and J.C. Dohrenwend. 1986. Influences of Quaternary climatic changes on processes of soil development on desert loess deposits of the Cima Volcanic Field, California. Catena 13:361-389.

McFadden, L.D., S.G. Wells, and M.J. Jercinovich. 1987. Influences of eolian and pedogenic processes on the origin and evolution of desert pavements. Geology 15:504-508.

McFadden, L.D. 1988. Climatic influences on rates and processes of soil development in Quaternary deposits of southern California. Geol. Soc. Am. Spec. Paper 216:153-177.

McFadden, L.D., S.G. Wells, W.J. Brown, and Y. Enzel. 1992. Soil genesis on beach ridges of pluvial Lake Mojave: Implications for Holocene lacustrine and eolian events in the Mojave Desert, southern California. Catena 19:77-97.

McFadden, L.D., E.V. McDonald, S.G. Wells, K. Anderson, J. Quade, and S.L. Forman. 1998. The vesicular layer and carbonate collars of desert soils and pavements: formation, age and relation to climate change. Geomorphology 24:101-145.

Meadows, D.G., M.H. Young, and E.V. McDonald. 2008. Influence of relative surface age on hydraulic properties and infiltration on soils associated with desert pavements. Catena 72:169-178.

Miller, D.E. 1971. Formation of vesicular structure in Soil. Soil Sci. Soc. Am. Proc. 35:635-637.

Miller, D.M., D.R. Bedford, D.L. Hughson, E.V. McDonald, S.E. Robinson, and K.M. Schmidt. 2009. Mapping Mojave Desert ecosystem properties with surficial geology. p. 225-251. *In* R. H. Webb, et al. (eds.) The Mojave Desert: Ecosystem Processes and Sustainability. University of Nevada Press, Reno, NV.

Minitab. 2007. MINITAB 15. Minitab, State College, PA.

Musick. 1975. Barrenness of desert pavement in Yuma County, Arizona. J. Arizona Acad. Sci. 10:24-28.

Noller, J.S. 1993. Late Cenozoic stratigraphy and soil geomorphology of the Peruvian Desert, 3^{o}-18^{o}S: A long-term record of hyperaridity and El Niño. Ph.D. Dissertation, University of Colorado, Boulder.

Painter, T.H., J.S. Deems, J. Belnap, A.F. Hamlet, C.C. Landry, and B. Udall. 2010. Response of Colorado River runoff to dust radiative forcing in snow. Proc. Natl. Acad. Sci. USA 107:17125-17130.

Paletskaya, L.N., A.P. Lavrov, and S.I. Kogan. 1958. Pore formation in takyr crust. Sov. Soil Sci. (Engl. Transl.) 3:245-250.

Pelletier, J.D., M. Cline, and S.B. DeLong. 2007. Desert pavement dynamics: numerical modeling and field-based calibration. Earth Surf. Process. Landforms 32:1913-1927.

Peterson, F.F. 1980. Holocene desert soil formation under sodium-salt influence in a playa-margin environment. Quat. Res. 13:172-186.

Peterson, F.F. 1981. Landforms of the Basin and Range Province: Defined for soil survey. Nevada Agric. Experiment Station Tech. Bull. 28. University of Nevada, Reno.

Quade, J. 2001. Desert pavements and associated rock varnish in the Mojave Desert: How old can they be? Geology 29:855-858.

Rossi, A.M. 2009. Soil development and clast weathering on a moraine chronosequence, eastern Sierra Nevada, California. M.S. Thesis, University of California, Riverside.

Schlesinger, W.H., J.F. Reynolds, G.L. Cunningham, L.F. Huenneke, W.M. Jarrell, R.A. Virginia, and W.G. Whitford. 1990. Biological feedbacks in global desertification. Science 247:1043-1048.

Schoeneberger, P.J., D.A. Wysocki, E.C. Benham, and W.D. Broderson (eds.) 2002. Field book for describing and sampling soils, Version 2.0. NRCS National Soil Survey Center, Lincoln, NE.

Shafer, D.S., M.H. Young, S.F. Zitzer, T.G. Caldwell, and E.V. McDonald. 2007. Impacts of interrelated biotic and abiotic processes during the past 125,000 years of landscape evolution in the Northern Mojave Desert, Nevada, USA. J. Arid Environ. 69:633-657.

Sheskin, D. 2007. Handbook of parametric and nonparametric statistical procedures. Chapman and Hall, Boca Raton, FL.

Smith, J.L., and K. Lee. 2003. Soil as a source of dust and implications for human health. Adv. Agron. 80:1-32.

Soil Survey Division Staff. 1993. Soil Survey Manual. USDA, Washington, DC.

Soil Survey Staff. 2007. Soil Extent Mapping Tool [Online]. Available by USDA-NRCS <http://www.cei.psu.edu/soiltool/semtool.html> (verified 31 August 2010).

Soil Survey Staff. 2009a. Official Soil Series Descriptions [Online]. Available by USDA-NRCS <http://soils.usda.gov/technical/classification/osd/index.html> (verified 24 June 2009).

Soil Survey Staff. 2009b. National Soil Survey Characterization Data, Soil Survey Laboratory, National Soil Survey Center [Online]. Available by USDA-NRCS <http://ssldata.nrcs.usda.gov/querypage.asp> (verified 29 June 2009).

Springer, M.E. 1958. Desert pavement and vesicular layer of some soils of the desert of the Lahontan Basin, Nevada. Soil Sci. Soc. Am. Proc. 22:63-66.

Sullivan, L.A., and A.J. Koppi. 1991. Morphology and genesis of silt and clay coatings in the vesicular layer of a desert loam soil. Aust. J. Soil. Res. 29:579-586.

Ugolini, F.C., S. Hillier, G. Certini, and M.J. Wilson. 2008. The contribution of aeolian material to an Aridisol from southern Jordan as revealed by mineralogical analysis. J. Arid Environ. 72:1431-1447.

USDA-NRCS. 2006. Digital General Soil Map of U.S [Online]. Available by USDA-NRCS <http://SoilDataMart.nrcs.usda.gov> (verified 7 Nov. 2010).

USEPA. 2006a. Omernik's Level III ecoregions of the continental United States [Online]. Available by National Atlas of the United States <http://nationalatlas.gov/atlasftp.html> (verified 22 Aug. 2009).

USEPA. 2006b. Ecological regions of North America [Online]. Available by USEPA < http://www.epa.gov/wed/pages/ecoregions/na_eco.htm> (verified 9 Mar. 2011).

USGS, 1997. Distribution of Non-Polar Arid Lands [Online]. Available by USGS <http://pubs.usgs.gov/gip/deserts/what/world.html> (verified 25 Jan. 2011).

U.S. Regional Salinity Laboratory. 1954. Diagnosis and improvement of saline and alkali soils. Agricultural Handbook No. 60. USDA, Washington, DC.

Valentin, C. 1994. Surface sealing as affected by various rock fragment covers in West-Africa. Catena 23:87-97.

Valentine, G.A., and C.D. Harrington. 2006. Clast size controls and longevity of Pleistocene desert pavements at Lathrop Wells and Red Cone volcanoes, southern Nevada. Geology 34:533-536.

Wells, S.G., J.C. Dohrenwend, L.D. McFadden, B.D. Turrin, and K.D. Mahrer. 1985. Late Cenozoic landscape evolution on lava flow surfaces of the Cima volcanic field, Mojave Desert, California. Geol. Soc. Am. Bull. 96:1518-1529.

Wells, S.G., L.D. McFadden, J. Poths, and C.T. Olinger. 1995. Cosmogenic ^{3}He surface-exposure dating of stone pavements: Implications for landscape evolution in deserts. Geology 23:613-616.

Western Regional Climate Center. 2011. RAWS USA Climate Archive. Available by Desert Research Institute < http://www.raws.dri.edu/> (verified 10 Mar. 2011).

Williams, A., B. Buck, D. Soukup, and D. Merkler. 2010. Biological soil crusts and the fertile island effect: Soil-geomorphic insights from the Mojave Desert, USA. ASA-CSSA-SSSA International Annual Meetings, Long Beach, CA.

Wood, M.K., W.H. Blackburn, R.E. Eckert, and F.F. Peterson. 1978. Interrelations of physical-properties of coppice dune and vesicular dune interspace soils with grass seedling emergence. J. Range Manage. 31:189-192.

Wood, Y.A., R.C. Graham, and S.G. Wells. 2005. Surface control of desert pavement pedologic process and landscape function, Cima Volcanic field, Mojave Desert, California. Catena 59:205-230.

Yonovitz, M., and P.J. Drohan. 2009. Pore morphology characteristics of vesicular horizons in undisturbed and disturbed arid soils; implications for arid land management. Soil Use Manage. 25:293-302.

Young, M.H., E.V. McDonald, T.G. Caldwell, S.G. Benner, and D.G. Meadows. 2004. Hydraulic properties of a desert soil chronosequence in the Mojave Desert, USA. Vadose Zone J. 3:956-963.

3. DISTURBANCE AND RECOVERY OF VESICUALR HORIZON POROSITY AND HYDRAULIC PROPERTIES UNDER FIELD CONDITIONS

ABSTRACT

Vesicular horizons are common surficial horizons in desert regions that are critical to the regulation of infiltration and run-off processes. Their position near the soil surface makes the vesicular horizon susceptible to disturbance by human activities. This study was conducted to evaluate the recovery of vesicular horizons from disturbance at field areas with varied vesicular horizon characteristics and climatic conditions. At 15 field sites located across the Sonoran, Mojave, and central Great Basin deserts, vesicular horizons were artificially disturbed, and allowed to recover for one year. Morphologic properties of the vesicular horizons were described before disturbance (pre-disturbance), and again after the one-year recovery period (post-disturbance), and intact samples were collected for analysis of the pore shape, size, and quantity using X-ray computed tomography (CT). Infiltration rates were measured in the pre- and post-disturbance soils using a tension disk infiltrometer. In addition to the artificially disturbed soils, vesicular horizon morphology was also examined in tire tracks and coppice dunes. Our results show that vesicular horizon recovery from disturbance was incomplete after one year. Vesicles and related pore morphologies (*i.e.*, vughs and interconnected pores) were smaller in the post-disturbance soils, but similar in quantity (*i.e.*, number of pores per sample volume). The difference in recovery between the field areas was best explained by the amount of precipitation received during the recovery period. Based on the relationship between precipitation and vesicular horizon recovery from disturbance, we predict that a recovery period of two to 11 years is required for complete recovery of

vesicular horizon properties. Vesicular horizons in tire tracks were thinner, but the pore morphology in the CT scans was similar to that of the undisturbed soils. In the vesicular horizons buried by coppice dunes, the vesicles, vughs, and interconnected pores were collapsed, resulting in stronger expression of platy structure and smaller pore volumes. Infiltration rates generally decreased following disturbance. Average saturated hydraulic conductivity (K_{sat}) decreased from 0.42 cm hr^{-1} before disturbance to 0.27 cm hr^{-1}, following disturbance and recovery. Likewise, Gardner's α decreased from 0.11 before disturbance to 0.08 cm^{-1} following disturbance and recovery. However, the decrease in both properties (K_{sat} and α) were statistically insignificant. Through this study we have found that: 1) recovery of vesicular horizons from disturbance is dependent on the amount and frequency of precipitation, 2) vesicular pore morphology is substantially altered in vesicular horizons that are buried by coppice dunes but show less alteration in tire tracks, and 3) the disturbance of the vesicular horizon does not severely alter the hydraulic properties.

INTRODUCTION

Vesicular horizons are a widely occurring feature of soils in arid and semi-arid lands, with critical implications for the surface hydrology of the water-limited ecosystems in which they occur. Vesicular horizons occur at or near the soil surface and are characterized by the predominance of discontinuous, nearly spherical vesicular pores. They occur on every continent on Earth and cover large areas of land in arid and semi-arid parts regions (Turk and Graham, 2011). For example, vesicular horizons cover approximately 156,000 km^2 of the western United States (Turk and Graham, 2011) and

an estimated 94,000 km^2 of the Karoo region of South Africa (Ellis, 1990). Within the arid Basin and Range province of the western United States, vesicular horizons are best expressed in the cold deserts of the Central and Northern Basin and Range, compared to the warm deserts of the Mojave and Sonoran Basin and Range (Turk and Graham, 2011). In addition to the broad-scale trends that explain their global and regional distribution, vesicular horizons display a fine-scale heterogeneity. They occur extensively in the inter-canopy soils between shrubs, but are absent or weakly expressed beneath the shrub canopy (Wood et al., 1978; Shafer et al., 2007).

Variability of surface properties in arid soils leads to heterogeneous infiltration rates, which control runoff and run-on patterns (Abrahams and Parsons, 1991). Soils with vesicular horizons have much lower infiltration rates compared to non-vesicular soils of shrub islands, ephemeral washes, and young alluvial deposits (Turk and Graham, 2011). With increasing surface age, there is a reduction in infiltration rates of vesicular soils, which is not observed when the vesicular horizon is removed and infiltration is measured directly into the underlying horizon (Young et al., 2004) or when infiltration rates are measured in the non-vesicular soils in the shrub islands (Shafer et al., 2007). Negative correlations have been observed between the amount of vesicular porosity in the surface horizon and infiltration rates (Blackburn, 1975; Valentin, 1994; Lebedeva et al., 2009).

Soil development in desert landscapes generally leads to increased plant water stress and a shift towards more xerophytic vegetation communities. The development of fine-textured vesicular and argillic horizons causes water to be held closer to the soil

surface, where it is more rapidly lost to evaporation, compared to water stored deeper in the soil (Noy-Meir, 1973; McAuliffe, 1994; Smith et al., 1995; Hamerlynck et al., 2002; Shafer et al., 2007). Root restrictive petrocalcic horizons prevent the extraction of water from greater depths in the soil (McAuliffe, 1994; Smith et al., 1995; Stevenson et al., 2009). Additionally, restrictive surface layers (*i.e.*, desert pavement and vesicular horizons) favor runoff over leaching, which limits the plant water supply and leads to decreased leaching of salts and plant osmotic stress due to high soil salinity (Musick, 1975; Wood et al., 2005). With increasing soil development, vegetation becomes more restricted to shrub islands and ephemeral washes, where run-on accumulates (Noy-Meir, 1973; Musick, 1975; McAuliffe, 1994).

Because of their rapid formation, vesicular horizons have been called a "diagnostic feature" of desert pedogenesis and the corresponding shift towards a more arid ecosystem (Lebedeva et al., 2009). Desert shrub communities are favored by heterogeneity of soil resources, including water (Schlesinger, 1990). Expansion of vesicular horizons has been observed in association with degradation of rangelands in northern Nevada (Eckert et al., 1986a) and southern Africa (Henning and Kellner, 1994). Vesicular horizons present a challenge to rangeland restoration projects due to poor seedling establishment (Wood et al., 1978), and the effects of slaking and crusting (Wood et al., 1982) and polygonal cracking (Eckert et al., 1986b), on the success of typical seeding methods.

Vesicular horizons are usually one to 10 cm thick (Miller, 1971; Evenari et al., 1974; Wood et al., 1978; Peterson, 1980; Dan et al., 1982; Van Vliet-Lanoë, 1985; Amundson et al.,

1989; McDonald et al., 1995; Joeckel and Clement, 1999; Quade, 2001; Ugolini et al., 2008; Miller et al., 2009; Yonovitz and Drohan, 2009; Turk and Graham, 2011). The vesicular pores range from less than one to a few mm in diameter (Evenari et al., 1974; Joeckel and Clement, 1999; Anderson et al., 2002) and can be equant, oblate, or prolate in shape, with smooth walls (Brewer, 1976; Sullivan and Koppi, 1991; Stoops, 2003). Vesicular pores are typically largest in the upper few mm of the vesicular horizon and smaller with increased depth (Hugie and Passey, 1964; Bouza et al., 1993). Vesicular horizons may be massive or platy, or they may have a primary structure consisting of columns or prisms that part to a secondary platy structure (Springer, 1958; Peterson, 1980; McFadden et al., 1998; Anderson et al., 2002; Caldwell et al., 2006). The platy structure is formed by fissures interconnecting large vesicles along a horizontal plane, which creates a plane of weakness that can be ruptured under minimal pressure (Brewer, 1976; Figueira and Stoops, 1983; Anderson et al., 2002). In cold deserts, freeze-thaw processes may contribute to the formation of polygonal structure and frost lenses may be a factor in platy structure formation (Hugie and Passey, 1964). Vesicular horizons occur primarily in soils with silt loam, loam, and sandy loam textures (Springer, 1958; Peterson, 1980; Wood et al., 1982; McFadden et al., 1998; Turk and Graham, 2011). Vesicular horizons may occur in soils with a wide-range of chemical and mineralogical properties. They have been described in soils with smectitic clays (Ugolini et al., 2008), kaolinitic clays (Sullivan and Koppi, 1991), and mixed clay mineralogy (Amundson et al., 1989). They often contain calcium carbonate, but also occur in non-calcareous soils (Bunting, 1977; Bockheim, 2010; Turk and Graham, 2011). Vesicular horizons are most often non-saline

(0.8-2.3 dS m^{-1}), non-sodic (1-6% exchangeable Na), with slight to moderate alkalinity (pH 7.3-8.4), and low organic carbon content (0.4-1.3%) (Turk and Graham, 2011).

Vesicular pores are formed by the entrapment of air in soil during wetting events (Hugie and Passey, 1964; Miller, 1971; Figueira and Stoops, 1983; Stoops, 2003). Bubbles can be observed rising through the vesicular horizon when it is in the fluid, supersaturated condition (Hugie and Passy, 1964). As the soil dries and hardens, the bubbles get trapped, forming vesicular pores. Vesicular horizons occur in association with "sealed" surfaces, which impede the escape of entrapped air. Surfaces that produce an effective seal include embedded gravels (Evenari et al., 1974; Figueira and Stoops, 1983; Valentin, 1994), physical crusts (Hugie and Passey, 1964; Miller, 1971; Brewer, 1976; Evenari et al., 1974; Hillel, 1998; Cantón et al., 2003), and biological surface crusts (Evenari et al., 1974; Issa et al., 1999; Joeckel and Clement, 1999; Cantón et al., 2003; Williams et al., 2010). The entrapment of air and formation of vesicular pores is promoted by the absence of vegetation, silt-rich textures, and structural instability (Miller, 1971; Brewer, 1976; Ellis, 1990). Vegetation canopy cover reduces surface sealing through the dissipation of raindrop kinetic energy, and by promoting the activity of burrowing animals, which disrupt the surface crust (Abrahams and Parsons, 1991). Vesicular horizons often occur beneath desert pavement, a mosaic of interlocking rock fragments that occurs at the soil surface (Wood et al., 2002), formed by entrapment of dust beneath a monolayer of rock fragments (McFadden et al., 1987; Wells et al., 1995). The desert pavement stabilizes the soil surface, preventing erosion of the silt-rich eolian layer, in which a vesicular horizon typically forms. In the Mojave Desert, periods of high

eolian activity, caused by the drying of pluvial lakes during the Pleistocene-to-Holocene transition period, have been hypothesized as a cause of widespread vesicular horizon formation (McFadden et al., 1998; Anderson et al., 2002).

Vesicular pores can be considered a dynamic feature of the soil. Chronosquence studies show that the vesicular horizon is one of the first pedologic features to form in desert soils (Dan et al., 1982; Reheis et al., 1989; McDonald et al., 1995). Vesicular pores can be rapidly formed in the lab by subjecting crushed soil material to repeated wetting and drying cycles (Springer, 1958; Miller, 1971; Evenari et al., 1974; Figueira and Stoops, 1983). In the field, vesicular pores can reform in disturbed vesicular horizons in as little as three to four months (Yonovitz, 2008). Vesicular horizons are often observed in geomorphic settings characterized by active deposition and erosion. They have been observed beneath playa crusts that are subject to disintegration, wind erosion, and burial by water-born sediments (Paletskaya et al., 1958; Evenari et al., 1974). Vesicular pores have been observed beneath biological and physical surface crusts in semi-arid badlands, where soil development is generally limited by high erosion rates (Cantón et al., 2003). Thin, patchy vesicular horizons (1-5 mm thick) have been observed on recent alluvial deposits (<100 yr old) (Gile and Hawley, 1968), and 1-cm thick vesicular horizons have been observed on alluvial surfaces with evidence of active transport (Peterson, 1980). In Arctic soils, transient vesicular layers are observed, which form in a thin layer of silt deposited by snowmelt and then erode in response to rainfall (Bunting, 1977). Vesicular pores have also been observed in sediments resulting from human modification of the landscape, including sediments infilling irrigation furrows

(Miller, 1971; Eckert et al. 1978) and sediments infilling tire tracks (Gile and Hawley, 1968).

In certain geomorphic settings, however, vesicular pores can be a stable feature that develops with soil age. In particular, surfaces with desert pavement may be stable for long periods of time. Desert pavement-mantled surfaces exceeding one million yrs old have been observed in the Negev Desert in Israel (Matmon et al., 2009) and in the dry valleys of Antarctica (Bockheim, 2010). In a chronosequence of alluvial fan deposits with desert pavement in the Mojave Desert, the thickness and vesicular porosity of the vesicular horizon increases with age in soils ranging up to 70,000 yrs old (McDonald et al., 1995; Turk and Graham, 2011). In vesicular horizons formed in such stable settings, clay, fine silt, and carbonate coatings lining the vesicular pores may reinforce them against collapse (Sullivan and Koppi, 1991; McFadden et al., 1998; Anderson et al., 2002). As many as 12 discrete layers have been observed within these coatings, suggesting the stability of the pores over successive wetting events (Sullivan and Koppi, 1991). In laboratory studies, the size of the vesicular pores increases with increasing number of wetting and drying cycles, indicating that the pores develop over successive wetting events (Miller, 1971; Figueira and Stoops, 1983), rather than being destroyed and reformed with each wetting event, as some observers have suggested (Springer, 1958; Hugie and Passey, 1964).

Desert lands in the western United States are subject to many forms of anthropogenic disturbance, including off-highway vehicle use, grazing, agriculture, urbanization, roads and utility corridors, and military training exercises (Lovich and

Bainbridge, 1999). In addition to existing activities that disturb desert lands, interest in developing the solar and wind power resources of deserts is bringing increasing human activity to desert lands. Currently, 73,000 km^2 of desert lands are under review for use in solar power generation (Associated Press, 2010). Disturbance of desert soils leads to the destruction of surface features that stabilize the soil, including biological surface crusts, physical crusts, and desert pavements (Lovich and Bainbridge, 1999). Off-highway vehicle use on vesicular soils leads to increased sediment loss with runoff (Eckert et al., 1978) and high rates of dust mobilization (Goossens and Buck, 2009). Disturbance of desert lands by military tracked vehicles leads to increase soil bulk density, increased penetration resistance, loss of fine particles, and loss of structure and macroporosity (Caldwell et al., 2006). Track scars on desert pavement are long-lasting features, which are still visible 60 years after abandonment of training grounds (Gilewitch, 2004).

Vesicular horizons associated with desert pavements are also subject to disturbance and recovery due to vegetation advances and contractions associated with climatic change. The most recent climatic transition from the Pleistocene pluvial climate to the drier Holocene climate is thought to have caused a decrease in vegetation cover throughout the lower elevations of the Basin and Range province (Harvey et al., 1999). Based on these past climatic conditions and associated changes in vegetation cover, it has been argued that desert pavements above 400 m elevation in the Mojave Desert cannot be older than latest Pleistocene in age (Quade, 2001). Others have found evidence suggesting that the desert pavements were not disrupted by past vegetation advances (Valentine and Harrington, 2006) or recovered rapidly following disturbance (Pelletier et

al., 2007). Reformation of desert pavement has been observed in plant scars left by past vegetation contractions, however, associated vesicular horizons are thinner and have a coarser texture than vesicular horizons beneath the surrounding desert pavement (McAuliffe and McDonald, 2006).

This study examined the changes in vesicular horizon morphology and hydraulic properties that occur with disturbance and recovery of the soil surface. Our objectives were to: 1) evaluate the recovery of vesicular horizon morphology over one year in artificially disturbed soils and determine the factors that influence their recovery, 2) analyze the impact of disturbance on vesicular horizon morphology and porosity in previously disturbed locations (*i.e.*, tire tracks and coppice dunes), and 3) determine the influence of disturbance on the hydraulic properties of the vesicular horizons.

MATERIALS AND METHODS

Field methods

Field studies were conducted over a two-year period. In the first year, three study plots were established at each site, all containing vesicular horizons and an overlying desert pavement layer. The study plots were approximately 0.3 by 0.3 m in size and located one to 30 m apart from each other, in places where the desert pavement displayed a similar clast cover and size distribution. In each plot, infiltration rates were measured using a 20 cm diam. tension disk infiltrometer. The desert pavement layer was carefully removed and contact sand was placed at the soil surface, so that continuous contact could be achieved between the tension disk and the soil. Steady-state infiltration rates were

recorded at four tensions (-1.2, -0.9, -0.6, and -0.3 kPa) and soil temperature was recorded following the completion of the infiltration measurements.

After infiltration measurement, the plots were allowed to dry for several days, so that they could be excavated without disrupting the vesicular horizon structure and porosity. One intact sample was extracted from each plot. In most cases, the vesicular horizon had a moderate to strong columnar structure and the intact sample consisted of one columnar ped. After this sample was collected, each plot was artificially disturbed in a manner that destroyed all vesicular porosity. First, the desert pavement clasts were removed and set aside. Then, the soil was excavated through the depth of the vesicular horizon. The vesicular horizon thickness, structure (size, grade, and shape), and porosity (abundance, size, and type) were recorded for each excavation according to standard methods and terminology (Schoeneberger et al., 2002). The excavated material was homogenized by crushing and passing through a 2-mm-mesh sieve and a small sample of the soil material was collected for laboratory analysis. After sieving, gravels were mixed back in with the <2-mm fraction and the excavation was refilled, followed by replacement of desert pavement clasts at the surface. The locations of the study plots were marked in the field and recorded in sketches of the field sites. After disturbance, one full year was allowed for recovery before the study plots were analyzed again. In the second year of the study, the original plots were located and the same procedures were followed for infiltration measurement, collection of an intact sample, and field description, as described above. Study plots at the sites in California and Arizona were

disturbed in June of 2010 and analyzed again in June of 2011, while study plots at the sites in Nevada were disturbed in August of 2010 and analyzed again in August of 2011.

In addition to the analysis of vesicular horizon recovery from disturbance in the study plots, vesicular horizons in disturbed parts of the landscape were observed and sampled. These included tire tracks on the desert pavement (Fig. 3.1a) and vesicular horizons that had been buried beneath coppice dunes (Fig. 3.1b). Based on observation of aerial imagery from Google Earth (Google Incorporated, 2011), the age of the tire tracks ranged from <4 to >15 yrs (Table 3.1). In coppice dune soils, the vesicular horizons occurred at the same microtopographical elevation as the vesicular horizons beneath the surrounding desert pavement, but were buried beneath five to 12 cm of loose sand. This is an indication that these vesicular horizons formed beneath the desert pavement and were subsequently buried by the coppice dune.

Soil and vegetation at each of the sites were characterized by standard methods. Hand-dug pits (0.5-1 m deep) were excavated to describe subsurface soil properties (Schoeneberger et al., 2002), which were used to classify the soils according to U.S. Soil Taxonomy (Soil Survey Staff, 2010). Shrub cover data were collected by the line-transect method (Barbour et al., 1999).

Study sites

Fifteen field sites were selected, including five sites within each of three ecological zones: the Sonoran Desert, the Mojave Desert, and the central Great Basin (Fig. 3.2). The Sonoran Desert sites were all within the western part of the Desert, also

Fig. 3.1. Examples of pre-existing disturbance features sampled during field work: (a) prominent tire tracks on desert pavement and (b) vesicular horizons buried beneath coppice dunes (scale in cm).

Table 3.1. Age of tire tracks based on visibility in aerial imagery[†]

Site	Age of tire tracks yrs	Evidence
S1	>5	Visible in 2006
S2	>6	Visible in 2005
S4	>15	Visible in 1996
S5	<4	Not visible in 2007
M2	<5	Not visible in 2006
M3	>1	Visible in 2010

[†]Aerial imagery from Google Earth (Google Incorporated, 2011)

Fig. 3.2. Location of field sites (S1-S5, M1-M5, and G1-G5) in relation to three ecological zones of the Basin and Range Province (Sonoran, Mojave, and central Great Basin).

referred to as the Colorado Desert. All sites were located on alluvial fan surfaces with desert pavement.

The elevation of the sites ranged from 231 to 457 m in the Sonoran Desert, 574 to 1048 m in the Mojave Desert, and 1426 to 1626 in the central Great Basin (Table 3.2). The vegetation consisted of creosotebush-bursage scrub communities at the Sonoran and Mojave Desert sites and saltbush-greasewood scrub communities at the central Great Basin sites (see Appendix A). The shrub cover at the sites varied between 1.8 and 7.3% in the Sonoran Desert, 8.3 and 18.8% in the Mojave Desert, and 9.4 to 19.2% in the central Great Basin (Table 3.2). The lithology of the desert pavements varied among the sites, and included pavements formed from volcanic, gneissic, limestone, sandstone, and mixed alluviums (Table 3.2, Appendix A). The soils at the sites were classified as either Aridisols or Entisols (Table 3.2, Appendix A). The vesicular horizon textures varied among the sites, but were most often loam or silt loam textures (Table 3.2).

Three sites within each ecological zone had an active weather station nearby (Table 3.3). Most of the weather stations were at elevations close to the field areas (within 50 m), with the exception of the Middlegate-Clifford weather station, which was 146 m higher than the G5 field area, and the Mountain Pass 1se weather station, which was 411 m higher than the M4 field area. For the M4 field area, adjustments for elevation were made, in order to get a better estimation of mean annual temperature (MAT) and mean annual precipitation (MAP). To estimate MAT a linear interpolation was made between the Mountain Pass 1se weather station and a lower elevation weather station located in Baker, CA (293 m). To account for the effect of elevation on MAP, the

Table 3.2. List of field areas and their characteristics.

Site	Elevation	Shrub Cover	Pavement Lithology	Soil Great Group[†]	Vesicular horizon texture[‡]
	m	%			
S1	457	7.3	Gneiss	Petrocalcids	l
S2	231	1.8	Mixed	Haplocambids	sil
S3	280	6.4	Mixed Volcanic	Torriorthents	l
S4	273	2.4	Mixed	Haplargids	sil
S5	431	2.2	Mixed	Haplocalcids	l
M1	875	18.8	Mixed	Haplocalcids	l
M2	1061	12.4	Mixed	Haplosalids	l
M3	574	8.3	Mixed Volcanic	Haplocambids	l
M4	1048	15.5	Limestone	Petrocalcids	scl
M5	863	16.6	Quartzitic Sandstone	Haplargids	sil
G1	1561	12.9	Mixed Volcanic	Haplocambids	lfs
G2	1512	12.3	Mixed Volcanic	Torriorthents	l
G3	1626	14.7	Mixed Volcanic	Haplocambids	cl
G4	1429	19.2	Mixed Volcanic	Haplargids	sil
G5	1246	9.4	Rhyolite	Haplosalids	l

[†]Soil field descriptions and laboratory data located in Appendix A, except for the soils at sites M1, which was classified based on the field description and laboratory data in Strathouse (1982) and M4, which was classified based on the field description by N. Pietrasiak (personal communication).

[‡]Field-determined textures (abbreviations: cl = clay loam, l = loam, lfs = loamy fine sand, scl = sandy clay loam, sil = silt loam).

Table 3.3. List of weather stations (WS) nearest to the field sites, their location relative to field areas, mean annual temperature (MAT), and mean annual precipitation (MAP).

Site	Weather station	Distance[†]	Elevation		MAT	MAP	Record length	Source[‡]
			WS	Site				
		km	m	m	°C	cm	yr	
S1	Hayfield	11 NE	429	457	20.8	11.4	77	NCDC
S2	Desert Center 2 NNE	17 NE	228	231	22.8	7.9	6	NCDC
S4	Quartzsite	3 SW	267	273	22.7	8.9	80	NCDC
M1	El Mirage	15 S	878	875	16.5	10.8	14	RAWS
M4	Mountain Pass 1se	15 SE	1459	1048	17.0[§]	14.5[¶]	4	NCDC
M5	Pahrump	21 SE	815	863	16.6	13.2	52	NCDC
G3	Tonopah	19 NE	1709	1626	11	14.8	65	NCDC
G4	Mina Airport	1 NE	1392	1429	12.7	15.4	62	NCDC
G5	Middlegate-Clifford	17 SE	1392	1246	9.4	13.0	22	NCDC

[†]Distance and direction of weather station from field area

[‡]NCDC = National Climate Data Center (Fenimore, 2011), RAWS = Remote automatic weather stations (Western Regional Climate Cent., 2011)

[§]Adjusted for elevation difference between weather station and site by linear interpolation between Mountain Pass 1se station and Baker NCDC station, located at 293 m elevation.

[¶]Adjusted for elevation difference between weather station and site using the logarithmic relationship between precipitation and elevation established by French (1983) for southern Nevada.

expected difference in precipitation between the weather station and the field area was calculated according to the logarithmic relationship between elevation and precipitation, previously established for the southern Nevada region (French, 1983). This difference in precipitation (3.7 cm) was subtracted from MAP recorded at the Mountain Pass 1se weather station, in order to represent the lower precipitation expected at lower elevation. Mean annual temperatures recorded by the weather stations ranged from 20.8 to 22.8^{o}C in the Sonoran Desert, 16.5 to 17.0^{o}C in the Mojave Desert, and 9.4 to 12.7^{o}C in the central Great Basin (Table 3.3). Mean annual precipitation ranged from 7.9 to 11.4 mm in the Sonoran Desert, 10.8 to 14.5 cm in the Mojave Desert, and 13.0 to 15.4 cm in the central Great Basin (Table 3.3).

Laboratory methods

Bulk samples of the vesicular horizons collected from each of the study plots were analyzed for particle-size distribution, pH, $CaCO_3$ percentage, electrical conductivity (EC), and exchangeable Na percentage (ESP). For samples below the vesicular horizon, $CaCO_3$ was measured if pedogenic carbonates were detected in the field, and EC and gypsum were measured if soluble salts were visible. Particle-size distribution was determined by the wet-sieving/laser-diffraction method (Segal et al., 2009). Soil pH was measured in a 1:1 soil:water suspension (Burt, 2004). Calcium carbonate was measured by the manometer method (Williams, 1948). Electrical conductivity was measured in saturation paste extracts (Burt, 2004). Exchangeable sodium was extracted with ammonium acetate and measured by inductively coupled

plasma (ICP) spectroscopy (Thomas, 1982). Cation exchange capacity (CEC) was determined by Na-saturation followed by ammonium acetate extraction and measurement of displaced Na by ICP spectroscopy (Bower and Hatcher, 1966). Soluble Na in saturation paste extracts was measured using a Na-selective electrode and exchangeable Na measurements were corrected for soluble sodium in the ESP calculation (Burt, 2004). Gypsum was measured by the acetone precipitation method (Burt, 2004)

Intact samples were analyzed by X-ray computed tomography (CT). One pre-disturbance and one post-disturbance sample from most of the field sites was CT-scanned, as well as a total of four samples collected from tire tracks and four samples of vesicular horizons buried beneath coppice dunes. Pre-and post-disturbance samples from site S3, and the post-disturbance sample from site S5, were not included in the CT analysis because the samples were too fragile to ship to the CT scanning facility. Scanning was performed with an inter-slice spacing of 0.08118 mm, and a resolution of 0.0752 mm per pixel.

Data analysis

Vesicular horizon index.

Vesicular horizon expression, according to the field descriptions, was quantified using the vesicular horizon index (VHI) (Turk and Graham, 2011). The VHI takes into account the horizon thickness, as well as vesicular pore size and quantity class. A vesicular pore term (X_{ve}) is calculated by summing values assigned to the size and quantity classes. The term is rescaled (0-1) by dividing by 220, which is the maximum

observed value of the term. Finally, the rescaled term is multiplied by the horizon thickness (in cm) to calculate the VHI.

The VHI of pre-disturbance soils was compared with the post-disturbance soils after one year of recovery. The statistical difference between pre-and post-disturbance VHI was evaluated using non-parametric analysis because the distribution of VHI is non-normal (Turk and Graham, 2011). At the field sites with nearby weather stations (Table 3.3), the influence of precipitation on recovery of vesicular horizons was evaluated by regression of VHI versus precipitation. This analysis was performed with precipitation expressed as depth, and also as events. Precipitation events were defined as more than five mm of precipitation occurring over consecutive days, separated by a drying period that varies by season (Jun.-Aug. = 1 d, Sept.-Nov. and Mar.-May = 3 d, Dec.-Feb. = 5 d) (Turk and Graham, 2011). The depth of water applied during infiltration measurement was included in the total precipitation depth during the year of recovery, and was also counted as one precipitation event. At site M4, the adjustment for elevation used to calculate MAP (Table 3.3) was also used to estimate the precipitation during the recovery period. However, no adjustment was made to precipitation expressed as events, since the relationship with elevation is unknown.

CT analysis

Images generated from the CT scans were analyzed using the Blob3D software (Ketcham et al., 2005). First the scans were cropped to a cylindrically- shaped volume of interest (VOI) (Brun et al., 2010). The VOIs were 20 to 40 mm in diam., depending on

the sample size, and oriented so that the z-axis corresponded to depth. The VOIs were 15 mm in height and extracted as close to the top surface of the sample as possible. This top zone of the vesicular horizon was selected for analysis because the vesicular pores were largest and most numerous near the surface.

Voids were segregated from the sample matrix using a general threshold filter, which was adjusted until the resulting binary image agreed well with visual segregation of voids in the grayscale image. Gravels were segregated using a general threshold/majority filter, to detect homogeneity of voxels within the grayscale value range of the gravels. Methods for characterization of pore geometry were developed based on the observation of 838 pores in one CT scan of an undisturbed vesicular horizon (from site G2). Each of these pores was classified as a vesicle, vugh, or interconnected pore network based on visual interpretation (Fig. 3.3). Vesicles are smooth, rounded pores, which are non-interconnected and may be equant, prolate, or oblate in shape (Brewer, 1976; Stoops, 2003). Vughs are large, irregular voids, which are usually non-oriented and have a random distribution, when vughs are numerous and highly-irregular, they may become interconnected (Brewer, 1976). The voids that we distinguished as interconnected pore networks consisted of interconnected vugh-like pores. Interstitial pores were not observable at the resolution of the CT scans and therefore were not included in our analysis. Volume and surface area were recorded for each pore and used to calculate a volumetric form of the two-dimensional lobation ratio (LR), a term previously used to characterize pore geometry in thin sections (Beckman, 1962; Figueira and Stoops, 1983). The two-dimensional LR is the ratio between the calculated perimeter

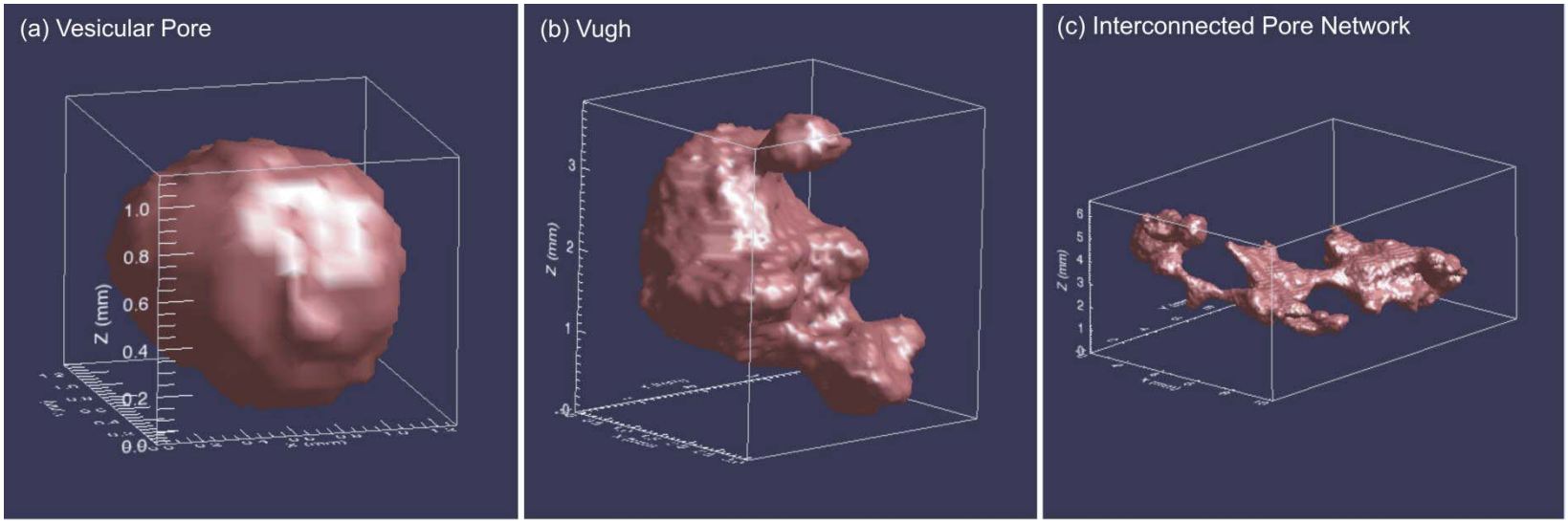

Fig. 3.3. Examples of the pore types classified according to visual observation: (a) vesicles, (b) vughs, and (c) interconnected pore networks. Three-dimensional images were generated using the Blob3D software (Ketcham, 2005).

and the actual perimeter of the pore, where the calculated perimeter is the perimeter of a hypothetical circle with an area equal to the measured pore area. A perfect circle will have a LR of one, while lower values indicate a less circular shape. The volumetric form of the LR (LR_v), introduced here, is the ratio between the calculated surface area and the actual surface area, where calculated surface area is the surface area of a hypothetical sphere with a volume equal to that of the measured pore volume. This formula can be simplified to:

$$LR_v = \frac{4.836V^{(2/3)}}{S} \qquad \text{(eq. 3.1)}$$

where, V = volume and S = surface area. The derivation of this equation is outlined in Appendix B. As with the two-dimensional LR, an LR_v of one indicates a perfect sphere, while a lower LR_v indicates a less spherical shape.

Significant differences in LR_v were observed between the visually-classified pore shapes (*i.e.*, vesicles, vughs, and interconnected pores) (Fig. 3.4a). LR_v was highest for the vesicles (median LR_v = 0.84), intermediate for the vughs (median LR_v = 0.73), and lowest for the interconnected pore networks (median LR_v = 0.40). Based on this analysis, LR_v cut-offs were established, so that the pore types could be classified using data extracted from the CT scans (*i.e.*, pore volume and surface area), without visual observation of each individual pore. The cut-offs were set at LR_v = 0.79, for distinguishing vesicles from vughs, and LR_v = 0.56, for distinguishing vughs from interconnected pores. Previous work using thin sections established a similar cut-off (LR = 0.75) to distinguish vesicles from vughs (Figueira and Stoops, 1983). The interconnected pore networks distinguished by LR_v were most often oriented with their

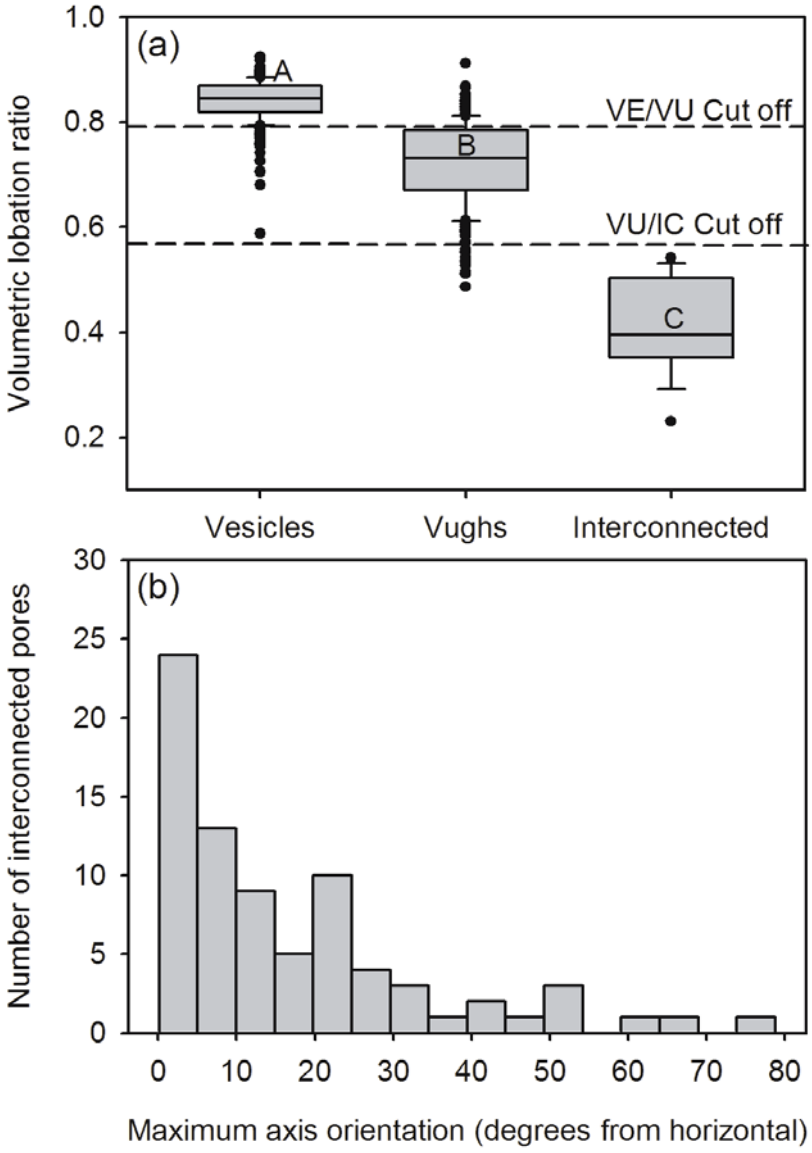

Fig. 3.4. Numerical characterization of visually-classified pore types: (a) box plot of volumetric lobation ratio for each pore type, (b) histogram showing the orientation of interconnected pore networks. In the box plots, boxes depict the upper and lower quartiles, center bars depict the median values, whiskers depict extreme values (within a distance from the box of 1.5 times the interquartile range), and points indicate outliers (outside a distance from the box of 1.5 times the interquartile range). Boxes in (a) labeled with different letters are significantly different, at the α (per family) = 0.05 level, according the Mann-Whitney test, using the Bonferroni correction for multiple comparisons. Dashed lines in (a) represent the cut-offs established for the separation of vesicles from vughs (VE/VU), and vughs from interconnected pores (VU/IC).

maximum axis close to the horizontal axis of the sample (Fig. 3.4b). This orientation suggests that the interconnected pore networks consist of horizontally interconnected vughs (*e.g.*, Fig. 3.3c). Similar pore networks have been previously observed in vesicular horizons and linked to the formation of lateral fractures between platy structural units (Figueira and Stoops, 1983). The LR_v is affected by elongation as well as regularity of the shape, therefore some prolate and oblate pores, which might otherwise be described as vesicles (Brewer, 1976), will be classified as vughs here. Based on the cut-off at LR_v = 0.79, prolate and oblate pores with aspect ratios exceeding 3:1 will be classified as vughs, rather than vesicles. This potential misclassification is unlikely to have a major effect on our results, however, since we focus on the upper part of the vesicular horizons (0-15 mm), in which the vesicles typically have the most equant shape (Bouza et al., 1993).

In the remaining samples, data were extracted for all voids with a volume greater than 0.0028 mm^3 (6 voxels). The values extracted for each void included volume, surface area, and side contact (*i.e.*, whether or not the pores contacted the edge of the VOI). The LR_v was calculated for each void and used to classify the voids as vesicles, vughs, or interconnected pores. For each pore type, the percentage of gravel-free volume occupied by pores ($V_{\%}$), number density of pores (N_p, in cm^{-3}), and geometric mean of pore volume ($\overline{V}$, in mm^3) were calculated using the following equations.

$$V_{\%} = \frac{\sum_{p=1}^{n} V_p}{\pi r^2 h - \sum_{g=1}^{m} V_g} \times 100 \qquad \text{(eq. 3.2)}$$

$$N_p = \frac{n}{\pi r^2 h - \sum_{g=1}^{m} V_g} \times 1000 \qquad \text{(eq. 3.3)}$$

$$\overline{V} = \left(\prod_{p0=1}^{k} V_{po} \right)^{\frac{1}{k}} \qquad \text{(eq. 3.4)}$$

In eq. 3.2 and eq. 3.3, $p_{1\ldots n}$ is the set of all pores of the designated class (*i.e.*, vesicles, vughs, or interconnected pores) within the VOI, n = the number of pores, V_p = the volume of pore p (in mm^3), $g_{1\ldots m}$ is the set of all gravels within the VOI, m = the number of gravels, V_g = the volume of gravel g (in mm^3), r = radius of the VOI (in mm), and h = height of the VOI (in mm). In eq. 3.4, $p0_{1\ldots k}$ is the set of all pores of the designated class (*i.e.*, vesicles, vughs, or interconnected pores) within the VOI that are not in contact with the VOI edge (*i.e.*, side contact = 0), k = the number of pores with no side contact, and V_{p0} = the volume of pore p0 (in mm^3).

The relationship between pore morphology and desert ecological zones was analyzed in the pre-disturbance soils, using statistical analysis by one-way ANOVA and Tukey's test. The effect of disturbance on vesicular horizons was analyzed by comparing: 1) porosity of pre-and post-disturbance samples from the study plots, 2) porosity of tire tracks relative to undisturbed desert pavement, and 3) porosity of vesicular horizons buried by coppice dunes relative to the unburied vesicular horizons. In each case, the statistical difference of all measured values (*i.e.*, $V_{\%}$, N_p, and $\overline{V}$) for each pore type (*i.e.*, vesicles, vughs, and interconnected pores) were determined using a paired t-test (paired by field site). Pairs from four study sites were included in the analysis of tire tracks (S4, S5, M2, and M3) and coppice dunes (G2, G3, G4, and G5). All statistical analyses were performed in MINITAB 16 (Minitab, 2010).

Infiltration

The relationship between steady-state infiltration rates at the four different tensions was used to calculate saturated hydraulic conductivity (K_{sat}) and Gardner's α (Gardner, 1958), by fitting the data to the Wooding's equation (Wooding, 1968; Young et al., 2004):

$$q(h) = K_{sat}\exp(\alpha h)\left(1 + \frac{4}{\pi r \alpha}\right) \qquad \text{(eq. 3.5)}$$

where q(h) is the steady-state infiltration rate (cm s^{-1}), α is a parameter related to pore-size distribution (cm^{-1}) (Gardner, 1958), h is the tension (cm), and r is the radius of the infiltrometer plate. The K_{sat} data was temperature-corrected to 20°C (Young et al., 2004) and log-normalized for statistical analyses (Young et al., 2004, Caldwell et al., 2006; Shafer et al., 2007). The geometric mean of K_{sat} for the three study plots at each site before disturbance was compared with the geometric mean of K_{sat} for the three study plots measured one year following disturbance, using a paired t-test. Pre- and Post-disturbance α were compared using the Mann-Whitney test, since these data were not normally distributed. In a few cases, the infiltration data for a plot did not fit well with the Wooding's equation ($p > 0.10$), in these cases, the data from that study plot were not used in the calculation of K_{sat} and α for the site. Non-linear regression analysis, used to fit the data to the Wooding's equation was performed by a user-defined regression equation in SigmaPlot 10 (Systat Software, 2007), and other statistical analyses were performed in MINITAB 16 (Minitab, 2010).

RESULTS AND DISCUSSION

Pore morphology of pre-disturbance vesicular horizons

The results of CT analysis show that the pore morphology of the vesicular horizons varies between sites grouped by desert, including the Great Basin, Mojave, and Sonoran Deserts (Fig. 3.5). Vesicles and vughs occupy a higher percentage of the sample volume in the Great Basin vesicular horizons relative to the Mojave Desert samples, and occupy the lowest percentage of sample volume in the Sonoran Desert (Fig. 3.5a). The number density of vesicles and vughs, however, is highest in the Sonoran Desert (Fig. 3.5b), which is in agreement with previous studies showing that smaller vesicular pores occur in greater numbers (Figueira and Stoops, 1983). The average volumes of vesicles and vughs are larger in the Great Basin than in the Mojave Desert, and smallest in the Sonoran Desert (Fig. 3.5c,d). Statistical analysis of these results shows that most of the differences between the deserts are not significant at the $\alpha = 0.05$ level, but the p-values range from 0.03 to 0.14, which suggests that the differences would be significant with slightly larger sample size.

These results are in agreement with previous analysis of vesicular horizon expression between the deserts of the Basin and Range Province, in which the VHI was applied to quantify vesicular horizon expression in field descriptions from the NRCS soil databases (Turk and Graham, 2011). In the previous study the vesicular porosity was quantified based on visual analysis in the field. Using the soil databases allowed for a very large sample size, including 1387 soil descriptions, but introduces additional variability related to the precision of visual estimations of porosity made by different observers. In the current study, CT analysis was used to collect data on the shape, size, and number of pores in the samples. While this approach allows better quantification and consistency of technique, a much smaller sample size was used, including only 14 samples. However, even with these different sources of uncertainty, both

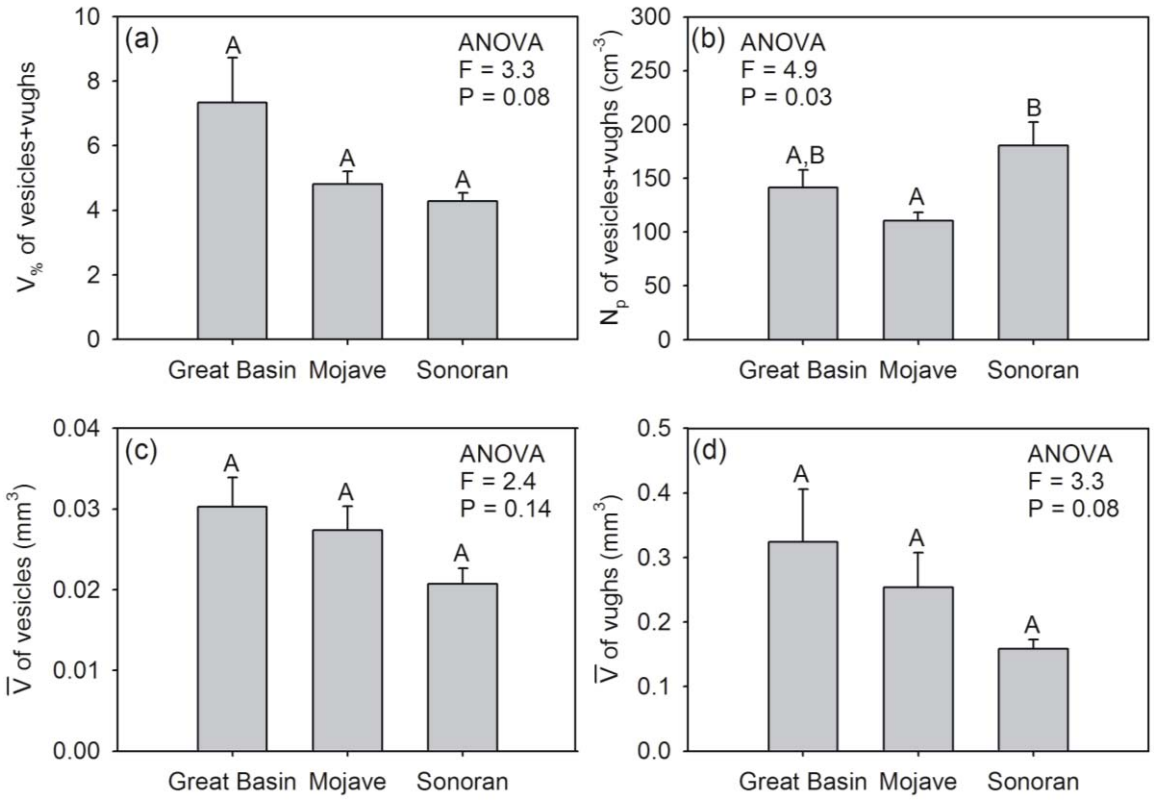

Fig. 3.5. Computed tomography analysis of vesicular pores and vughs in pre-disturbance vesicular horizons grouped by desert: (a) percentage of gravel-free volume occupied by vesicles and vughs ($V_{\%}$), (b) number density of vesicles and vughs (N_p), (c) geometric mean volume ($\overline{V}$) for vesicles, and (d) geometric mean volume for vughs.

studies show the same general trend, which is better expression of vesicular horizons in the cold desert (*i.e.,* the Great Basin), relative to the warm deserts (*i.e.*, the Mojave and Sonoran Deserts). Two possible reasons for this trend were discussed by Turk and Graham (2011): 1) more extensive sources of eolian dust due to the drying of large pluvial lakes in the Great Basin, and 2) more frequent precipitation events in the cold deserts relative to the warm deserts.

Recovery of vesicular horizons following disturbance

Vesicular pores formed in all of the study plots within one year following disturbance. However, the post-disturbance vesicular horizons were weakly developed compared to the pre-disturbance vesicular horizons (Fig. 3.6). The pre-disturbance vesicular horizons displayed moderate to strong columnar structure, often parting to moderate to strong platy structure. In contrast, the vesicular horizons formed following disturbance had weak prismatic or massive structure. The pre-disturbance vesicular pores were very fine to medium in size (<1 to 5 mm diam.) and occurred in a layer that was 1 to 8 cm thick; while the reformed vesicular pores were very fine to fine in size (<1 to 2 mm diam.) and occurred in a thin layer, ranging from 0.3 to 3 cm thick. In pre-disturbance soils, the vesicular pores were often observed to be largest near the soil surface and the large pores tended to be more irregular in shape. Vesicular horizon morphology was quantified according to the VHI and a statistically significant reduction in VHI was observed in the post-disturbance soils relative to the pre-disturbance soils, according to the Mann-Whitney test ($p < 0.0001$) (Fig. 3.7).

A previous study of vesicular horizon disturbance at the Lake Mead National Recreation Area (LMNRA) also demonstrated the reformation of vesicular pores within

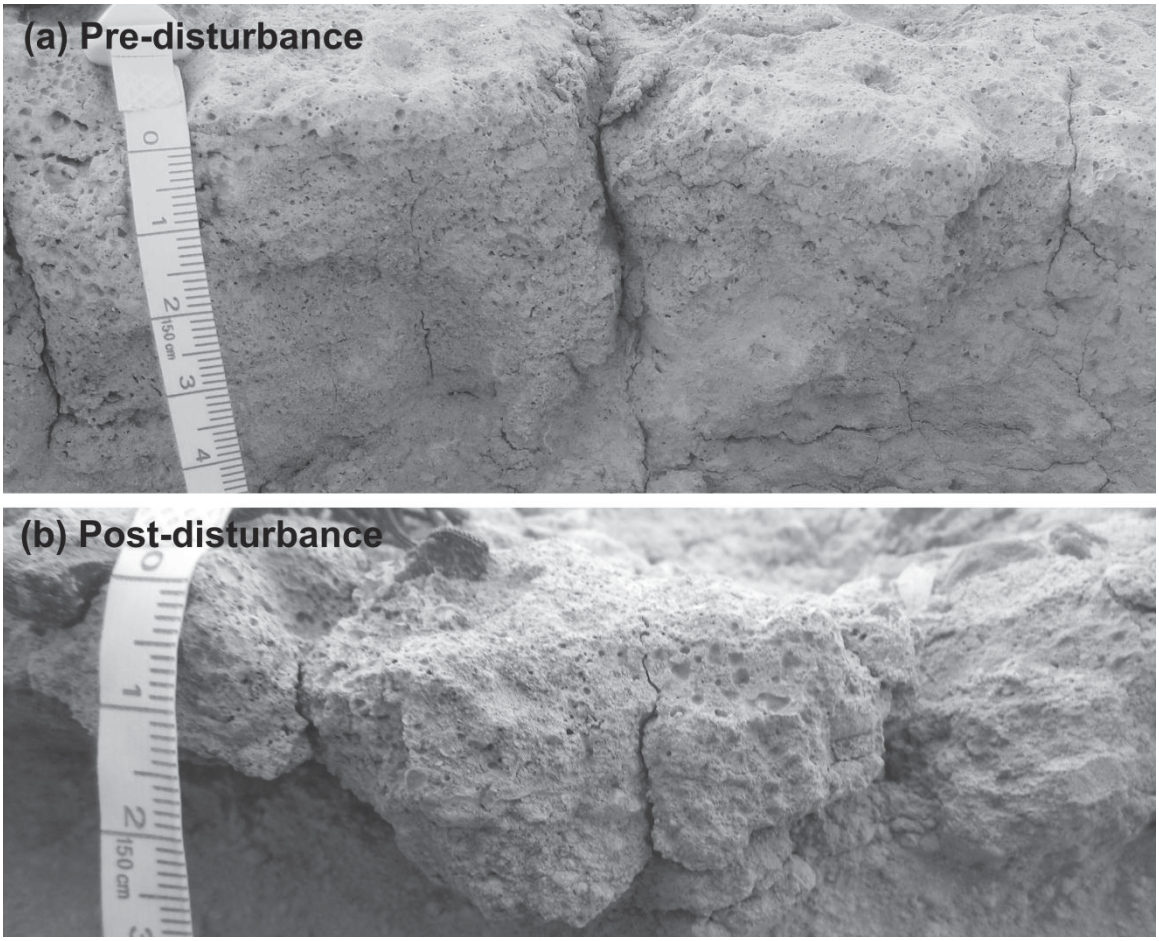

Fig. 3.6. Examples of vesicular horizons before and after disturbance: (a) pre-disturbance vesicular horizon, (b) post-disturbance vesicular horizon formed during the one year recovery period. Both photos are from site S4 (Quartzsite, AZ). Scales are in cm.

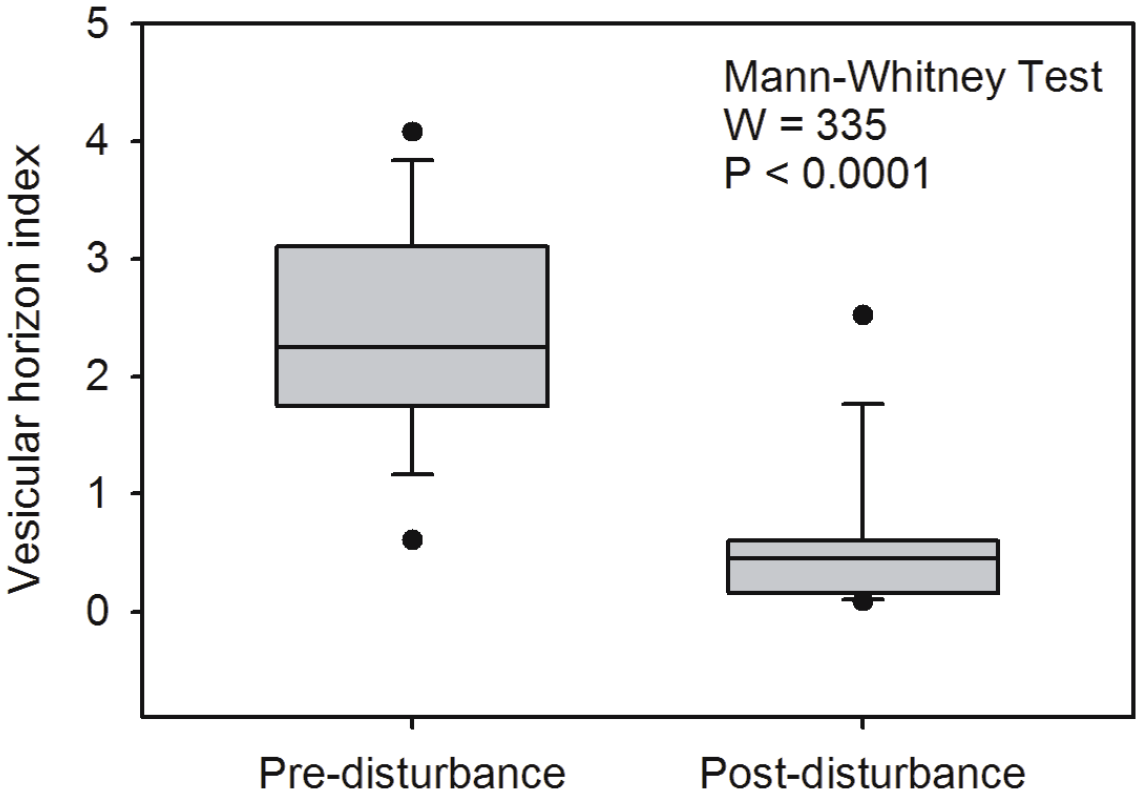

Fig. 3.7. Box plots of vesicular horizon index for pre-and post-disturbance vesicular horizons. Post-disturbance soils were analyzed following the one-year recovery period. Boxes depict the upper and lower quartiles, center bars depict the median values, whiskers depict extreme values (within a distance from the box of 1.5 times the interquartile range), and points indicate outliers (outside a distance from the box of 1.5 times the interquartile range).

one year following disturbance (Yonovitz and Drohan, 2009). In this study, platy structure was observed to reform following disturbance, which we did not observe in our study plots. At LMNRA, moderate platy structure was observed in undisturbed soils and weak platy structure was observed in the vesicular horizons that reformed following disturbance. The range of vesicular horizon thickness observed following disturbance at LMNRA (0.3-3 cm) was the same as the range of vesicular horizon thickness observed in the post-disturbance soils in our study. However, in the study at LMNRA the size of the vesicular pores was observed to be unaltered by disturbance; in contrast, we found that the largest pores (2-5 mm) did not reform within a year following disturbance.

The difference between the pre-and post-disturbance vesicular horizons was observed in more detail using data from the CT scans. The decreased vesicular horizon thickness and pore size is apparent in slices from pre- and post-disturbance scans (Fig. 3.8). Following disturbance, vesicles, vughs, and interconnected pores in the upper 15 mm occupy less of the sample volume relative to the pre-disturbance soils (Fig. 3.9a, 3.10a, 3.11a). Pores in the post-disturbance soils were similar or greater in number density relative to the pre-disturbance soils (Fig. 3.9b, 3.10b, 3.11b), but the individual pores formed following disturbance were smaller in volume (Fig. 3.9c, 3.10c, 3.11c). The vesicular pores had a greater number density in the post-disturbance soils relative to the pre-disturbance soils (Fig. 3.9a), although the difference was not significant at the $\alpha = 0.05$ level ($p = 0.08$). Analysis of vesicular pore formation in the lab has shown that the number of vesicular pores declines as the soil undergoes repeated wetting and drying cycles, due to the merging of the pores as they grow (Figueira and Stoops, 1983). The

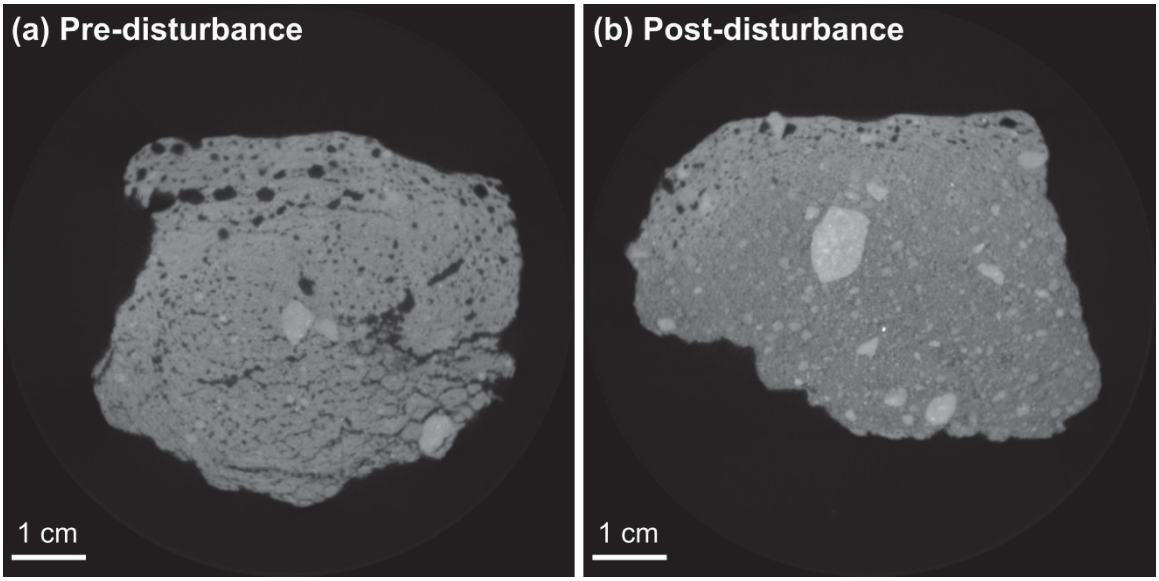

Fig. 3.8. Examples of slices from computed tomography scans of samples collected before and after disturbance at site G5 (Dixie Valley, NV): (a) pre-disturbance sample, (b) post-disturbance sample collected following the one-year recovery period.

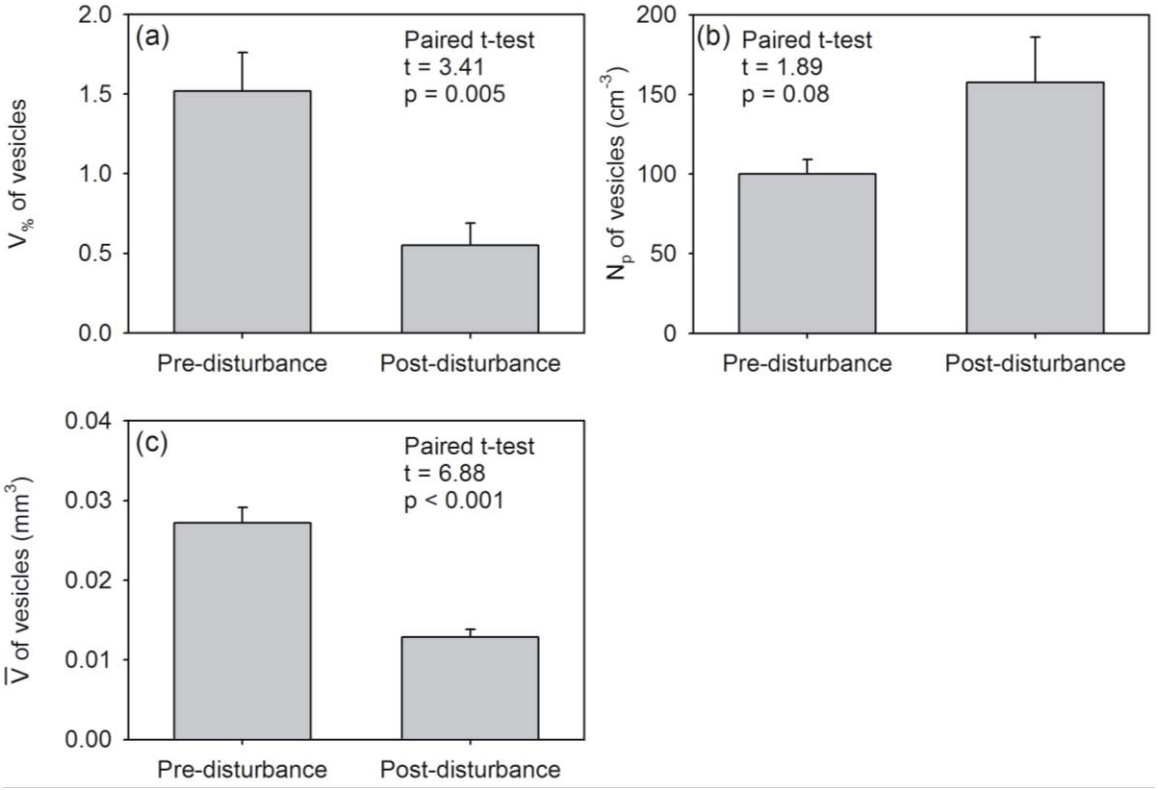

Fig. 3.9. Vesicular pore data from computed tomography scans of pre-and post-disturbance soils: (a) percentage of gravel-free volume occupied by vesicles ($V_{\%}$), (b) number density of vesicles (N_p), and (c) geometric mean of vesicular pore volume ($\overline{V}$). Height of bars is the mean for 13 samples and error bars are one standard error.

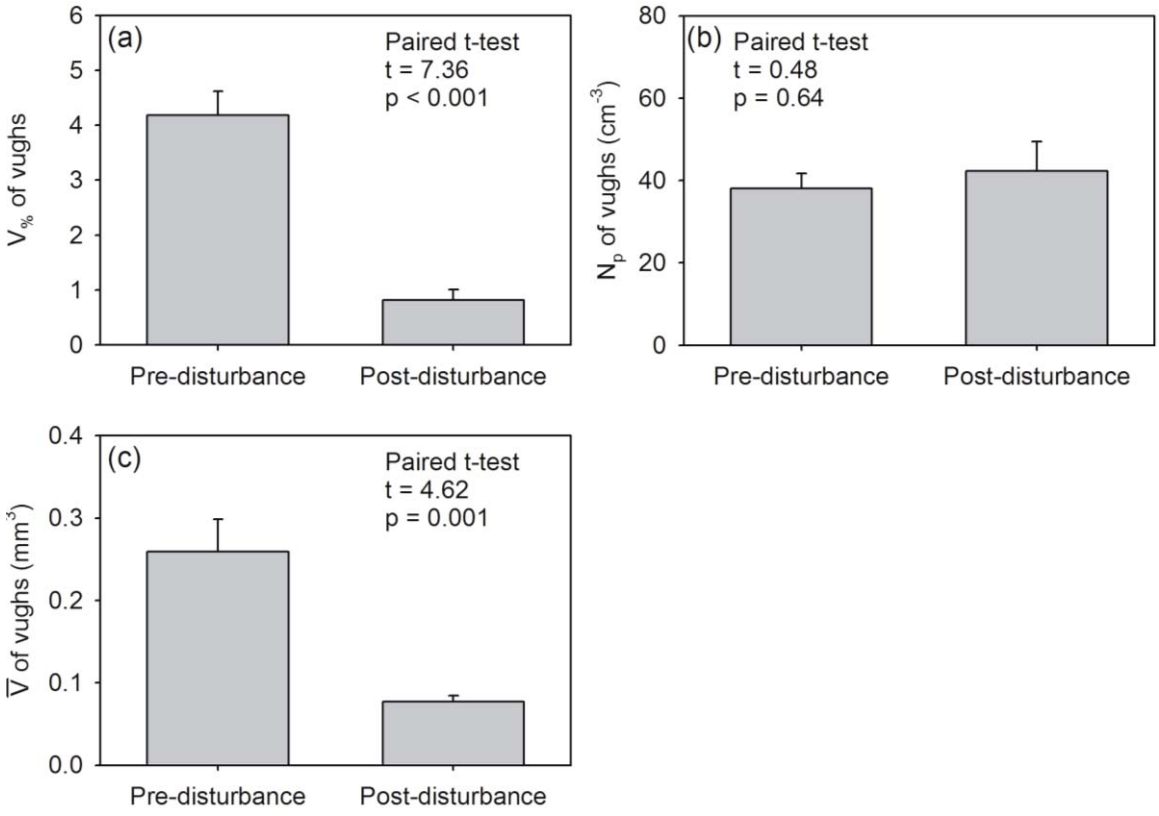

Fig. 3.10. Vugh data from computed tomography scans of pre- and post-disturbance soils: (a) percentage of gravel-free volume occupied by vughs ($V_{\%}$), (b) number density of vughs (N_p), and (c) geometric mean of vugh volume ($\overline{V}$). Height of bars is the mean for 13 samples and error bars are one standard error.

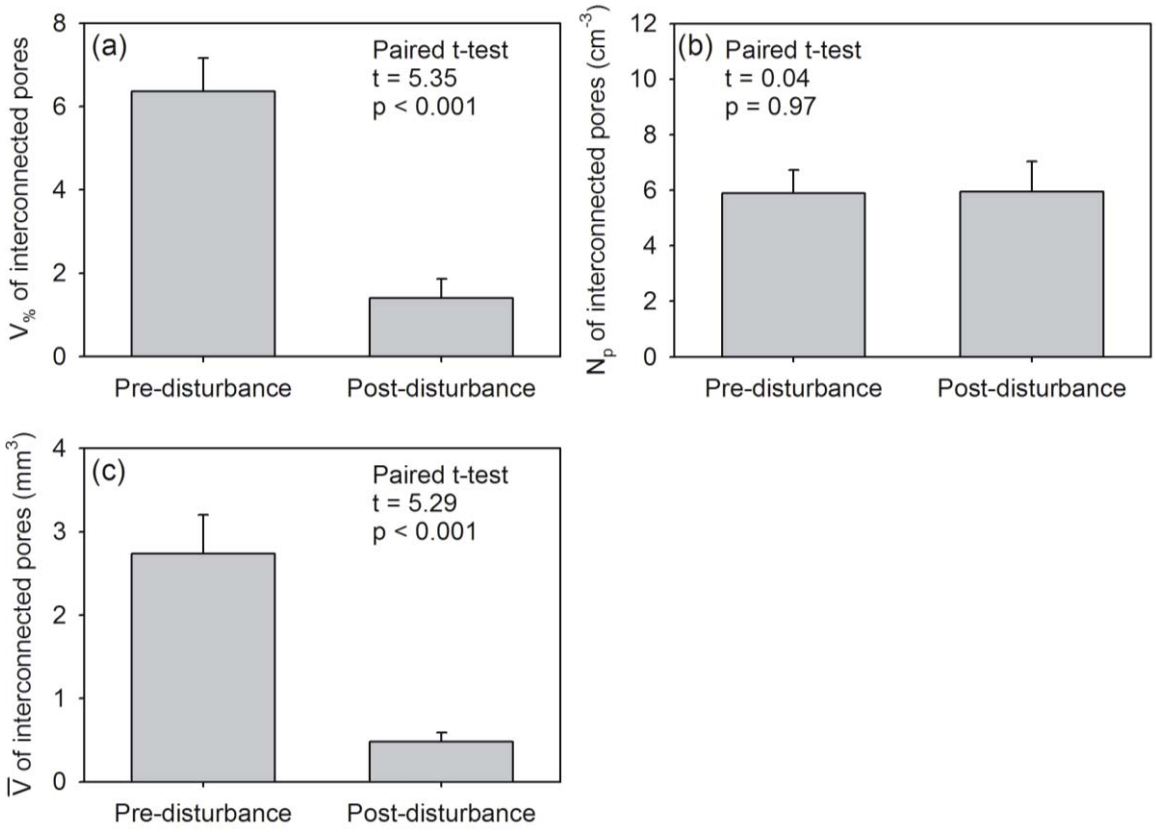

Fig. 3.11. Interconnected pore data from computed tomography scans of pre- and post-disturbance soils: (a) percentage of gravel-free volume occupied by interconnected pores ($V_{\%}$), (b) number density of interconnected pore networks (N_p), and (c) geometric mean of interconnected pore network volume ($\overline{V}$). Height of bars is the mean for 13 samples and error bars are one standard error.

greater number of vesicular pores in the post-disturbance soils is indicative of an earlier stage of pore development. These results differ from the LMNRA study, which showed no significant difference in the size of vesicles and vughs between the disturbed and undisturbed vesicular horizons, based on measurements of pore area in thin sections (Yonovitz and Drohan, 2009).

We observed that vughs were generally larger and less numerous than vesicles, which agrees with previous characterization of these pore types (Brewer, 1976). However, the vughs that occur in vesicular horizons are unlikely to have formed by mechanisms proposed in the literature, which include flocculation of clays, differential weathering of minerals, faunal activity, and welding of aggregates (Brewer, 1976; Stoops, 2003). Rather, we suggest that the vughs that occur in the vesicular horizon develop from pores that were initially vesicular. Their irregular shape appears to result from growth of vesicular pores through the "capture" of adjacent vesicular pores, adding lobes to the pore shape. The presence of interconnected pores has been previously observed in some studies that have analyzed vesicular horizons in thin sections (Figueira and Stoops, 1983; Sullivan and Koppi, 1991), while other studies have found the vesicles and vughs to display no interconnection (Yonovitz and Drohan, 2009). Our results show that interconnected pore networks are common in vesicular soils, and their reformation following disturbance follows similar trends as the reformation of vesicles and vughs.

Rate of vesicular horizon recovery following disturbance

The variation in vesicular horizon recovery from disturbance among the different field areas may be explained by: 1) the characteristics of the disturbed soil material, or 2) by external factors, such as weather conditions during the period of recovery. This study includes vesicular horizons with a wide range of chemical properties (EC: 0.5-20.3 dS m^{-1}, pH: 7.8-8.9, ESP: 1.5-62.3%, $CaCO_3$: 2.6-22.8%), and particle size distributions (sand: 27-57%, silt: 32-57%, and clay: 10-25%) (Table 3.4). Past studies have suggested that certain soil characteristics, including ESP (Bouza et al., 1993) and texture (Evenari et al., 1974), can influence vesicular pore formation. It has been suggested that vesicular horizons on old geomorphic surfaces may be pre-disposed to recovery from disturbance due to the accumulation of eolian material throughout the history of these surfaces, producing a silt-rich texture that is conducive to vesicular pore formation (Yonovitz and Drohan, 2009). However, in this study, most of the variability in vesicular horizon recovery could be explained by precipitation patterns during the period of recovery (Fig. 3.12), pointing to a significant role of external factors in determining vesicular horizon recovery from disturbance.

The VHI of the post-disturbance vesicular horizons showed a linear relationship ($r^2 = 0.64$, $p = 0.009$) with the total depth of precipitation during the recovery period (Fig. 3.12a). This relationship was improved by considering precipitation as events, rather than depth ($r^2 = 0.88$, $p = 0.0002$). The precipitation events that influence vesicular pore formation in the field can be considered analogous to the wetting and drying cycles that drive vesicular pore formation in the lab (Miller, 1971; Figueira and Stoops, 1983). The

Table 3.4. Laboratory characterization data for the vesicular horizons, including electrical conductivity (EC), pH in 1:1 H_2O, exchangeable sodium percentage (ESP), calcium carbonate percent by weight, and the percentage of the three soil separates (sand, silt, and clay). Data presented are the average of the three study plots at each site and their standard error (SE).

Site		EC	pH	ESP	$CaCO_3$	Sand	Silt	Clay
		ds m^{-1}		%	%	%	%	%
S1	Average	7.1	8.5	21.2	8.0	38.4	46.9	14.8
	SE	3.1	0.1	1.9	0.4	1.2	3.1	1.9
S2	Average	12.0	8.8	42.2	7.9	31.7	49.1	19.2
	SE	3.6	0.0	6.7	0.5	2.2	1.8	2.4
S3	Average	1.6	7.8	1.5	7.8	57.1	31.5	11.4
	SE	0.6	0.1	0.1	1.7	2.6	2.7	1.1
S4	Average	4.0	8.4	17.0	11.9	27.0	56.8	16.2
	SE	1.4	0.1	0.2	1.7	2.7	2.1	1.9
S5	Average	1.5	8.4	11.4	4.3	33.1	53.3	13.7
	SE	0.1	0.1	1.5	0.9	1.6	2.0	4.3
M1	Average	4.7	8.1	8.7	8.4	36.1	43.2	20.6
	SE	2.0	0.0	3.0	0.7	2.8	2.0	1.4
M2	Average	3.1	7.9	6.8	4.4	33.4	51.1	15.5
	SE	2.0	0.1	3.1	0.4	2.3	1.6	1.1
M3	Average	1.1	8.8	28.0	2.9	49.4	33.9	16.8
	SE	0.4	0.1	3.6	0.5	1.1	1.3	2.7
M4	Average	5.7	8.5	20.4	22.8	33.10	46.7	19.5
	SE	0.9	0.1	4.8	1.2	7.2	7.4	2.7
M5	Average	3.3	8.9	43.6	6.2	33.4	48.3	18.3
	SE	1.7	0.1	7.9	1.3	2.0	0.8	2.6
G1	Average	20.3	8.3	25.5	9.4	43.6	46.4	10.1
	SE	17.9	0.2	13.0	2.2	4.7	3.7	1.4
G2	Average	5.4	8.8	62.9	8.4	32.5	42.4	25.1
	SE	0.1	0.1	4.1	0.6	2.4	2.6	0.6
G3	Average	0.7	8.5	14.6	6.5	46.1	39.1	14.8
	SE	0.2	0.0	3.1	0.7	1.7	1.9	0.7
G4	Average	1.3	8.8	31.6	4.2	45.5	40.2	14.2
	SE	0.3	0.0	1.4	0.2	4.3	2.6	1.0
G5	Average	10.9	8.0	15.2	2.6	51.3	34.0	14.6
	SE	1.3	0.0	1.1	0.9	4.3	4.8	0.6

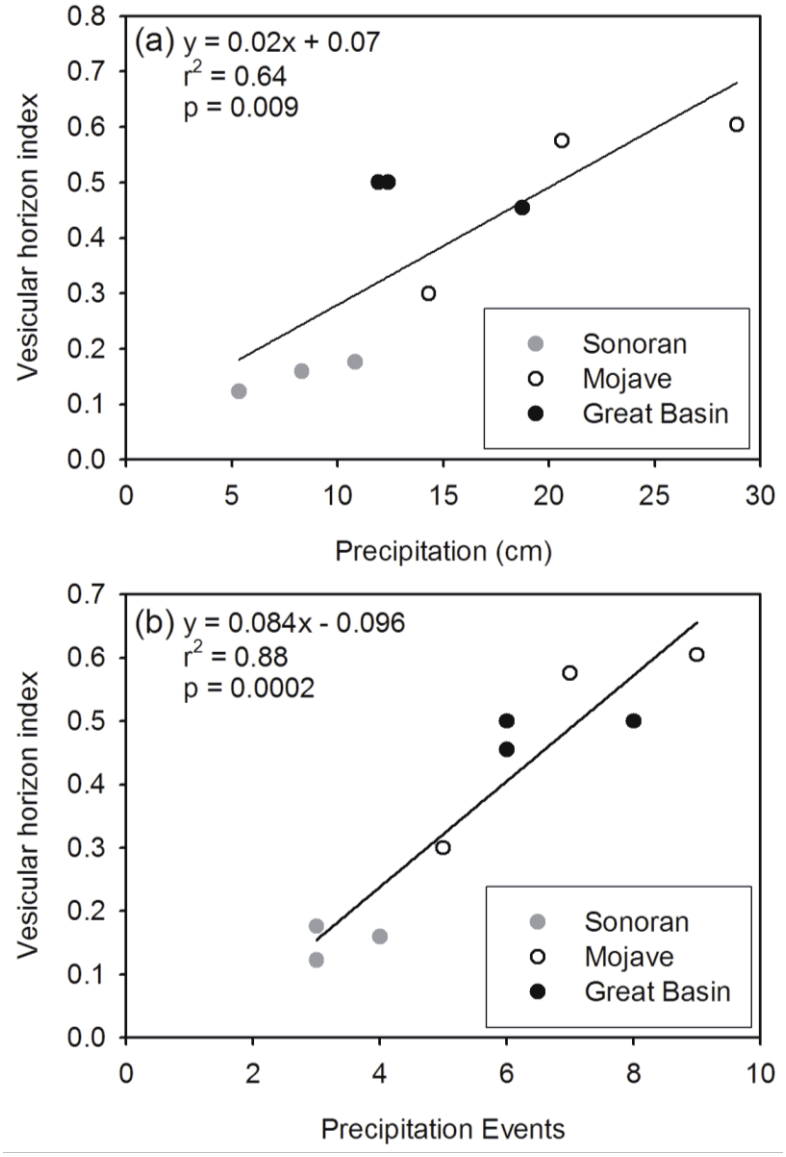

Fig. 3.12. Relationship between precipitation received during the one-year recovery period and vesicular horizon index of the post-disturbance vesicular horizons formed during the recovery period. Precipitation is expressed as: (a) total depth and (b) number of events. Only field areas with nearby weather stations were included in this analysis (see Table 3.3).

role of precipitation in the recovery of vesicular horizons may explain why we observed differences in pore volume between the pre- and post-disturbance vesicular horizons, while the study at LMNRA concluded that there was no significant difference in pore size (Yonovitz and Drohan, 2009). The study at LMNRA took place over 2004 to 2005, which was an exceptionally rainy year in the Mojave Desert. The Willow Beach weather station in LMNRA recorded 34.5 cm of precipitation between June 2004 and May 2005, which is more than double the precipitation received in normal year (14.1 cm) (Fenimore, 2011). In the current study, precipitation during the recovery period ranged from 3.4 to 26.3 cm at the various field sites.

Using the relationship between VHI and precipitation events (Fig. 3.12b), along with knowledge of the initial VHI and the typical precipitation patterns at a site, it is possible to predict the period of time required for the recovery of the vesicular horizon from disturbance. This prediction may be expressed as follows:

$$\mathrm{RT} = \frac{\mathrm{VHI} + 0.096}{0.084(\mathrm{P_E})} \qquad (\mathrm{eq.}\ 3.6)$$

where, RT = recovery time (in yrs), VHI = vesicular horizon index before disturbance, and P_E = average number of precipitation events per year. Using data from the local weather stations, we were able to predict recovery times for the sites examined in this study (Table 3.5). The average number of precipitation events for each site was calculated by examining the most recent 10 yrs of weather records, except at those sites with shorter record lengths, for which all available data was examined (Table 3.3). Using average P_E, the predicted recovery times ranged from two to 11 yrs. However, predicted

Table 3.5. Estimated recovery time (RT) for vesicular horizons by site. Recovery times were calculated according to Eq. 3.6, using initial vesicualr horizon index for the site (VHI), and records of precipitation events (P_E) from nearby weather stations. Location and details about weather stations are in Table 3.3.

Site	Initial VHI	Average P_E	Min. P_E	Max. P_E	RT (Average P_E)	RT (Min. P_E)	RT (Max. P_E)
		yr^{-1}	yr^{-1}	yr^{-1}	yr		
S1	3.3	5	1	10	8	40	4
S2	3.1	4	1	6	11	38	6
S4	2.9	6	3	10	6	12	4
M1	2.2	4	1	8	6	27	3
M4	1.7	10	7	16	2	3	1
M5	1.7	6	1	11	4	22	2
G3	2.0	6	2	10	4	12	2
G4	2.8	7	3	10	5	12	4
G5	1.5	7	2	10	3	10	2

recovery times using the minimum and maximum P_E data show that the recovery rate varies dramatically from year to year, due to high inter-annual variation in precipitation. The slowest recovery rates are predicted for the sites in the Sonoran Desert, which receives the least precipitation. These predicted recovery rates suggest that vesicular horizons recover rapidly following disturbance, relative to other metrics of recovery in disturbed desert lands, including recovery of vegetation, alleviation of soil compaction, and recovery of biological soil crusts, which require between 20 and >1000 yrs (Webb et al., 2009).

This prediction offers some insight into the time that may be required for vesicular horizons to reform following disturbance; however, several limitations must be noted. First, the predictions are based on an extrapolation beyond the range of observation, therefore it is not known if the linear relationship between P_E and VHI continues into the later stages of recovery. Second, while VHI of the post-disturbance soils could be related to precipitation events during the recovery period, a similar relationship was not found between the porosity data collected from the CT scans and precipitation received during the recovery period. This may be because the scale of observation used in the CT scans (one clod per site) was not sufficient to characterize the overall recovery of vesicular horizons at the whole site. In calculating VHI, all three study plots were described and several clods were examined during the description of each plot, providing a broader scale of observation.

Another limitation is that VHI deals only with the horizon thickness, and quantity and size of vesicular pores, but not with structure, which is more difficult to quantify. The

recovery of vesicular horizon structure is a significant concern because of the role that interpedal voids play in infiltration (Meadows et al., 2008) and seedling establishment (Eckert et al., 1986b). In chronosquence studies, platy structure is observed in very young vesicular horizons (750 yrs), whereas columnar or prismatic structure in the vesicular horizon is only observed in soils older than 10,000 yrs (McDonald, 1994; Meadows et al., 2008). The development of these structures in initially coarse-textured parent material requires modification of texture through eolian input, a process that may limit the rate of initial structure development. The formation of structure following disturbance may occur much more rapidly, assuming that the soil texture has not been severely modified by the disturbance. The relatively rapid formation of vesicular horizon structure following disturbance is supported by our observations of weak prismatic structure in some of the reformed vesicular horizons, which had developed in one year following disturbance. Previous studies have also observed the reformation of polygonal structure in vesicular soils during one year following trampling by grazing animals (Eckert et al., 1986b). At our field areas, platy structure was not observed to reform in the disturbed soils during the one year recovery period; however, the reformation of platy structure was observed in the disturbed soils at LMNRA (Yonovitz and Drohan, 2009). Laboratory studies of vesicular pore formation have shown that platy structure is formed by the growth of fissures between horizontally interconnected vesicular pores (Figueira and Stoops, 1983), a process that occurs after many (20-30) wetting and drying cycles. Based on the typical number of rainfall events at the field areas (Table 3.5), this process is likely to take between two and six years.

Impacts of pre-existing disturbance on vesicular horizon morphology

Tire Tracks

Vesicular horizons in pre-existing tire tracks were analyzed in order to determine the impact that real-world disturbance has on vesicular horizon morphology. The vesicular horizons in the tire tracks were one to five cm thick, while those beneath the desert pavement were three to eight cm thick. Very fine- to medium-sized (<1 to 5 mm) vesicular pores were observed in both the tire tracks and the undisturbed vesicular horizons. In most of the tire tracks, moderate to strong prismatic structure was observed, compared to moderate to strong columnar structure observed beneath the desert pavement (Fig. 3.13). This suggests that the top surface of the polygons was flattened, but the polygonal cracking, was either unaffected, or recovered within the time period following disturbance.

Data from the CT scans show that the pore morphology of vesicular horizons in the tire tracks are not substantially altered relative to those beneath the undisturbed desert pavement (Fig. 3.14). Vesicles and vughs show no significant difference in $V_{\%}$, N_p, or $\overline{V}$ between the pre-and post-disturbance soils (Fig. 3.15, 3.16). The interconnected pores show a reduction of $V_{\%}$ and $\overline{V}$ in the tire tracks relative to the undisturbed soils (Fig. 3.17); though these differences were also not significant at the $\alpha = 0.05$ level ($p = 0.11$ for $V_{\%}$, $p = 0.18$ for $\overline{V}$). Within the analyzed depth (0-15 mm), the pores are likely to have been crushed when the tire tracks were formed. The CT results indicate that there has been a full recovery of the vesicular pores and vughs within this upper zone of the

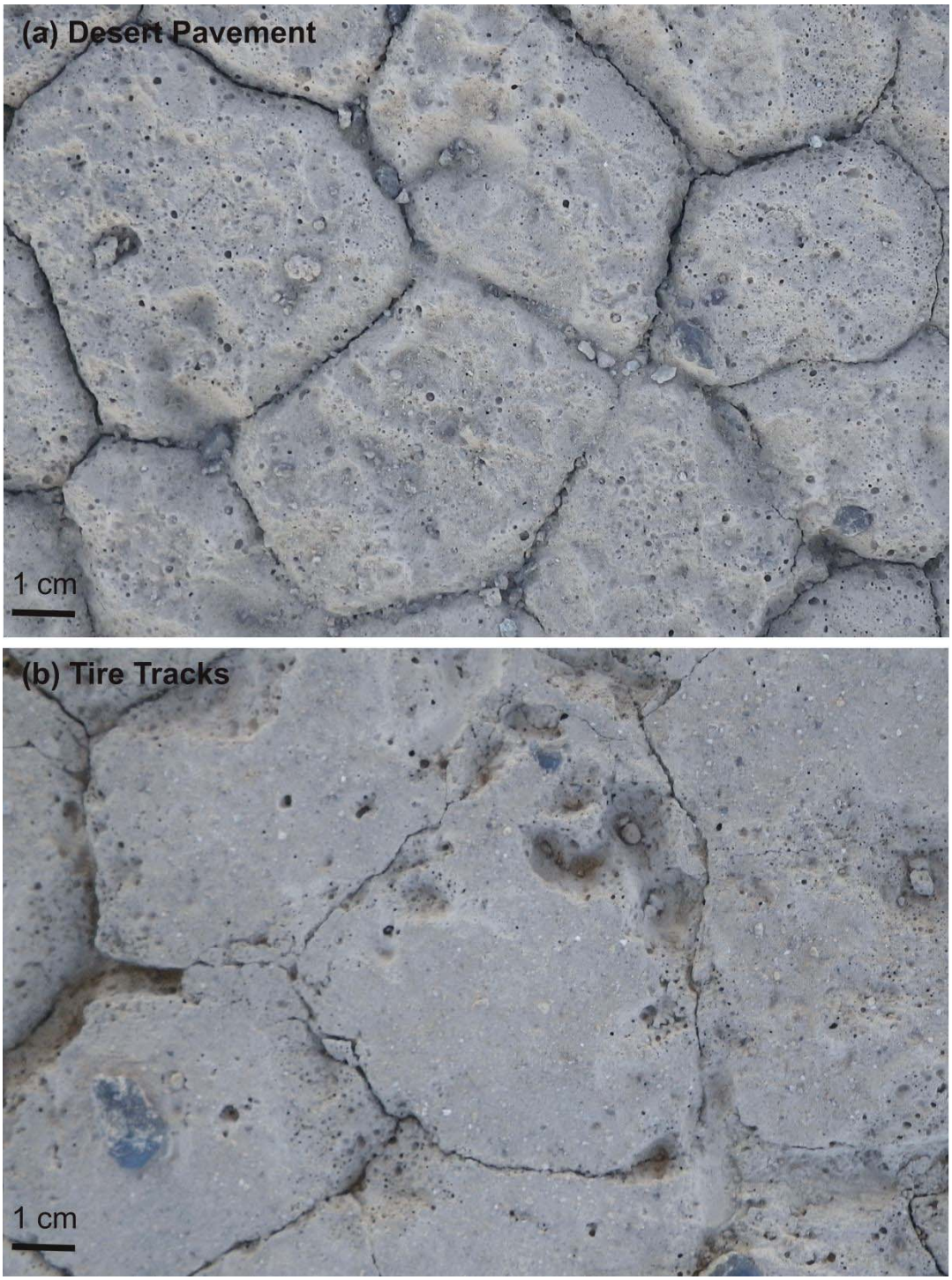

Fig. 3.13. Polygonal surface cracks in the vesicular horizons: (a) beneath the undisturbed desert pavement and (b) in tire tracks. Both photos were taken at site S4 (Quartzsite, AZ).

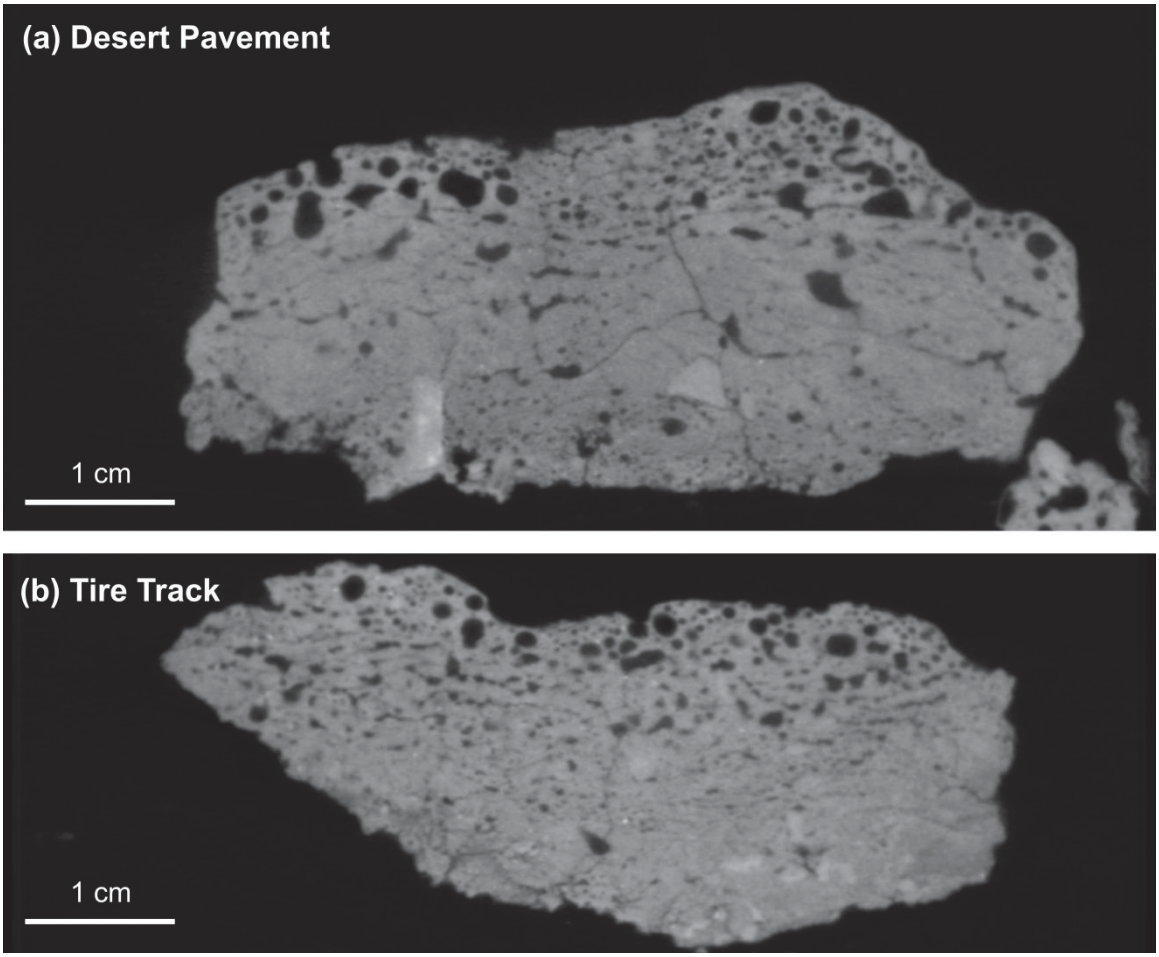

Fig. 3.14. Examples of slices from computed tomography scans of samples collected from tire tracks and undisturbed desert pavement at site M2 (Johnson Valley, CA): (a) desert pavement sample, (b) tire track sample.

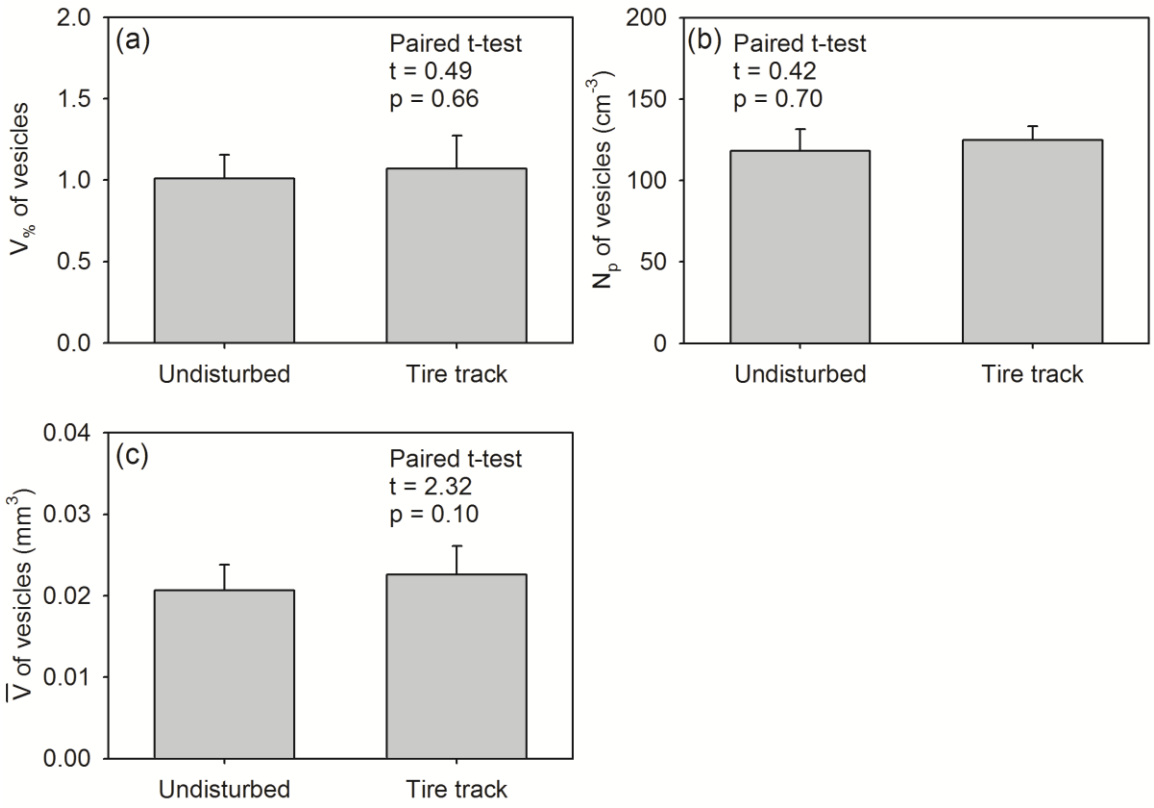

Fig. 3.15. Vesicular pore data from computed tomography scans of soils from tire tracks and surrounding undisturbed desert pavement: (a) percentage of gravel-free volume occupied by vesicles ($V_{\%}$), (b) number density of vesicles (N_p), and (c) geometric mean of vesicular pore volume ($\overline{V}$). Height of bars is the mean for 13 samples and error bars are one standard error.

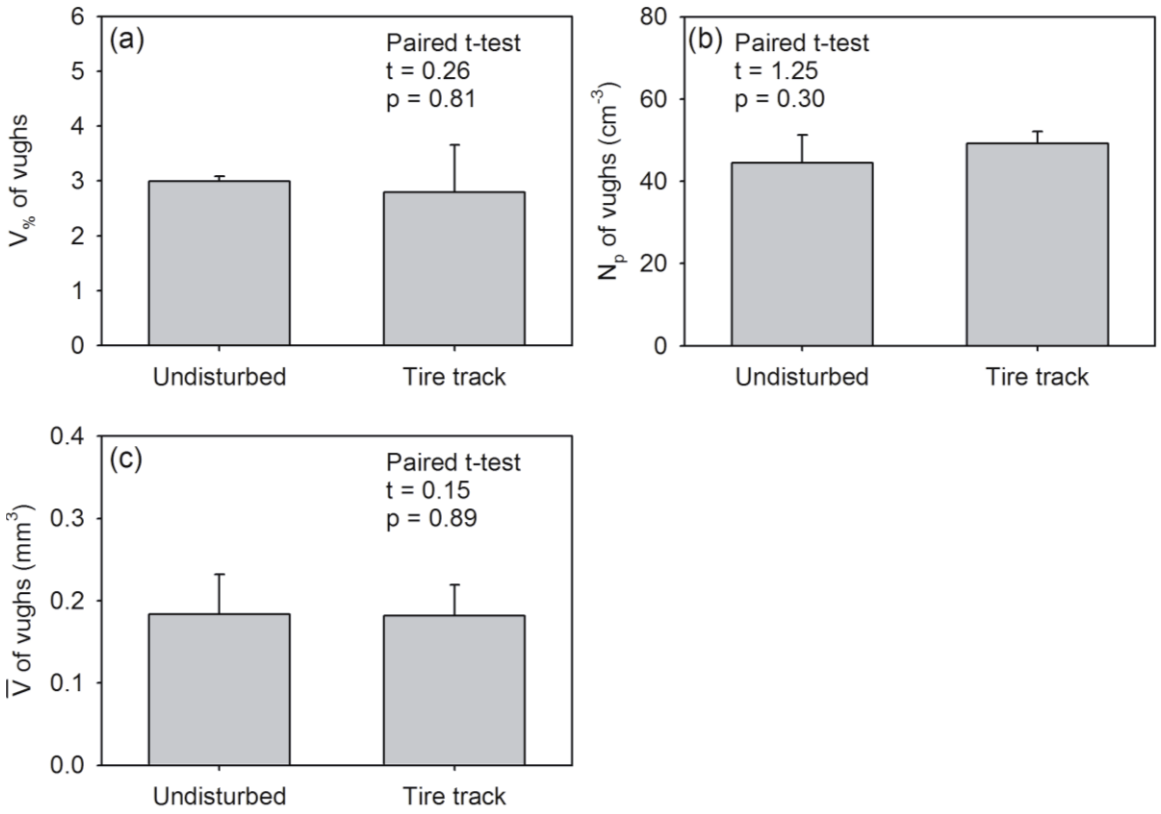

Fig. 3.16. Vugh data from computed tomography scans of soils from tire tracks and surrounding undisturbed desert pavement: (a) percentage of gravel-free volume occupied by vughs ($V_{\%}$), (b) number density of vughs (N_p), and (c) geometric mean of vugh volume ($\overline{V}$). Height of bars is the mean for 13 samples and error bars are one standard error.

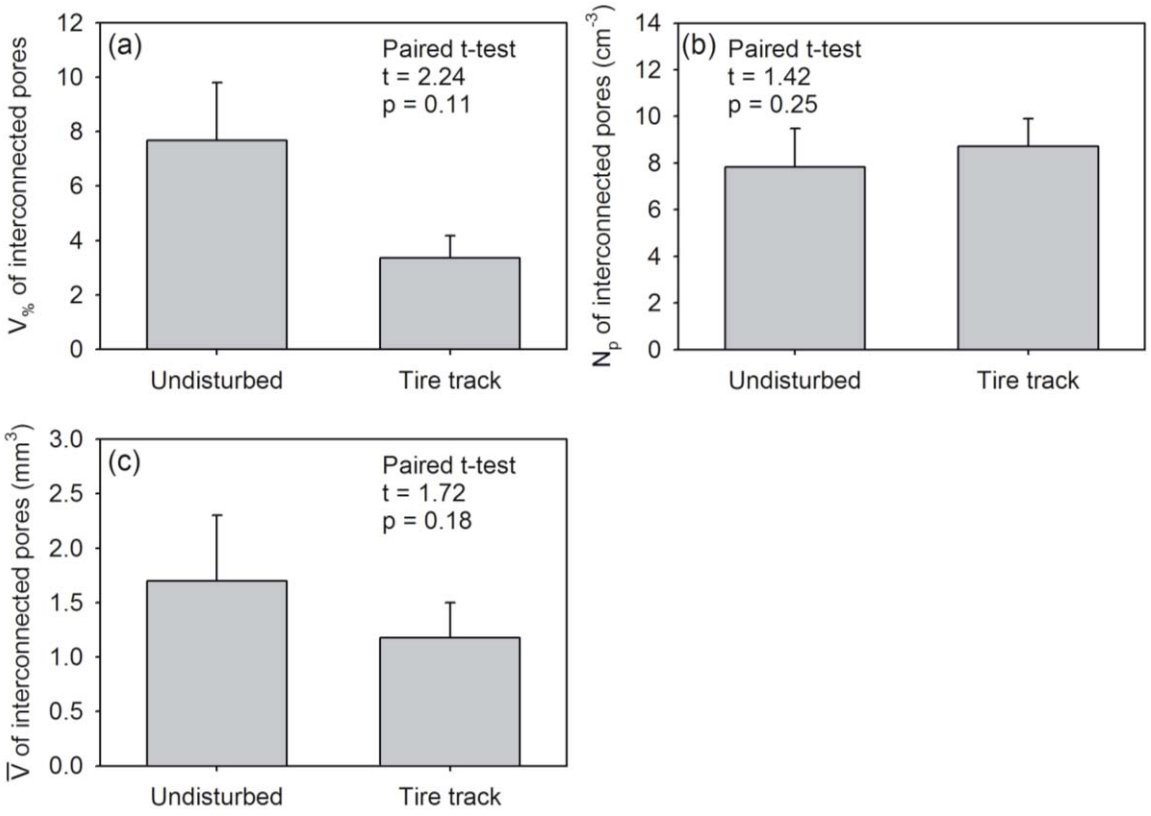

Fig. 3.17. Interconnected pore data from computed tomography scans of soils from tire tracks and surrounding undisturbed desert pavement: (a) percentage of gravel-free volume occupied by interconnected pores ($V_{\%}$), (b) number density of interconnected pore networks (N_p), and (c) geometric mean of interconnected pore network volume ($\overline{V}$). Height of bars is the mean for 13 samples and error bars are one standard error.

vesicular horizon, and nearly complete recovery of the interconnected pore networks. However, our field observations indicate that the vesicular horizons were thinner in the tire tracks, which suggests a slower recovery in the lower part of the vesicular horizon.

Coppice Dunes

Vesicular horizons were sometimes observed beneath coppice dunes at our field areas (Fig. 3.1b). Vesicular horizons beneath coppice dunes were also observed by Shafer et al. (2007) in the Mojave Desert. Coppice dunes have sandier textures than soils in the shrub interspace and are subject to mixing by bioturbation, creating conditions which typically prevent the formation of vesicular horizons (Eckert et al., 1978; McFadden et al., 1998). Therefore, the vesicular horizons observed beneath the coppice dunes are most likely relicts; *i.e.*, they formed in a shrub interspace and were subsequently buried when a new shrub, and corresponding coppice dune, was established. These vesicular horizons were examined in order to evaluate changes in vesicular horizon morphology that occur following shrub establishment.

The vesicular horizons observed beneath coppice dunes were three to six cm thick, and occurred beneath five to 12 cm of loose sandy material that formed the coppice dune. The vesicular horizons contained mostly very fine to fine vesicular pores (<1-2 mm diam.) and occasional very fine root channels. The structure was either massive or platy. Vesicular horizons beneath the adjacent desert pavement were of a similar thickness (3-7 cm), but contained very fine- to medium-sized vesicular pores (<1-5 mm diam.), and displayed columnar structure parting to platy structure. Beneath some

coppice dunes, a vesicular horizon remnant could be identified based on color, texture, and position relative to the surrounding desert pavement, but no vesicular pores were observed.

Examination of CT scans indicates that vesicular horizons undergo a loss of their characteristic porosity when they become buried beneath a coppice dune. Representative slices from CT scans of vesicular horizons beneath a coppice dune and a desert pavement are shown in Fig. 3.18. In these slices, the reduction in vesicular pore size and increase in planar voids with horizontal orientation is apparent. These observations suggest that the vesicular pores collapse under the weight of the coppice dune sediments, producing the planar voids, which separate platy structural units. A similar zone of collapsed vesicles is sometimes described in the lower part of cumulic vesicular horizons, in these soils vesicular porosity is prominent in the upper part of the vesicular horizon, while a platy subcrust, with some remaining vesicles occurs in the lower part of the horizon (Miller, 1971; Brewer, 1976; McFadden et al., 1998; Joeckel and Clement, 1999; Lebedeva et al., 2009).

The porosity of the vesicular horizons is notably altered in the buried vesicular horizons (Figs. 3.19, 3.20, 3.21). None of the differences described here were significant at the $\alpha = 0.05$ level, which is most likely due to an insufficient sample size ($N = 4$). Vesicles and vughs in the buried vesicular horizons occupy less of the sample volume compared to the un-buried vesicular horizons (Figs. 3.19a, 3.20a). The vesicles and vughs were similar in number density between the buried and un-buried soils (Figs. 3.19b, 3.20b), but were smaller in volume (Figs. 3.19c, 3.20c). In contrast to the vesicles

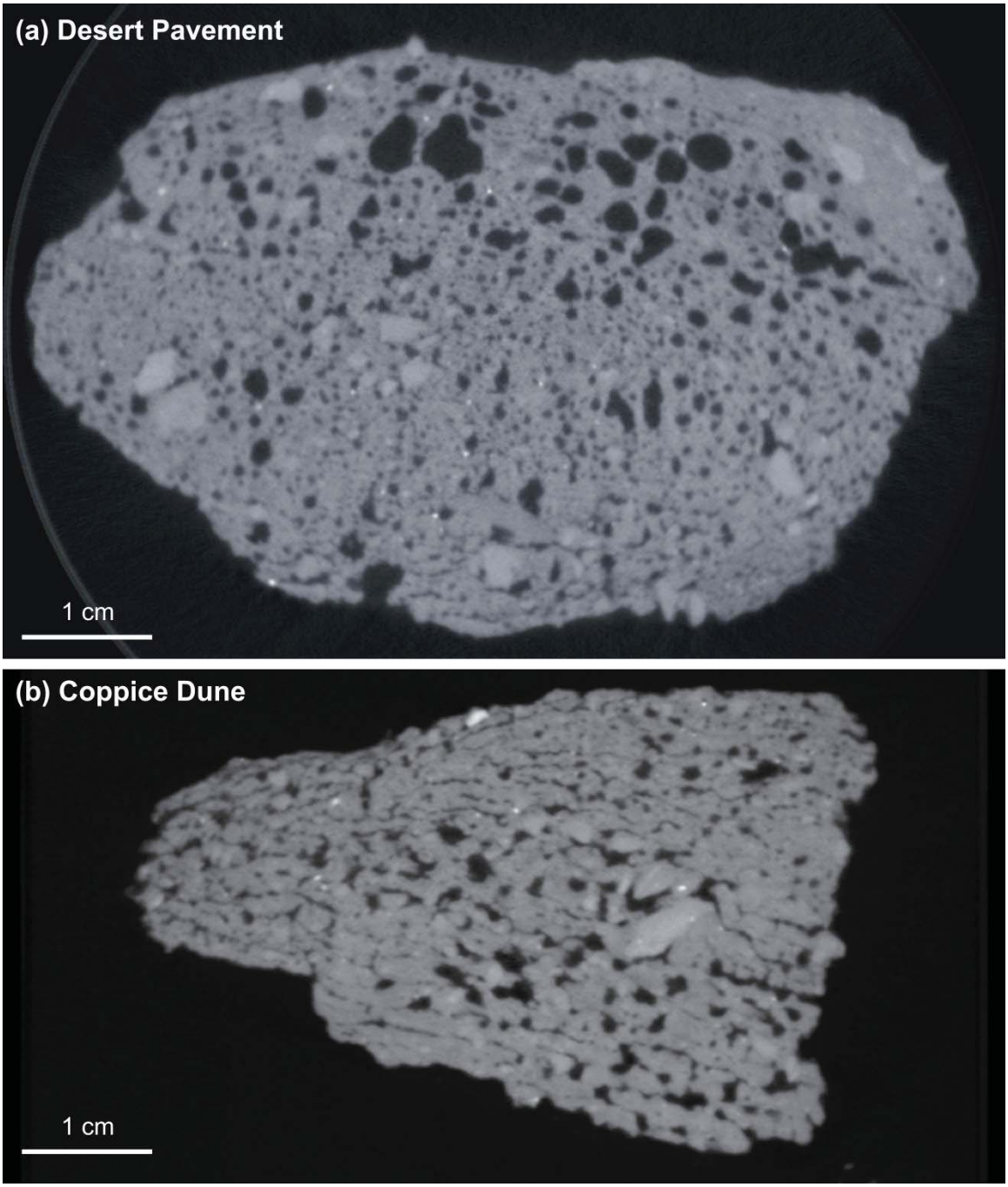

Fig. 3.18. Examples of slices from computed tomography scans of samples collected from beneath coppice dunes and desert pavement at site G3 (Tonopah, NV): (b) desert pavement sample, (b) coppice dune sample.

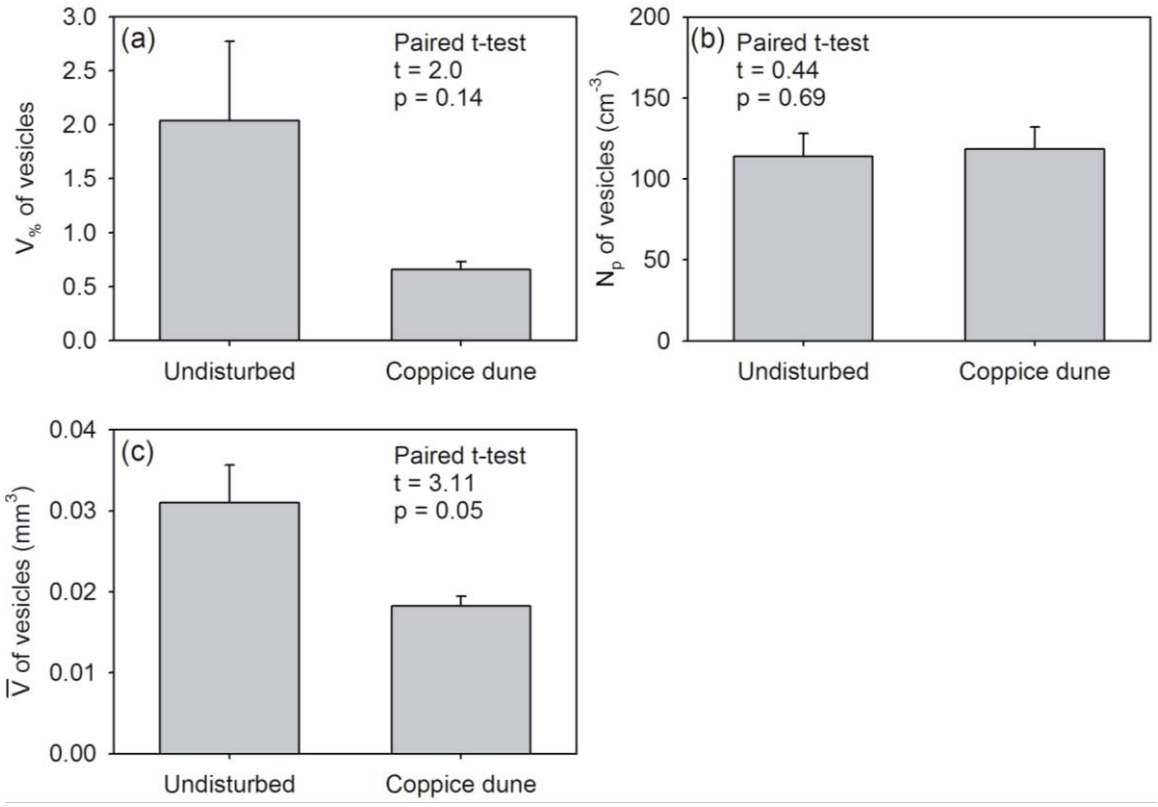

Fig. 3.19. Vesicular pore data from computed tomography scans of soils from beneath coppice dunes and surrounding undisturbed desert pavement: (a) percentage of gravel-free volume occupied by vesicles ($V_{\%}$), (b) number density of vesicles (N_p), and (c) geometric mean of vesicular pore volume ($\overline{V}$). Height of bars is the mean for 13 samples and error bars are one standard error.

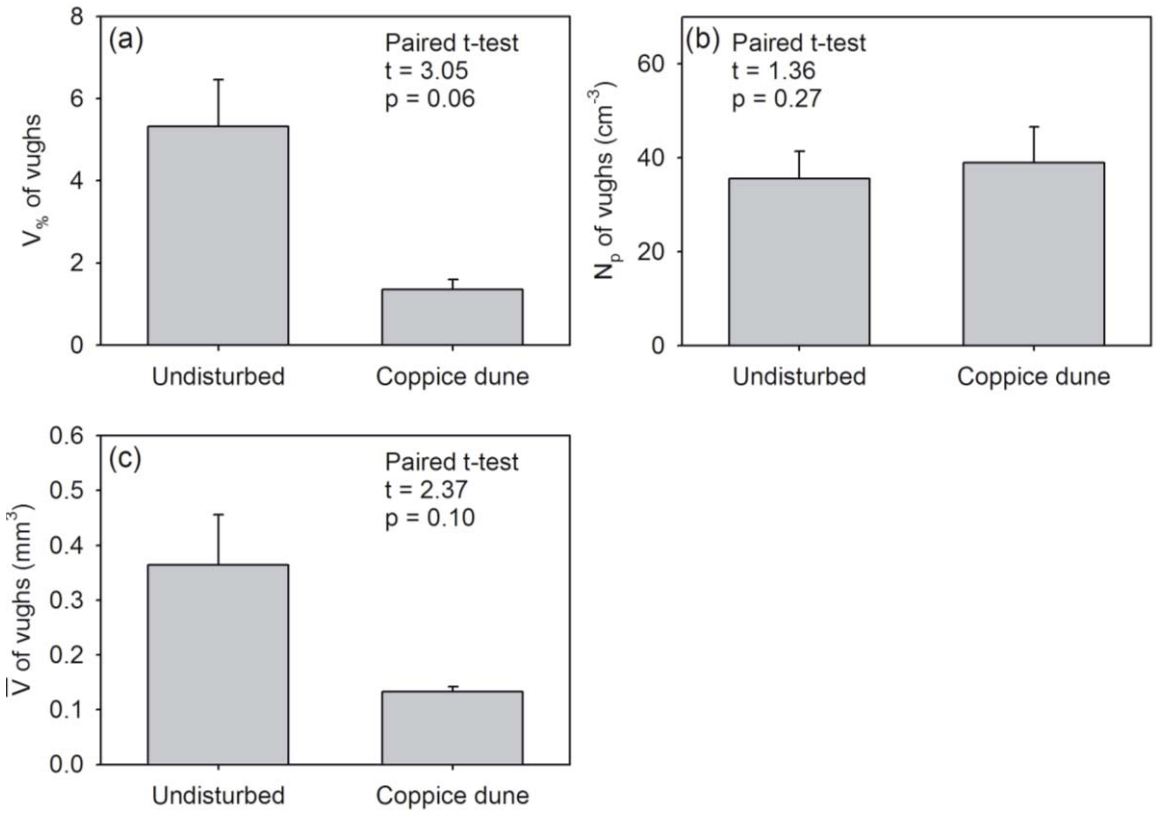

Fig. 3.20. Vugh data from computed tomography scans of soils from beneath coppice dunes and surrounding undisturbed desert pavement: (a) percentage of gravel-free volume occupied by vughs ($V_{\%}$), (b) number density of vughs (N_p), and (c) geometric mean of vugh volume ($\overline{V}$). Height of bars is the mean for 13 samples and error bars are one standard error.

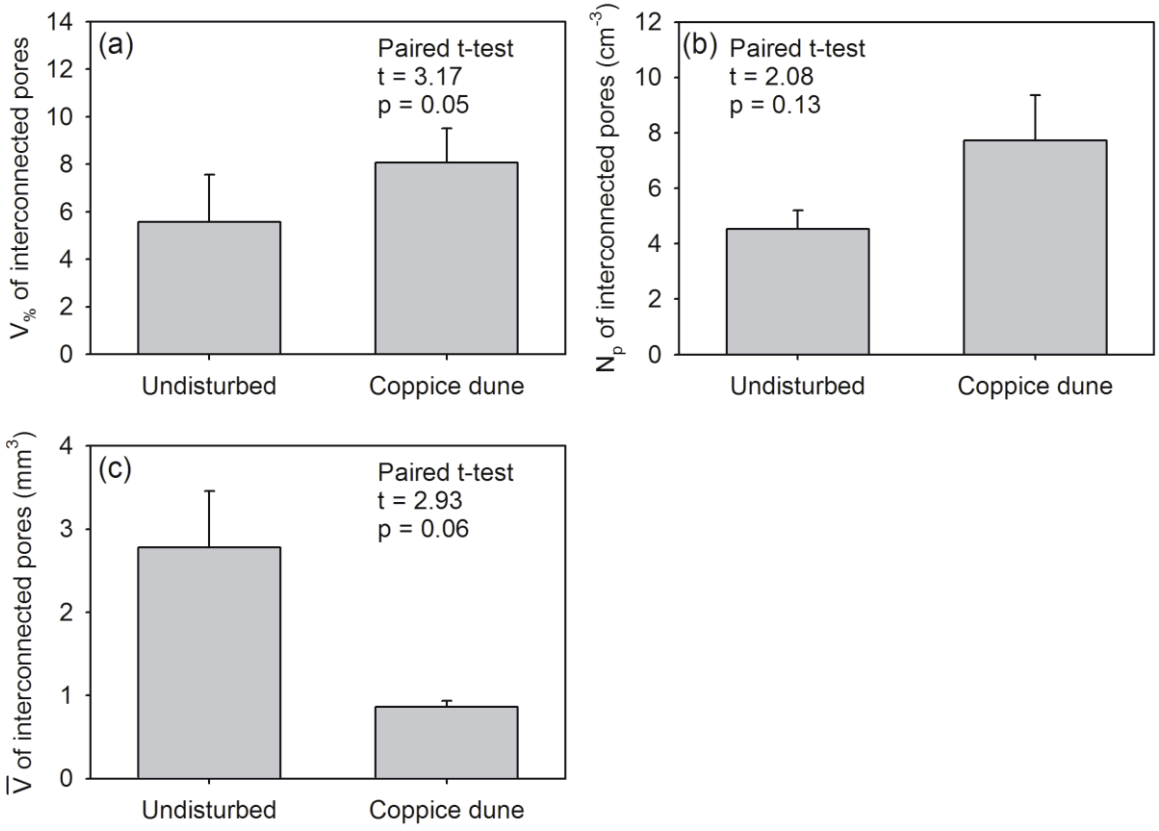

Fig. 3.21. Interconnected pore data from computed tomography scans of soils from beneath coppice dunes and surrounding undisturbed desert pavement: (a) percentage of gravel-free volume occupied by interconnected pores ($V_{\%}$), (b) number density of interconnected pore networks (N_p), and (c) geometric mean of interconnected pore network volume ($\overline{V}$). Height of bars is the mean for 13 samples and error bars are one standard error.

and vughs, the interconnected pore networks occupy a greater percentage of the sample volume in the buried vesicular horizons (Fig. 3.21a). Like the vesicles and vughs, the individual interconnected pore networks were smaller in volume in the buried vesicular horizons (Fig. 3.21c), but the number density increased (Fig. 3.21b). The smaller pore volumes reflect the collapse of vesicles, vughs, and interconnected pore networks under the weight of the coppice dune sediments. This process of collapse leads to the formation of more interconnected pore networks, aligned along the horizontal plane.

Previous work has shown that shrub abandonment and degradation of the coppice dune can lead to the formation of a new vesicular horizon (McAuliffe and McDonald, 2006). The role of buried vesicular horizon remnants in this recovery process is unknown, but they may lead to more rapid recovery of desert pavements disturbed by past vegetation advances (Valentine and Harrington, 2006; Pelletier et al., 2007).

Impact of disturbance on hydraulic properties

Infiltration rates were generally lower following disturbance. The data fit well with Wooding's equation (eq. 3.5), with an average r^2 of 0.962 in the pre-disturbance plots, and an average r^2 of 0.923 in the post-disturbance plots. The geometric mean of the pre-disturbance K_{sat} measurements was 0.42 cm hr^{-1}, while the geometric mean of the post-disturbance K_{sat} measurements was 0.27 cm hr^{-1}. These K_{sat} values are within the range measured on alluvial fan surfaces with vesicular horizons in a previous study (0.3-0.8 cm hr^{-1}), but much lower than those measured on younger alluvial fan surfaces that did not have vesicular horizons (6.8-15 cm hr^{-1}) (Young et al., 2004). The paired t-test

between log-normalized K_{sat} data before and after disturbance indicates that the decrease in K_{sat} following disturbance was not significant at the $\alpha = 0.05$ level ($p = 0.063$) (Fig. 3.22a). The median pre-disturbance Gardner's α was 0.11 cm^{-1}, while the median post-disturbance α was 0.08 cm^{-1} (Fig. 3.22b). Gardner's α defines the slope of the unsaturated hydraulic conductivity (K_{unsat}) function, which relates K_{unsat} to tension, and a decrease in α is indicative of a loss of macroporosity (Caldwell et al., 2006). However, according to the Mann-Whitney test, the decrease in Gardner's α was also not statistically significant at the $\alpha = 0.05$ level ($p = 0.07$).

The reduction of infiltration rates in the disturbed soils, which have drastically less vesicular porosity (Fig. 3.9), is evidence that vesicular pores do not directly inhibit infiltration. No significant correlation was observed between VHI and K_{sat}, in either the pre-disturbance ($r = 0.23$, $p = 0.41$) or post-disturbance ($r = -0.25$, $p = 0.38$) soils, as previously hypothesized (Turk and Graham, 2011). This suggests that vesicular pores are a consequence rather than a cause of low infiltration rates in the vesicular horizon. Vesicular pores are associated with soils that have restricted K_{sat} for various reasons, including silt- and clay-rich textures generated through eolian inputs (McFadden et al., 1998; Anderson et al., 2002; Turk and Graham, 2011), low aggregate stability (Bouza et al., 1993), and low canopy cover, which promotes surface crusting through raindrop impact (Abrams and Parsons, 1991; Hillel, 1998). We find no evidence that the non-connected vesicular pores and vughs have a direct effect on infiltration, as suggested by some past studies (Blackburn, 1975; Valentin, 1994; Brown and Dunkerley, 1996; Lebedeva et al., 2009).

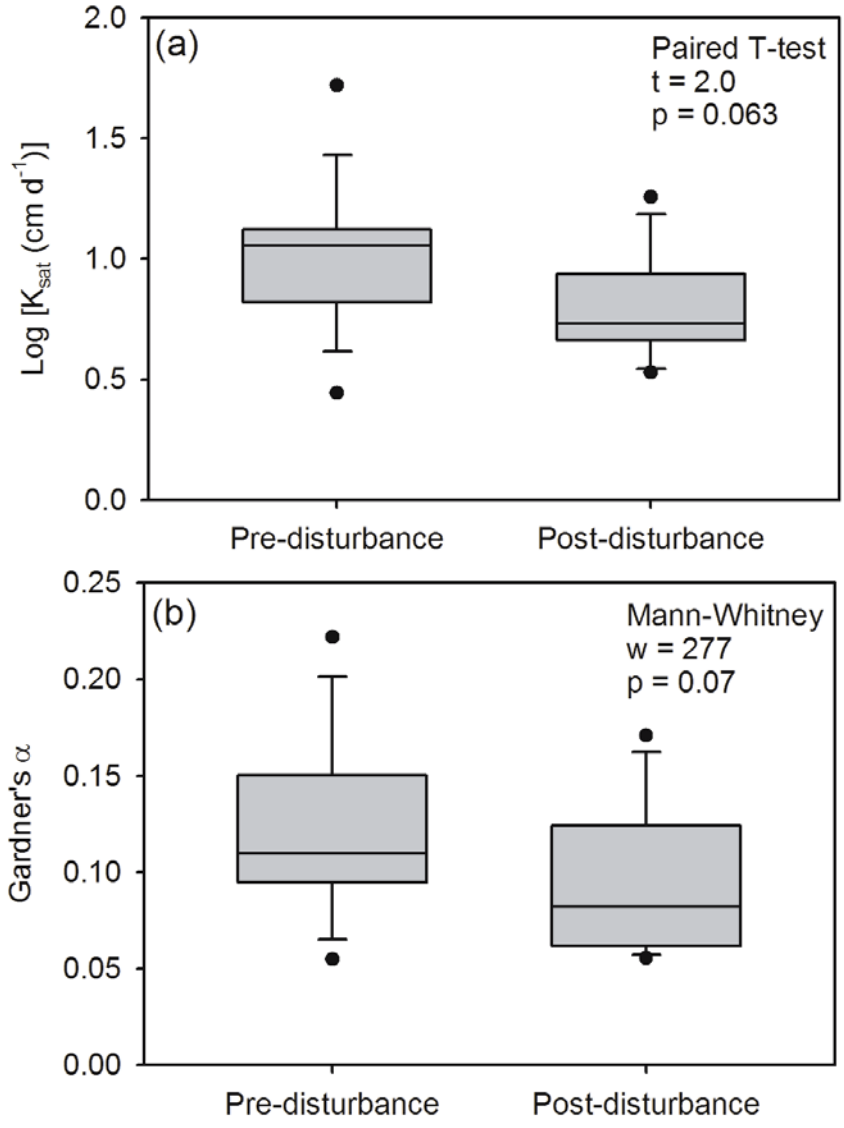

Fig. 3.22. Box plots of the hydraulic properties for pre-and post-disturbance vesicular horizons: (a) the logarithm of saturated hydraulic conductivity (K_{sat}) and (b) Gardner's α. Boxes depict the upper and lower quartiles, center bars depict the median values, whiskers depict extreme values (within a distance from the box of 1.5 times the interquartile range), and points indicate outliers (outside a distance from the box of 1.5 times the interquartile range).

Similar changes to the hydraulic properties of vesicular soils were shown by Caldwell et al. (2006), following disturbance by military tracked vehicles. That study showed that the impact of disturbance on K_{sat} is dependent on the intensity of disturbance. Low intensity disturbance (e.g., individual tracks made by one or two passes), led to an increase in K_{sat}, which was attributed to disruption of the surface crust. High intensity disturbance (e.g., repeatedly trafficked areas), led to a decrease in K_{sat} and α, reflecting the loss of macroporosity due to compaction. The artificial disturbance applied in the current study is most similar to the high-intensity disturbance, because it results in elimination of structure and macroporosity. Thus, the reduction of K_{sat} and α that we observed following disturbance is in agreement with the findings of Caldwell et al. (2006). The decrease in K_{sat} may be primarily due to the destruction of the columnar structure, which was either absent or weakly reformed following the recovery period. A previous study, using dye to indicate the flow path of water moving through vesicular soils, showed that most infiltration occurs through the cracks between polygonal structural units (Meadows et al., 2008).

Anthropogenic disturbance that impacts the hydraulic properties of soils are of critical concern in desert ecosystems. Water is the most limiting resource in desert ecosystems and soil hydraulic properties partition water between runoff, drainage, evaporation, and transpiration (Noy-Meir et al., 1973). Vesicular horizons typically have very low infiltration rates (Turk and Graham, 2011), but we have shown that infiltration rates can be further reduced through disturbance that results in a loss of macroporosity and interpedal cracks (Fig. 3.14). This can be expected to increase runoff, resulting in a

more patchy pattern of water storage, and potentially increasing erosion of the vesicular horizon (Eckert et al., 1979).

Based on our observations in this study, it can be predicted that the hydraulic properties of the vesicular horizons will recover from disturbance as the vesicular horizon morphology recovers. The observed decrease in K_{sat} and α were not statistically significant, indicating that the alteration of hydraulic properties following disturbance was relatively minor. The loss of infiltration capacity following disturbance can be attributed to the loss of macroporosity, which we expect to recover over a period of two to 11 years (Table 3.5). Although the vesicular pores and vughs are isolated pores, which do not conduct water, interconnected pore networks are formed by fissures between the isolated pores (Figs. 3.3c and 3.10). Calcitans and argillans that line the surface of interconnected pores in vesicular soils, suggest that water is transported through these pores (Sullivan and Koppi, 1991; Anderson et al., 2002). Horizontal fissures between platy units in the vesicular horizons promote water transport from the exterior to the interior of polygonal structural units (Anderson et al., 2002). We do not know how much time is required for the recovery of columnar structure and polygonal cracks that promote infiltration in vesicular soils (Meadows et al., 2008); however, we did observe weak prismatic structure in some of the disturbance plots, following only one year of recovery (Fig. 3.6b). Polygonal cracks were also observed in tire tracks (Fig. 3.13b), which suggests that preferential flow through polygonal cracks between structural units would be unaffected in the tire tracks.

The results of our study support the conclusion of Caldwell et al. (2006), that ripping, a practice sometimes used to alleviate compaction for the remediation of disturbed desert lands, should not be recommended for vesicular soils. This practice would slow the recovery of structure and porosity that naturally reform following disturbance in response to repeated wetting and drying by precipitation events.

SUMMARY AND CONCLUSIONS

Vesicular pores were observed to form in disturbed soils during a one-year recovery period following disturbance. However, in contrast to previous findings (Yonovitz and Drohan, 2009), significant differences were observed between the pre- and post-disturbance soils, suggesting that more than one year is required for complete recovery of the vesicular horizons. The post-disturbance vesicular horizons formed during the recovery period were thinner than the pre-disturbance vesicular horizons (Fig. 3.8) and contained less total volume of vesicles, vughs, and interconnected pores (Figs. 3.9a, 3.10a, and 3.11a). For all types of pores, the number of pores that reformed following disturbance was similar to the pre-disturbance soils (Figs. 3.9b, 3.10b, and 3.11b), but the individual pores were smaller in volume (Figs. 3.9c, 3.10c, and 3.11c). Variation in recovery between field sites was best explained by the number of precipitation events experienced during the recovery period (Fig. 3.12b). This relationship can be used to predict the time required for recovery of vesicular horizon properties following disturbance (eq. 3.6, Table 3.5). We predict recovery periods between two and 11 yrs for the field areas considered in the study; however, longer-term observations are required to verify these predictions.

Previously disturbed vesicular horizons, indicated by tire tracks and coppice dunes, were observed in order to determine the effects of real-world disturbance on vesicular horizon properties. Vesicular horizons in the tire tracks were thinner than those beneath the undisturbed

desert pavement; however, the pore morphology in the upper part of the horizon (0-15 mm) was similar to that of the undisturbed vesicular horizons. In the vesicular horizons beneath the coppice dunes, vesicular pores, vughs, and interconnected pores were smaller in volume. Planer voids were prominent in the buried vesicular horizons, resulting from the collapse of large pores along horizontal planes of weakness.

Vesicular horizon disturbance led to a decrease in K_{sat} and Gardner's α, however, neither of these hydraulic properties were significantly changed at the $\alpha = 0.05$ level (Fig. 3.22). The decreased infiltration rates in the post-disturbance soils are most likely attributable to the loss of polygonal cracks, which promote preferential flow through the vesicular horizon (Meadows et al., 2008).

REFERENCES

Abrahams, A.D., and A.J. Parsons. 1991. Relation between infiltration and stone Cover on a semiarid hillslope, southern Arizona. J. Hydrol. 122:49-59.

Amundson, R.G., O.A. Chadwick, J.M. Sowers, and H.E. Doner. 1989. Soil evolution along an altitudinal transect in the eastern Mojave Desert of Nevada, USA. Geoderma 43:349-371.

Anderson, K., S. Wells, and R. Graham. 2002. Pedogenesis of vesicular horizons, Cima Volcanic Field, Mojave Desert, California. Soil Sci. Soc. Am. J 66:878-887.

Associate Press. 2010. Solar showdown in tortoises' home. Available at <http://www.msnbc.msn.com/id/34659369/ns/us_news-environment/> (accessed 11 Nov 2010). MSNBC.

Barbour, M.G., J.H. Burk, W.D. Pitts, F.S. Gilliam, and M.W. Schwartz. 1999. Methods of sampling the plant community. *In* Barbour et al. Terrestrial plant ecology. Benjamin/Cummings, Menlo Park, CA.

Beckman, W. 1962. Zur Mikromorphometrie von hohlräumen und aggregaten im boden. (in German) Zeitsh Pflazern, Düng, Bodend 99:129-139.

Blackburn, W.H. 1975. Factors influencing infiltration and sediment production of semiarid rangelands in Nevada. Water Resour. Res. 11:929-937.

Bockheim, J.G. 2010. Evolution of desert pavements and the vesicular layer in soils of the Transantarctic Mountains. Geomorphology 118:433-443.

Bouza, P., H.F. Delvalle, and P.A. Imbellone. 1993. Micromorphological, physical, and chemical characteristics of soil crust types of the central Patagonia region, Argentina. Arid Soil Res. Rehabilitation 7:355-368.

Bower, C.A., and J.T. Hatcher. 1966. Simultaneous determinations of surface area and cation exchange capacity. Soil Sci. Soc. Am. Proc. 30:525-527.

Brewer, R. 1976. Fabric and mineral analysis of soils. Robert E. Krieger, Huntington, NY.

Brown, K.J., and D.L. Dunkerley. 1996. The influence of hillslope gradient, regolith texture, stone size and stone position on the presence of a vesicular layer and related aspects of hillslope hydrologic processes: A case study from the Australian arid zone. Catena 26:71-84.

Brun, F., L. Mancini, P. Kasae, S. Favretto, D. Dreossi, and G. Tromba. 2010. Pore3D: A software library for quantitative analysis of porous media. Nucl. Instrum. Meth. A. 615:326-332.

Bunting, B.T. 1977. The occurrence of vesicular structures in arctic and subarctic soils. Z. Geomorphol. 21:87-95.

Burt, R. (ed.) 2004. Soil Survey Laborator Methods Manual. Soil Suvey Investigations Report No. 42. USDA, Washington, DC.

Caldwell, T.G., E.V. McDonald, and M.H. Young. 2006. Soil disturbance and hydrologic response at the National Training Center, Ft. Irwin, California. J. Arid Environ. 67:456-472.

Cantón, Y., A. Solé-Benet, and R. Lázaro. 2003. Soil-geomorphology relations in gypsiferous materials of the Tabernas Desert (Almeria, SE spain). Geoderma 115:193-222.

Dan, J., D.H. Yaalon, R. Moshe, and S. Nissim. 1982. Evolution of reg soils in southern Israel and Sinai. Geoderma 28:173-202.

Eckert, R.E., M.K. Wood, W.H. Blackburn, F.F. Peterson, J.L. Stephens, and M.S. Meurisse. 1978. Effects of surface-soil morphology on improvement and management of some arid and semiarid rangelands. p. 299-301. *In* D.N. Hyder (ed.) Proc. of the First Int. Rangeland Congr., Denver, CO. 14-18 Aug. 1978. Society for Range Mangement, Denver, CO.

Eckert, R.E., F.F. Peterson, and J.T. Belton. 1986a. Relation between ecological-range condition and proportion of soil-surface types. J. Range Manage. 39:409-414.

Eckert, R.E., F.F. Peterson, M.S. Meurisse, and J.L. Stephens. 1986b. Effects of soil-surface morphology on emergence and survival of seedlings in big sagebrush communities. J. Range Manage. 39:414-420.

Ellis, F. 1990. Note on soils with vesicular structure and other micromorphological features in Karoo soils. p. 326-336. *In* Proc. 16th Congress of the Soil Science Society of South Africa, Pretoria, South Africa. July 9-12 1990. Soil Science Society of South Africa, Erasmusrand, South Africa.

Evenari, M., D.H. Yaalon, and Y. Gutterman. 1974. Note on soils with vesicular structure in deserts. Z. Geomorphol. 18:162-172.

Figueira, H., and G. Stoops. 1983. Application of micromorphometric techniques to the experimental study of vesicular layer formation. Pedologie 33:77-89.

Fenimore, C. 2011. NCDC: Locate Weather Observation Station Record. Available at http://www.ncdc.noaa.gov/oa/climate/stationlocator.html (verified 15 Jan. 2012). Natl. Oceanic and Atmospheric Administration, Natl. Climatic Data Cent., Ashville, NC.

French, R.H. 1983. Precipitation in southern Nevada. J. Hydraul. Eng. 109:1023-1038.

Gardner, W.R. 1958. Some steady-state solutions of the unsaturated moisture flow equation with application to evaporation from a water table. Soil Sci 85:228-232.

Gile, L.H., and J.W. Hawley. 1968. Age and comparative development of desert soils at Gardner Spring radiocarbon site, New Mexico. Soil Sci. Soc. Am. Proc. 32:709-716.

Gilewitch, D.A. 2004. The effect of military operations on desert pavement: a case study from Butler Pass, AZ (USA). p. 243-258. *In* D. R. Caldwell et al. (ed.) Studies in military geography and geology. Kluwer Academic Publishers, Alphen aan den Rijn, The Netherlands.

Google Incorporated, 2011. Google Earth 6.1.0.5001. Google Inc., Mountain View, CA.

Goossens, D., and B. Buck. 2009. Dust emission by off-road driving: Experiments on 17 arid soil types, Nevada, USA. Geomorphology 107:118-138.

Hamerlynck, E.P., J.R. McAuliffe, E.V. McDonald, and S.D. Smith. 2002. Ecological responses of two Mojave Desert shrubs to soil horizon development and soil water dynamics. Ecology 83:768-779.

Harvey, A.M., P.E. Wigand, and S.G. Wells. 1999. Response of alluvial fan systems to the late Pleistocene to Holocene climatic transition: contrasts between the margins of pluvial Lakes Lahontan and Mojave, Nevada and California, USA. Catena 36:255-281.

Henning, J.A.G., and K. Kellner. 1994. Degradation of a soil (Aridosol) and vegetation in the semiarid grasslands of southern Africa. Bot. Bull. Acad. Sin. 35:195-199.

Hillel, D. 1998. Environmental Soil Physics Academic Press, San Diego, CA.

Hugie, V.K., and H.B. Passey. 1964. Soil surface patterns of some semiarid soils in northern Utah, southern Idaho, and northeastern Nevada. Soil Sci. Soc. Am. Proc. 28:786-792.

Issa, O.M., J. Trichet, C. Defarge, A. Coute, and C. Valentin. 1999. Morphology and microstructure of microbiotic soil crusts on a tiger bush sequence (Niger, Sahel). Catena 37:175-196.

Joeckel, R.M., and B.A. Clement. 1999. Surface features of the Salt Basin of Lancaster County, Nebraska. Catena 34:243-275.

Ketcham, R.A. 2005. Computational methods for quantitative analysis of three-dimensional feature in geological specimens. Geosphere 1:32-41.

Lebedeva, M.P., D.L. Golovanov, and S.A. Inozemtsev. 2009. Microfabrics of desert soils of Mongolia. Euras. Soil Sci. 42:1204-1217.

Lovich, J.E., and D. Bainbridge. 1999. Anthropogenic degradation of the southern California desert ecosystem and prospects for natural recovery and restoration. Environ. Manag. 24:309-326.

Matmon, A., O. Simhai, R. Amit, I. Haviv, N. Porat, E. McDonald, L. Benedetti, and R. Finkel. 2009. Desert pavement-coated surfaces in extreme deserts present the longest-lived landforms on Earth. Geol. Soc. Am. Bull. 121:688-697.

McAuliffe, J.R. 1994. Landscape evolution, soil formation, and ecological patterns and processes in Sonoran Desert bajadas. Ecol. Monogr. 64:111-148.

McAuliffe, J.R., and E.V. McDonald. 2006. Holocene environmental change and vegeation contraction in the Sonoran Desert. Quat Res 65:204-215.

McDonald, E.V. 1994. The relative influences of climatic change, desert dust, and lithologic control on soil-geomorphic processes and soil hydrology of calcic soils formed on quaternary alluvial-fan deposits in the Mojave Desert, California. Ph.D. Dissertation, The University of New Mexico, Albuquerque, NM.

McDonald, E.V., L.D. McFadden, and S.G. Wells. 1995. The relative influences of climate change, desert dust, and lithologic control on soil-geomorphic processes on alluvial fans, Mojave Desert, California: Summary of results. p. 35-42. *In* R. E. Reynolds and J. Reynolds (ed.) Ancient surfaces of the East Mojave Desert: a volume and field trip guide prepared in conjunction with the 1995 Desert Research Symposium. Quarterly of the San Bernardino County Museum Association. San Bernardino County Museum Association, Redlands, CA.

McFadden, L.D., E.V. McDonald, S.G. Wells, K. Anderson, J. Quade, and S.L. Forman. 1998. The vesicular layer and carbonate collars of desert soils and pavements: formation, age and relation to climate change. Geomorphology 24:101-145.

McFadden, L.D., S.G. Wells, and M.J. Jercinovich. 1987. Influences of eolian and pedogenic processes on the origin and evolution of desert pavements. Geology 15:504-508.

Meadows, D.G., M.H. Young, and E.V. McDonald. 2008. Influence of relative surface age on hydraulic properties and infiltration on soils associated with desert pavements. Catena 72:169-178.

Miller, D.E. 1971. Formation of vesicular structure in soil. Soil Sci. Soc. Am. Proc. 35:635-637.

Miller, D.M., D.R. Bedford, D.L. Hughson, E.V. McDonald, S.E. Robinson, and K.M. Schmidt. 2009. Mapping Mojave Desert ecosystem properties with surficial geology. p. 225-251. *In* R. H. Webb et al. (ed.) The Mojave Desert: Ecosystem Processes and Sustainability. University of Nevada Press, Reno, NV.

Minitab. 2010. MINITAB 16. Minitab, State College, PA.

Musick. 1975. Barrenness of desert pavement in Yuma County, Arizona. J. Arizona Acad. Sci. 10:24-28.

Noy-Meir, I. 1973. Desert ecosystems: environment and producers. Annu. Rev. Ecol. Syst. 4:25-51.

Paletskaya, L.N., A.P. Lavrov, and S.I. Kogan. 1958. Pore formation in takyr crust. Sov. Soil Sci. (Engl. Transl.) 3:245-250.

Pelletier, J.D., M. Cline, and S.B. DeLong. 2007. Desert pavement dynamics: numerical modeling and field-based calibration. Earth Surf. Process Landforms 32:1913-1927.

Peterson, F.F. 1980. Holocene desert soil formation under sodium-salt influence in a playa-margin environment. Quat. Res. 13:172-186.

Quade, J. 2001. Desert pavements and associated rock varnish in the Mojave Desert: How old can they be? Geology 29:855-858.

Reheis, M.C., J.W. Harden, L.D. McFadden, and R.R. Shroba. 1989. Development rates of late quaternary soils, Silver Lake Playa, California. Soil Sci. Soc. Am. J. 53:1127-1140.

Schlesinger, W.H., J.F. Reynolds, G.L. Cunningham, L.F. Huenneke, W.M. Jarrell, R.A. Virginia, and W.G. Whitford. 1990. Biological feedbacks in global desertification. Science 247:1043-1048.

Schoeneberger, P.J., D.A. Wysocki, E.C. Benham, and W.D. Broderson. (eds.) 2002. Field book for describing and sampling soils, Version 2.0. NRCS National Soil Survey Center, Lincoln, NE.

Segal, E., P.J. Shouse, S.A. Bradford, T.H. Skaggs, and D.L. Corwin. 2009. Measuring particle size distribution using laser diffraction: implications for predicting soil hydraulic properties. Soil Sci. 174:639-645.

Shafer, D.S., M.H. Young, S.F. Zitzer, T.G. Caldwell, and E.V. McDonald. 2007. Impacts of interrelated biotic and abiotic processes during the past 125 000 years of landscape evolution in the Northern Mojave Desert, Nevada, USA. J. Arid Environ. 69:633-657.

Smith, S.D., C.A. Herr, K.L. Leary, and J.M. Piorkowski. 1995. Soil-plant water relations in a Mojave Desert mixed shrub community: a comparison of three geomorphic surfaces. J Arid Environ 29:339-351.

Soil Survey Staff. 2010. Keys to Soil Taxonomy, 11th ed. USDA Natural Resources Conservation Service, Washington, DC.

Springer, M.E. 1958. Desert pavement and vesicular layer of some soils of the desert of the Lahontan Basin, Nevada. Soil Sci. Soc. Am. Proc. 22:63-66.

Stevenson, B.A., E.V. McDonald, and T.G. Caldwell. 2009. Root patterns of Larrea tridentata in relation to soil morophology in Mojave Desert soils of different ages. p. 225-251, *In* R. H. Webb et al. (ed.) The Mojave Desert: Ecosystem Processes and Sustainability. University of Nevada Press, Reno, NV.

Stoops, G. 2003. Guidelines for Analysis and Description of Soil and Reolith Thin Sections Soil Science Society of America, Madison, WI.

Strathouse, S.M. 1982. Genesis and mineralogy of soils on an alluvila fan, western Mojave Desert, California. Ph.D. Dissertation, University of California, Riverside, CA.

Sullivan, L.A., and A.J. Koppi. 1991. Morphology and genesis of silt and clay coatings in the vesicular layer of a desert loam soil. Aust. J. Soil Res. 29:579-586.

Systat Software. 2007. SigmaPlot 10. Systat Software, Chicago, IL.

Thomas, G.W. 1982. Exchangeable Cations. p. 159-165. *In* A. L. Page, (ed.) Methods of Soil Analysis. Part 2. 2nd ed. Agron. Monogr. 9. ASA and SSSA, Madison, WIl

Turk, J.K., and R.C. Graham. 2011. Distribution and properties of vesicular horizons in the western United States. Soil Sci. Soc. Am. J. 75:1449-1461.

Ugolini, F.C., S. Hillier, G. Certini, and M.J. Wilson. 2008. The contribution of aeolian material to an Aridisol from southern Jordan as revealed by mineralogical analysis. J. Arid Environ. 72:1431-1447.

Valentin, C. 1994. Surface sealing as affected by various rock fragment covers in West-Africa. Catena 23:87-97.

Valentine, G.A., and C.D. Harrington. 2006. Clast size controls and longevity of Pleistocene desert pavements at Lathrop Wells and Red Cone volcanoes, southern Nevada. Geology 34:533-536.

Van Vliet-Lanoë, B. 1985. Frost effects in soils. *In* J. Boardman (ed.) Soils and quaternary landscape evolution. John Wiley and Sons, Chichester, UK.

Webb, R.H., J. Belnap, and K.A. Thomas. 2009. Natural recovery from severe disturbance in the Mojave Desert. p. 343-377, *In* R. H. Webb et al. (ed.) The Mojave Desert: Ecosystem Processes and Sustainability. University of Nevada Press, Reno, NV.

Wells, S.G., L.D. McFadden, J. Poths, and C.T. Olinger. 1995. Cosmogenic ^{3}He surface-exposure dating of stone pavements: Implications for landscape evolution in deserts. Geology 23:613-616.

Western Regional Climate Cent. 2011. RAWS USA climate archive. Available at <http://www.raws.dri.edu/> (accessed 15 Jan. 2012). Desert Research Institute, Reno, NV.

Williams, D.E. 1948. A rapid manometric method for determination of carbonate in soils. Soil Sci. Soc. Am. Proc. 13:127-129.

Williams, A., B. Buck, D. Soukup, and D. Merkler. 2010. Biological soil crusts and the fertile island effect: Soil-geomophic insights from the Mojave Desert, USA. *In* Abstracts, ASA-CSSA-SSSA Int. Annu. Meet., Long Beach, CA. 31 Oct.-3 Nov. 2010. ASA-CSSA-SSSA, Madison, WI.

Wood, M.K., W.H. Blackburn, R.E. Eckert, and F.F. Peterson. 1978. Interrelations of physical-properties of coppice dune and vesicular dune interspace soils with grass seedling emergence. J. Range Manage. 31:189-192.

Wood, M.K., R.E. Eckert, W.H. Blackburn, and F.F. Peterson. 1982. Influence of crusting soil surfaces on emergence and establishment of crested wheat-grass,

squirreltail, thurber needlegrass, and fourwing saltbush. J. Range Manage. 35:282-287.

Wood, Y.A., R.C. Graham, and S.G. Wells. 2002. Surface mosaic map unit development for a desert pavement surface. J. Arid Environ. 52:305-317.

Wood, Y.A., R.C. Graham, and S.G. Wells. 2005. Surface control of desert pavement pedologic process and landscape function, Cima Volcanic field, Mojave Desert, California. Catena 59:205-230.

Wooding, R.A. 1968. Steady infiltration from a shallow circular pond. Water Resour Res 4:1259-1273.

Yonovitz, M., and P.J. Drohan. 2009. Pore morphology characteristics of vesicular horizons in undisturbed and disturbed arid soils; implications for arid land management. Soil Use Manage. 25:293-302.

Yonovitz, M.L. 2008. Pedogenesis of vesicular horizons in disturbed and undisturbed soils. M.S. Thesis, University of Nevada, Las Vegas.

Young, M.H., E.V. McDonald, T.G. Caldwell, S.G. Benner, and D.G. Meadows. 2004. Hydraulic properties of a desert soil chronosequence in the Mojave Desert, USA. Vadose Zone J. 3:956-963.

4. MECHANISMS OF VESICULAR PORE FORMATION IN DESERT SOILS

ABSTRACT

Vesicular horizons are common surficial horizons in desert soils, which are critical to the regulation of surface hydrology in desert ecosystems. They are characterized by the prevalence of bubble-like vesicular pores, but little is known about how these pores form. In this study, we test two hypotheses about the formation of vesicular pores: 1) that vesicular pores are formed by CO_2 gas bubbles that are produced through microbial respiration, and 2) that vesicular pore growth is promoted by thermal expansion of gases. The hypotheses were tested by recreating vesicular pores in the laboratory through exposure to repeated wetting and drying. In the first experiment, vesicular pore growth was compared in sterile, innoculated, and glucose-amended soil material. In the second experiment, the temperature increase between wetting and drying was varied. The treatment groups included a 33^{o}C temperature increase (7^{o}C to 40^{o}C), a 17^{o}C temperature increase (23^{o}C to 40^{o}C), and a 0^{o}C temperature increase (40^{o}C to 40^{o}C). We found indirect evidence for the role of biological processes in vesicular pore formation including: 1) increased vesicular pore formation in response to a labile C source (*i.e.*, glucose), and 2) decreased vesicular pore formation in soils wet at temperatures near biological zero. However, there was no significant effect of sterilization on vesicular pore formation, which indicates that there is also an abiotic mechanism of vesicular pore formation. Vesicular pore formation through thermal expansion of gases was not supported by our experiments, which showed the greatest vesicular pore formation when soils were wet and dried at constant temperature. Overall,

these experiments indicate that both biotic and abiotic mechanisms are involved in vesicular pore formation and that thermal expansion of gases does not promote vesicular pore formation.

INTRODUCTION

Vesicular horizons are a common feature of soils in arid and semi-arid lands. They are distinguished by the prevalence of non-interconnected, nearly spherical vesicular pores. Vesicular horizons restrict infiltration rates and thereby regulate the distribution of water in arid and semi-arid landscapes (Blackburn, 1975; Valentin, 1994; Brown and Dunkerley, 1996; Young et al., 2004). The redistribution of water in arid landscapes can lead to large subsurface accumulations of soluble salts (Musick, 1975; Young et al., 2004; Wood et al., 2005; Graham et al., 2008), and is critical to defining plant-water relations (Noy-Meir, 1973; Musick, 1975; Smith et al., 1990; McAuliffe, 1994; Hamerlynck et al., 2002; Wood et al., 2005; Miller et al., 2009). Crusting and polygonal cracking in vesicular horizons affect the response of these soils to seeding methods used in rangelands restoration (Wood et al., 1978; Wood et al., 1982; Eckert et al., 1986). Vesicular horizons are a dynamic soil feature, capable of forming in a short period of time (Yonovitz and Drohan, 2009), and have been considered diagnostic of a shift towards a more arid ecosystem and desert pedogenesis (Lebedeva et al., 2009).

Vesicular horizons are widespread in deserts of the western United States, where they cover an estimated 156,000 km^2 of the land area (Turk and Graham, 2011). Vesicular horizons occur in landscapes with sparse vegetation (Brewer, 1976; Amundson et al., 1989; Ellis, 1990; McFadden et al., 1998; Joeckel and Clement, 1999); and within

these landscapes, the vesicular horizons occur in the intercanopy soils, and are not typically observed beneath the shrub canopy (Eckert et al., 1978; Wood et al., 1978). Vesicular horizons often occur beneath desert pavement (Peterson, 1980; Amit and Gerson, 1986; Amundson et al., 1989; Ellis, 1990; Bouza et al., 1993; Anderson et al., 2002; Valentine and Harrington, 2006; Matmon et al., 2009; Bockheim, 2010), but may also occur in soils with a physical surface crust (Brewer, 1976; Eckert et al., 1978; Ellis, 1990; Hillel, 1998; Cantón et al., 2003) or biological surface crust (Issa et al., 1999; Joeckel and Clement, 1999; Cantón et al., 2003; Williams et al, 2010). They are commonly formed in a silt-rich layer that is formed by eolian additions to the soil (Hugie and Passey, 1964; McFadden et al, 1987; Amundson et al., 1989; Reheis et al., 1992; McFadden et al., 1998; Anderson et al., 2002).

Vesicular horizons are typically one to 10 cm thick (Miller, 1971; Evenari et al., 1974; Wood et al., 1978; Peterson, 1980; Dan et al., 1982; Van Vliet-Lanoë, 1985; Amundson et al., 1989; McDonald et al., 1995; Joeckel and Clement, 1999; Quade, 2001; Ugolini et al., 2008; Miller et al., 2009; Yonovitz and Drohan, 2009; Turk and Graham, 2011). The vesicular pores occur as non-interconnected pores with smooth walls and an equant, oblate, or prolate shape (Brewer, 1976; Sullivan and Koppi, 1991; Stoops, 2003). They typically range in size from less than one to three millimeters in diameter (Evenari et al., 1974; Peterson, 1980; Joeckel and Clement, 1999). The texture of the vesicular horizon is most often in the sandy loam, loam, or silt loam textural classes (Peterson, 1980; Wood et al., 1982; Turk and Graham, 2011). Vesicular horizons may be massive or platy, or they may have a primary structure consisting of columns or prisms that part to

a secondary platy structure (Springer, 1958; Peterson, 1980; McFadden et al., 1998; Anderson, 2002; Caldwell et al., 2006).

Although vesicular horizons are a common and dynamic feature of the arid landscape, little is known about the mechanisms that drive their formation. Vesicular pores form through repeated wetting and drying of the soil and they can be recreated in the laboratory by application of repeated wet/dry cycles (Springer, 1958; Miller, 1971; Evenari et al., 1974; Figueira and Stoops, 1983). Vesicular pore formation is generally attributed to gas bubbles that form during soil wetting that become "frozen" in place as the soil dries (Hugie and Passey, 1964; Brewer, 1976; Stoops, 2003). However, the mechanisms by which gases become trapped and grow over successive wet/dry cycles have not been evaluated. Several mechanisms have been proposed, which are summarized and discussed below.

(1) *$CaCO_3$ precipitation.* When $CaCO_3$ precipitates, CO_2 gas is released:

$$Ca^{2+} + 2HCO_3^- \rightarrow CaCO_3 + H_2O + CO_2 \qquad \text{(eq. 4.1)}$$

This has led some authors to suggest that $CaCO_3$ precipitation is what forms the gas bubbles that generate vesicular pores (Paletskaya et al., 1958; Evenari et al., 1974; Lebedeva et al., 2009). However, given the low solubility of $CaCO_3$ in the soil solution (0.0006 mol L^{-1}) (Turk et al., 2011), it is unlikely that the dissolution and re-precipitation of $CaCO_3$ during wetting and drying could contribute significantly to the production of vesicular pores. Furthermore vesicular pores are noted to occur in soils that contain no

$CaCO_3$ (Bunting, 1977; Bockheim, 2010, Turk and Graham, 2011), which means that other mechanisms must contribute to the formation of vesicular pores.

(2) *Biological production of gases*. The rapid microbial response to precipitation in arid environments (Austin et al., 2004; Huxman et al., 2004) may play a role in the production of gas bubbles that form vesicular pores. An early experiment examined the role of O_2 bubbles, produced through algal photosynthesis, in vesicular pore formation, but found no evidence to support this hypothesis (Paletskaya et al., 1958). Another possibility is that the CO_2 released by microbial respiration is responsible for the gas bubbles. Some authors have discounted this mechanism, due to the low biological activity of soils with vesicular pores (Paletskaya et al., 1958) and the observation of vesicular pores beneath, but not within, biological soil crusts (Joeckel and Clement, 1999). However, no further investigation of this mechanism has been made.

(3) *Decrease in pressure*. The ideal gas law defines an inverse relationship between pressure and volume of a gas:

$$PV = nRT \qquad \text{(eq. 4.2)}$$

where, P = pressure, V = volume, n = number of moles of gas, R = gas constant, and T = temperature. A decrease in pressure could cause vesicular pore formation by reducing the solubility of gases in the soil solution and promoting expansion of trapped gases. This mechanism has been invoked to explain the formation of vesicular pores in cryoturbated soils. In these soils, the formation of vesicular pores was attributed to the

reduction in pressure in upward thrust soil masses (Bunting, 1977). In desert soils, production of vesicular pores has been attributed to a reduction in pressure, due to the formation of a surface seal (Hillel, 1998). This seal prevents further entry of water or air, under which condition, drainage of water from the vesicular layer would generate negative pressure. The formation of bubbles in silt-rich soil material often occurs during vacuum extraction of saturation pastes, which has been observed by the current author, as well as others (Bunting, 1977). However, such a dramatic decrease in pressure is unlikely to occur under field conditions.

(4) *Increase in temperature*. The ideal gas law (eq. 4.2) defines a positive relationship between temperature and volume of a gas. Similar to decreasing pressure, increasing temperature could cause vesicular pore formation by reducing the solubility of gases in the soil solution and promoting the expansion of trapped gases. Expansion of trapped gases by solar heating is a commonly cited explanation for the formation of vesicular pores (Evenari et al., 1974; Henning and Kellner, 1994; Brown and Dunkerley, 1996), and the thermal gradient at the soil surface is often offered as an explanation for the occurrence of larger, more equant vesicles in the upper part of the vesicular horizon (Paletskaya et al., 1958; Hugie and Passey, 1964; Ellis, 1990; Bouza et al., 1993; McFadden et al., 1998). However, no past study has tested the role of thermal expansion in the formation of vesicular pores.

All of the mechanisms described above may contribute to the formation of vesicular pores, to varying degrees, in different soil-forming environments. We have selected two for evaluation in the current study: 1) production of CO_2 bubbles by microbial respiration, and 2) thermal expansion.

MATERIALS AND METHODS

Sampling and laboratory characterization

A bulk sample of soil material was collected from a well-developed vesicular horizon in the Mojave Desert for use in all of the laboratory experiments on vesicular pore formation. The sampling location was on the northern end of the Johnson Valley Off-Highway Vehicle area in San Bernardino County, California (34°35'13.5''N, 115°38'23.6''W). The vesicular horizons at this site occurred on alluvial fan remnants, beneath a desert pavement layer. The soil mapped in this part of the landscape was the Oldwoman soil series, a loamy-skeletal, mixed, superactive, thermic Typic Calciargid (Soil Survey Staff, 2012).

Laboratory characterization data of the vesicular horizon are provided in Table 4.1. Electrical conductivity was measured in the saturation paste extract and pH was measured in 1:1 soil:water suspension (Burt, 2004). Cation exchange capacity was measure by Na saturation, followed by extraction with ammonium acetate (Bower and Hatcher, 1966), and measurement of Na by inductively coupled plasma (ICP) spectroscopy. Exchangeable Na was extracted in 1 N ammonium acetate (Thomas, 1982), and also measured by ICP spectroscopy. Soluble Na was measured in the

Table 4.1. Laboratory characterization data of the soil material, including electrical conductivity of the saturation paste extract (EC_e), pH in 1:1 H_2O, exchangeable sodium percentage (ESP), calcium carbonate percent by weight, and the percentage of the three soil separates (sand, silt, and clay).

EC_e	pH	ESP	$CaCO_3$	Sand	Silt	Clay
ds m^{-1}		%	%	%	%	%
2.7	8.75	28.2	3.4	28.2	49.5	22.3

saturation paste extract using a sodium-selective electrode. Exchangeable Na was corrected for soluble sodium in the calculation of exchangeable sodium percentage (Burt, 2004). Calcium carbonate was measured by the manometer method (Williams, 1948) and particle size distribution was evaluated by the wet sieving/laser diffraction method (Segal et al., 2009).

Vesicular pore formation and analysis

Vesicular pores were recreated in the laboratory through exposure to repeated wetting and drying (Springer, 1958; Miller, 1971; Evenari et al., 1974; Figueira and Stoops, 1983). The methods that we followed are closest to those of Miller (1971). The soil material was air-dried and sieved to 1 mm. In plastic cups, 350 g of soil was mixed to a saturation state with 50 mL of deionized water. Parchment-lined aluminum columns, 7.5 cm in diameter and 7.5 cm tall, were placed on ceramic plates, with five columns per plate. The saturation pastes were transferred to the columns and then dried for five days in a 40^{o}C oven. After the drying period, the samples were wet again by placing the ceramic plate in water and allowing the samples to wet by capillary rise for 24 hrs, and then adding five to 10 mL of water to the top of the columns. Preliminary experiments using other methods of wetting were unsuccessful at forming vesicular pores. If the dry soil was wet by capillary rise without initially making a saturation paste, the vesicular pores did not form because the surface did not form a dispersion crust, which prevents air from escaping at the soil surface (Evenari et al., 1974). If the soil was wet by flooding in

a closed-bottom container, the air trapped in the soil formed a large pocket at the bottom of the container, rather than vesicular pores within the soil matrix.

Wetting by capillary rise was repeated 19 times, with a five day drying period at 40^{o}C between each wetting. After every five drying periods the samples were removed from the columns, and bulk density was measured by the three-dimensional laser scanning method (Rossi et al., 2008). At the end of the experiment, four of the samples from each treatment group were scanned by X-ray computed tomography (CT), with a resolution of 0.0752 mm and an inter-slice spacing of 0.08118 mm.

The CT-generated images were analyzed using the Blob3D software (Ketcham et al., 2005). All pores within a cylindrical volume of interest (60 mm diam., 16.2 mm height), positioned near the top surface of the sample, were segregated and analyzed. The pores were segregated using a general threshold filter, which was adjusted until the binary image produced by the filter showed good agreement with visual segregation of voids in the grayscale image. The volume and surface area of all voids were extracted from the scans and used to calculate a volumetric form of the lobation ratio (LR), previously used for two-dimensional analysis of pore-shape in thin sections (Beckman, 1962; Figueira and Stoops, 1983). The LR is the ratio between the actual perimeter of the pore and the calculated perimeter, which is the perimeter of a hypothetical circle with an area equal to the measured area of the pore. The volumetric form of the LR (LR_v) is the ratio between the actual surface area of the pore and the calculated surface area, which is the surface area of a hypothetical sphere with a volume equal to the measured pore volume. Pores were identified as vesicular when they had a LR_v greater than 0.79, a

cutoff determined by previous analysis of visually classified vesicles. For each CT scan, the percentage of sample volume occupied by vesicular pores ($V_{\%}$), number density of vesicular pores (N_p), and geometric mean of the individual pore volumes ($\overline{V}$) were calculated, as described in Chapter 3.

Microbial respiration treatments

Three treatment groups were established to determine the influence of microbial respiration on vesicular pore formation; these were sterile, inoculated, and glucose-amended inoculated soils. Each treatment was applied to five of the columns in which vesicular pores were recreated, as described above. Columns in the same treatment group were placed on the same ceramic plate, to prevent contamination of the sterile columns and to allow separate application of glucose solution to the glucose-amended soils. For all three treatment groups, the soils were first sterilized by autoclaving five times, with a one week period between each autoclaving. All columns and ceramic plates were also sterilized by autoclaving. For the sterile treatment group, the saturation paste used to fill the columns was made using sterile deionized water. For the inoculated treatment group, the sterile deionized water was mixed with unsterilized soil (10 g of soil per 50 mL of water) and shaken for 10 minutes before making the saturation paste. For the glucose amended inoculated soils, a sterile glucose solution (6.6 g L^{-1}) was mixed with unsterilized soil (10 g of soil per 50 mL of glucose solution) and shaken for 10 minutes before making the saturation paste. The final concentration of glucose in the columns was one mg per g of soil, which is the concentration of glucose used to maximize

respiration rates in the physiological method for microbial biomass determination (Anderson and Domsch, 1978). The sterilization and re-inoculation of the inoculated and glucose-amended treatments was intended to control for any side-effects that accompany autoclaving, such as increased soluble organic carbon concentration (Venterea, 2007). During drying, the columns were placed in sterilized dishpans that were covered with a double layer of gauze, to prevent contamination, while allowing the soil to dry. During wetting, the dishpans were covered with foil and sterile deionized water was used to wet all of the treatment groups. Every five wetting cycles, the glucose-amended soils were wet with glucose solution instead of sterilized water, in order to sustain high respiration rates.

The effectiveness of the treatments was verified by applying the same treatments to another set of soils, in which respiration rates were measured by the NaOH trap method (Zibilske, 1994). In addition to the treatments used in the experiment, the respiration rate of glucose-amended sterile soil was also measured in order to verify that there was no response to glucose following sterilization. The respiration rate of non-autoclaved soils was also measured, in order to test their similarity to the soils that were re-inoculated following sterilization. In addition, a set of repeated respiration measurements were made for the glucose-amended soils, in which the soils were dried at 40^{o}C between each measurement and then re-wet for the next respiration measurement. This treatment was applied to test the duration of the glucose response under cyclic wetting and drying conditions. All respiration measurements were made in replicates of five.

Temperature treatments

In this experiment, the soils in each treatment group were wet at three different temperatures (7^{o}C, 23^{o}C, and 40^{o}C) and then dried at the same temperature (40^{o}C). The treatments were each applied to five columns. Soil columns in the same treatment group were placed on the same ceramic plate, so that they could be co-located in the various temperature locations. Before each wetting cycle, the soil columns and the water were both placed at the wetting temperature overnight. After wetting the columns were moved to a 40^{o}C oven for the five day drying period.

Statistical Analysis

Statistical significance of the respiration results were analyzed by five t-tests, using the Bonferroni correction for multiple comparisons (Abdi, 2007). The five t-tests were: 1) sterile vs. inoculated, 2) sterile vs. glucose-amended sterile, 3) inoculated vs. glucose-amended inoculated, 4) non-autoclaved vs. inoculated, 5) glucose-amended non-autoclaved vs. glucose-amended inoculated. To achieved an α(per family) of 0.05, we used an α(per test) of 0.01 (Abdi, 2007).

Statistical significance of the bulk density results was determined by two-way ANOVA, using the treatment group and number of wet/dry cycles as factors. For the CT scan results, one-way ANOVA and Tukey's test were performed, to determine the influence of treatment group on vesicular pore formation. All statistical analyses were performed in MINITAB 16 (Minitab, 2010).

RESULTS AND DISCUSSION

Effect of microbial respiration on vesicular pore formation

Respiration data demonstrate that the methods used to create sterile, non-sterile, and glucose-amended soils did have the intended effects on microbial activity of the soils (Fig. 4.1a). Carbon dioxide was emitted from the sterile soils (Fig. 4.1a), however, CO_2 emissions from the sterile soils were significantly lower than those of the inoculated soils ($t = -7.41$, $p = 0.002$), which demonstrates the effectiveness of the sterilization treatment. Furthermore, there was no significant increase in CO_2 emissions from the sterile soils in response to glucose-amendment ($t = 0.71$, $p = 0.531$). This indicates that the CO_2 emitted from the sterile soils was most likely a product of an abiotic reaction, such as $CaCO_3$ precipitation (eq. 4.1), rather than evidence that the soils were not completely sterilized. In the inoculated soils, there was a significant increase in CO_2 emissions in response to glucose-amendment ($t = 36.2$, $p < 0.001$), which demonstrates the effectiveness of glucose-amendment for increasing respiration rates. There was no significant difference between the inoculated and non-autoclaved soils, in either the non-amended soils ($t = 0.0$, $p = 1.0$) or glucose-amended soils ($t = 1.55$, $p = 0.17$). This demonstrates the effectiveness of the inoculation treatment at reintroducing the microorganisms back to the soil following sterilization. In the repeated respiration measurements of glucose-amended soils (Fig. 4.1b), we observed that response of the soils to glucose-amendment declines over repeated wetting cycles; however, addition of glucose after five wetting cycles brought the respiration rates back up.

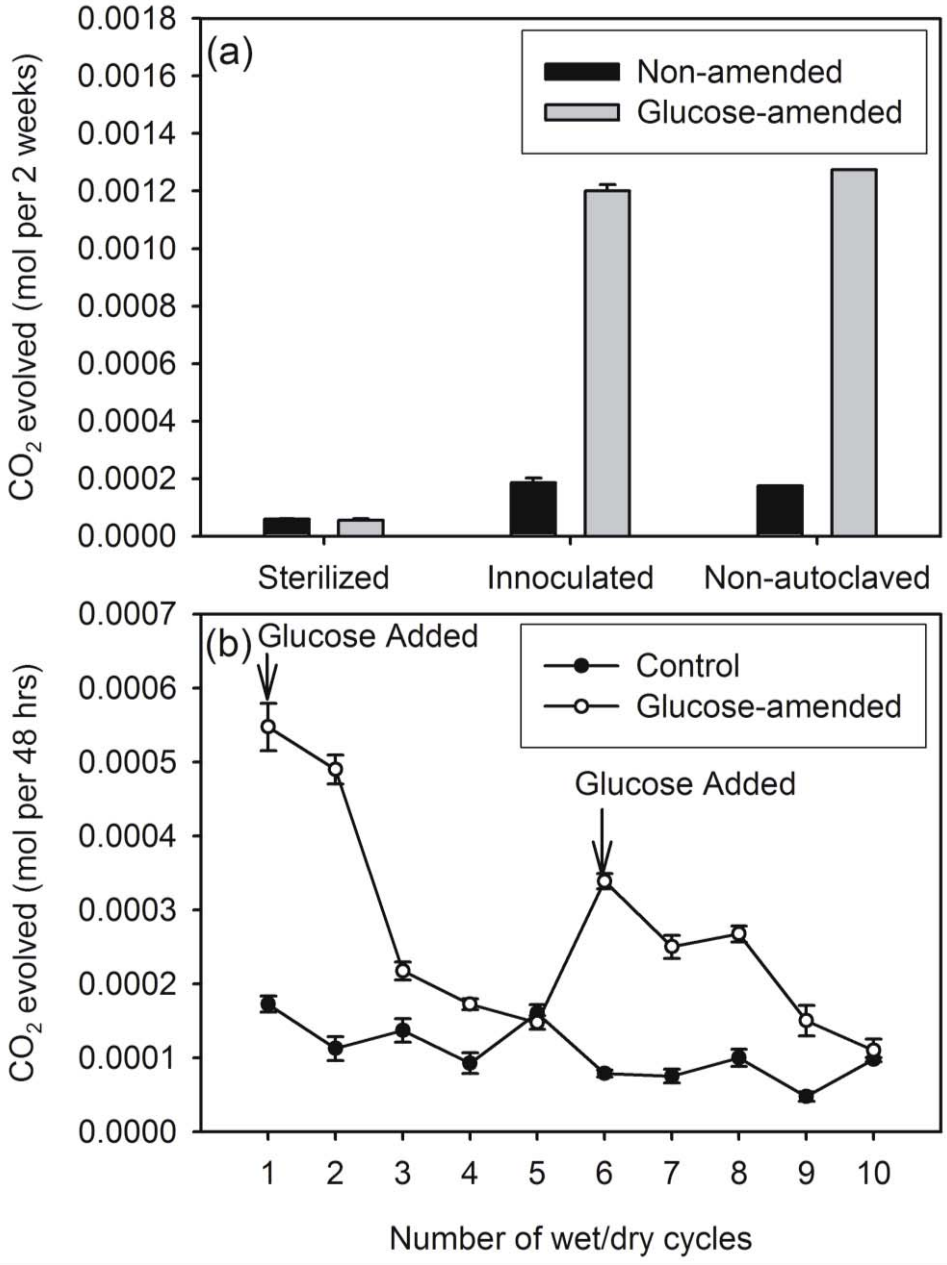

Fig. 4.1. Respiration rates of treated soils: (a) comparison of sterilized, sterilized/inoculated, and non-autoclaved soils with and without glucose-amendment and (b) duration of glucose response in sterilized-inoculated over successive wetting and drying cycles. Error bars show the standard error of the mean.

If soil respiration drives the formation of vesicular pores, we expect to see an inhibition of vesicular pore growth in the sterilized soils and enhanced vesicular pore formation in the glucose-amended soils. Bulk density can be used as an indication of total porosity in soils, and if vesicular pores are the predominant pore type, the decline in bulk density can be used as a measure of vesicular pore growth (Miller, 1971). Experimental results show that the decline in bulk density was greatest in the sterile soil, followed by the inoculated soil, and lowest in the glucose-amended soil (Fig. 4.2). There was a significant effect of treatment ($p < 0.001$) and number of wet/dry cycles ($p < 0.001$) on bulk density, according to the two-way ANOVA test. However, examination of internal pore structure by CT, shows the growth of both planar voids and vesicles are affected by the treatments (Fig. 4.3). Planar voids were most abundant in the sterile soils relative to the nonsterile soils, and were least abundant in the glucose-amended soils. The growth of these voids had a dominant effect on the bulk density of the soils, which means that the bulk density was not directly related to the formation of vesicular pores.

The planar voids formed in this study appear to result from shrink-swell processes (Stoops, 2003), rather than the collapse of interconnected vesicular pores (Brewer, 1976). The orientation of the planar voids shifts towards vertical near the edges of the sample, which is an indication the voids are linked to differential rates of drying. If the planar voids were formed through collapse of vesicular pores we would expect a predominantly horizontal orientation throughout the sample. Both processes (*i.e.*, shrink-swell and collapse of vesicular pores), may contribute to the formation of platy structure in the field. Shrink-swell processes may be particular effective at forming platy structure in

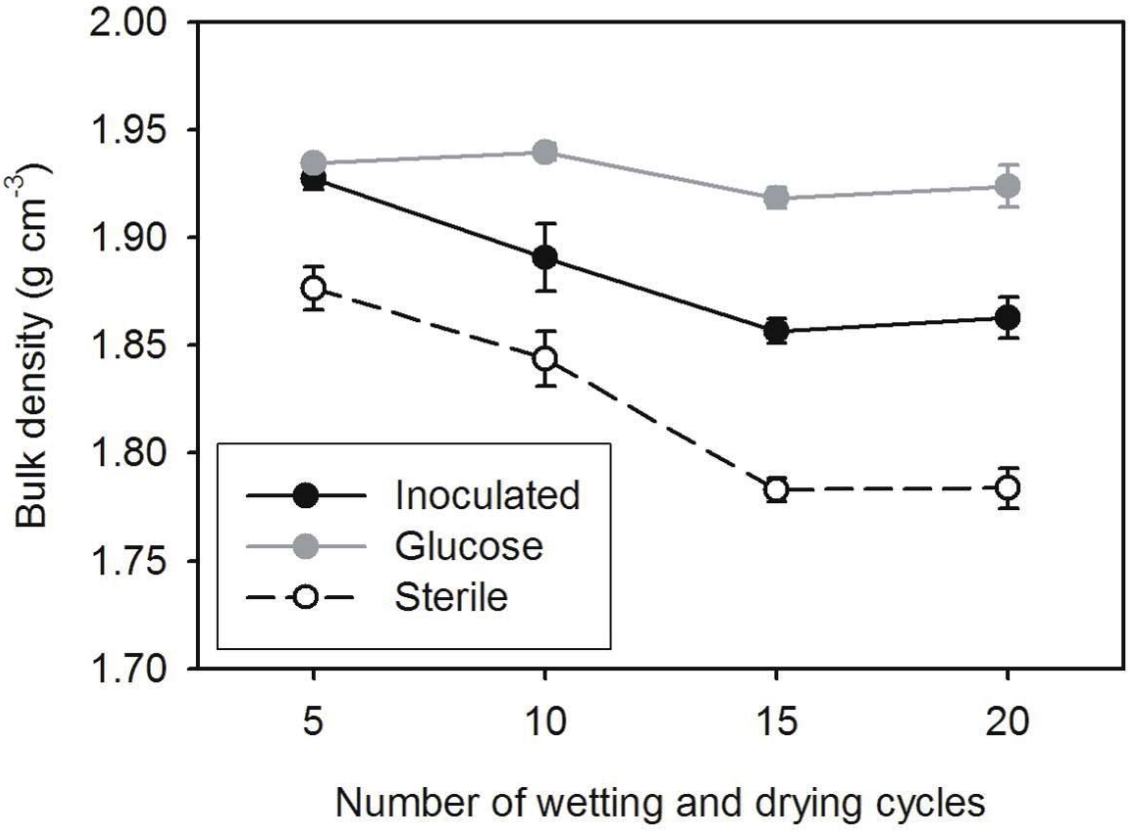

Fig. 4.2. Bulk densities of inoculated, glucose-amended inoculated, and sterile soil, measured after every 5 wet/dry cycles. Error bars represent ±1 standard error.

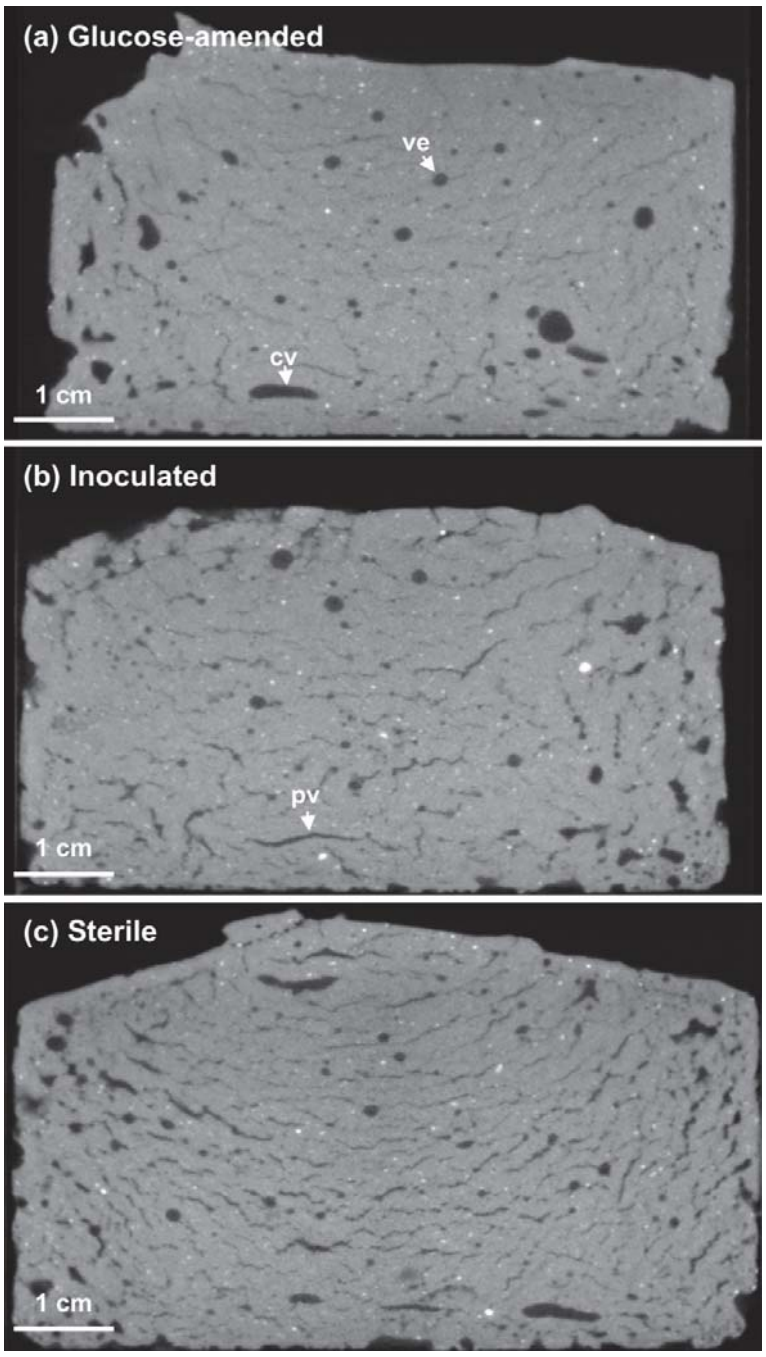

Fig. 4.3. Slices from computed tomography scans of vesicular pores created after 20 wet/dry cycles in: (a) sterile soil, (b) inoculated soil, and (c) glucose-amended inoculated soil. Examples of major pore types are labeled: ve = vesicular pore, cv = collapsed vesicle, pv = planar void.

deserts where summer rainfall is followed by high temperatures and rapid drying of the soil surface.

Vesicular pores formed in soils in all three treatment groups, but varied in their size and number (Fig. 4.4). Vesicular pores occupied the largest percentage of sample volume in the glucose-amended soils ($p = 0.02$). The number of vesicular pores was greatest in the sterilized soils ($p = 0.004$), but the pores were largest in the glucose-amended soils ($p = 0.001$). As vesicular pores grow and merge with each other, the number of vesicles is reduced (Figueira and Stoops, 1983). This trend may explain why the vesicular pores were most numerous in the sterile soils, which had the smallest vesicular pore volume. These results indicate that vesicular pore growth was promoted by the addition of glucose, but was not inhibited sterilization. This suggests that vesicular pore growth is promoted by microbial respiration, but that abiotic processes are equally, or perhaps more important in driving vesicular pore formation. The relationship between vesicular horizon formation and soil organic matter is likely to be complex. Soil organic matter stabilizes soil aggregates, which prevents crusting and entrapment of air bubbles (Wood et al., 1978). However, the results of the current study demonstrate that addition of a labile carbon source increases the formation of vesicular pores by increasing soil respiration rates.

Effect of thermal expansion on vesicular pore formation

The rate of total porosity formation was affected by the treatment groups exposed to varied temperature increase between wetting and drying. The soils that experienced

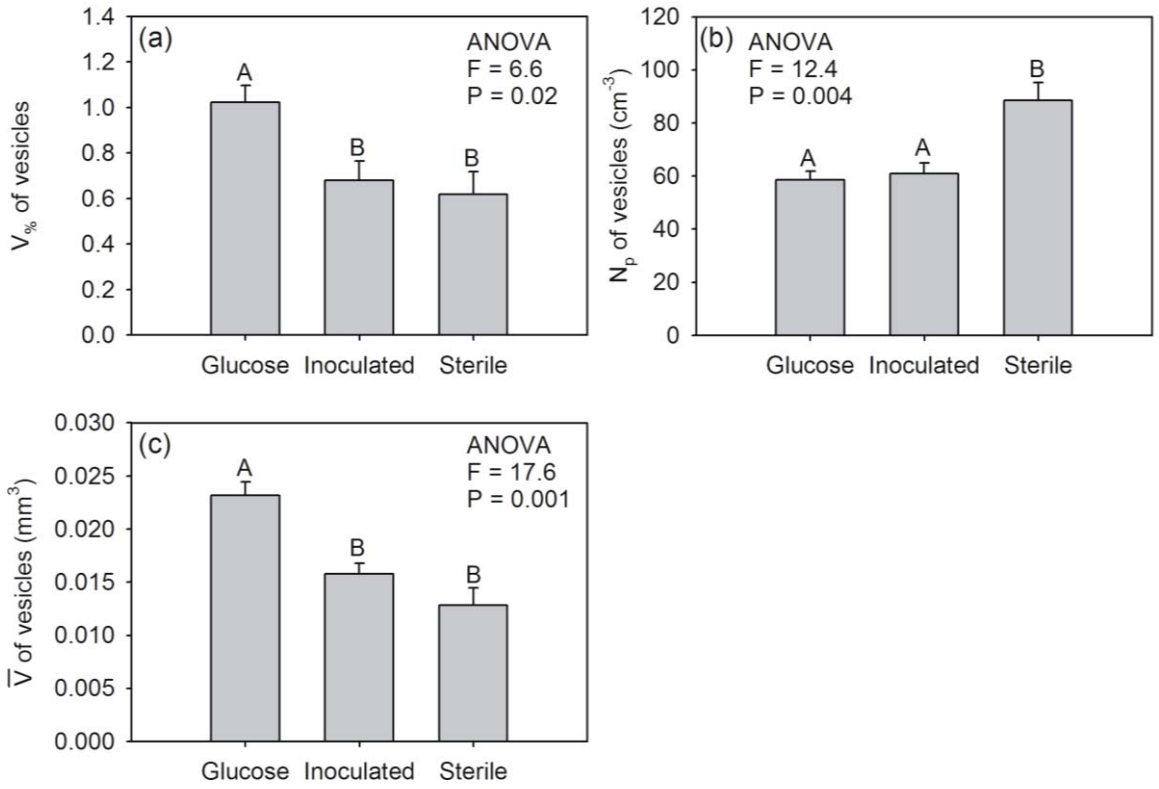

Fig. 4.4. Vesicular pore data from computed tomography scans sterile, inoculated, and glucose-amended soils after 20 wet/dry cycles: (a) percent of sample volume occupied by vesicular pores ($V_{\%}$), (b) number density of vesicular pores (N_p), and (c) average vesicular pore volume (geometric mean) ($\overline{V}$). Error bars represent 1 standard error and bars on the same graph labeled with different letters are significantly different according to Tukey's test.

the greatest increase in temperature (wet at 7°C, dried at 40°C) showed the greatest decrease in bulk density over the course of the experiment, while those that experienced a smaller increase in temperature (wet at 23°C and dried at 40°C) had an intermediate decrease in bulk density, and those that experienced no increase in temperature (wet and dried at 40°C) had the least decline in bulk density (Fig. 4.5). There was a significant effect of both wetting temperature ($p < 0.001$) and number of wet/dry cycles ($p < 0.001$) on bulk density, according to the two-way ANOVA. However, as with the results of the previous experiment, bulk density was not a reliable indicator of vesicular pore growth due to the dominance of planar voids formed through shrink-swell processes (Fig. 4.6). Soils exposed to greater temperature increase had more planar voids.

The percentage of sample volume occupied by vesicular pores was greatest in the soils that were wet and dried at the same temperature (40°C) and lowest in the soils that experienced the greatest increase in temperature (7°C to 40°C) (Fig. 4.7a). There was no significant difference in the number density of vesicular pores or the individual vesicular pore volume between the treatment groups (Fig. 4.7b,c). These results do not support the role of thermal expansion in vesicular pore formation. Rather, the relationship between temperature and vesicular pore formation may be microbially-mediated. Mesophyllic microorganisms are most active between 15 and 45°C (Tate, 2000), but are relatively inactive at temperatures below 5 to 10°C (Rabenhorst, 2005). The inhibition of vesicular pore growth in the soils wet at 7°C may be explained by low microbial activity at this temperature. This relationship could be confirmed by an experiment combining the two treatment sets applied in this study; that is, by exposing sterile, inoculated, and glucose-

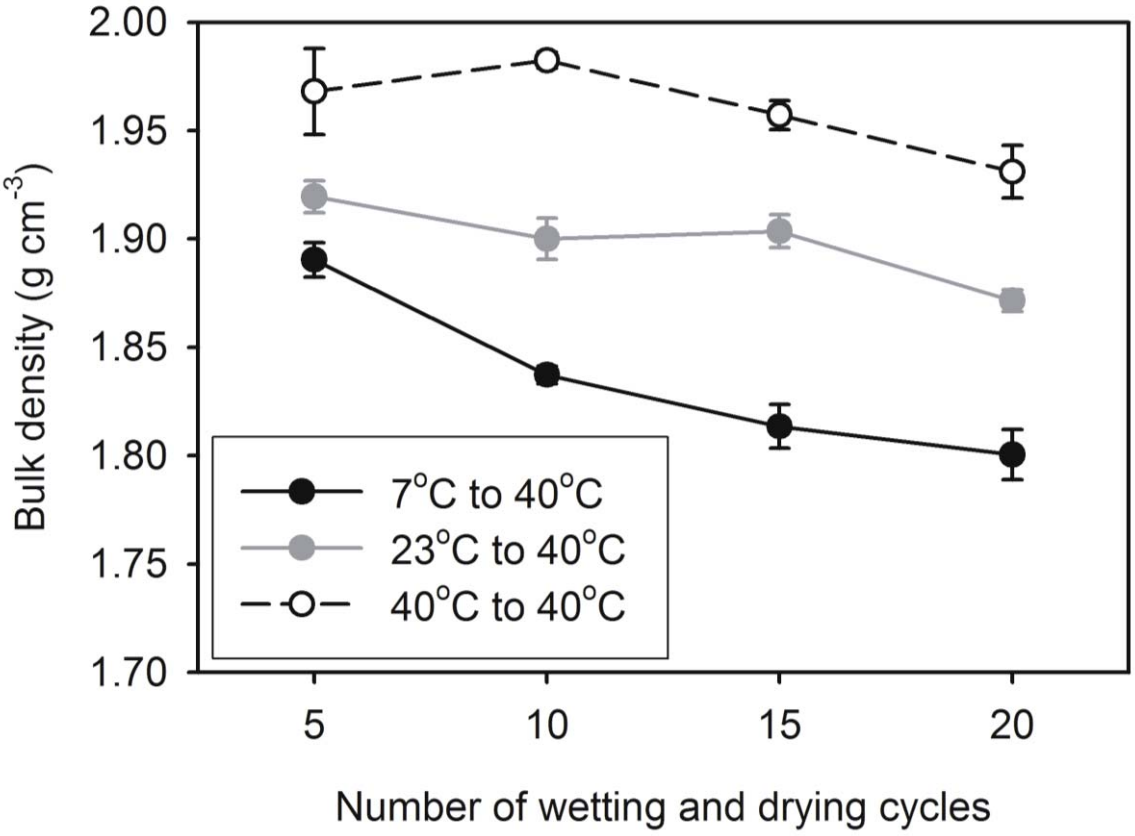

Fig. 4.5. Bulk densities of soils exposed to different temperature increases during drying, measured after every 5 wet/dry cycles. Error bars represent ±1 standard error.

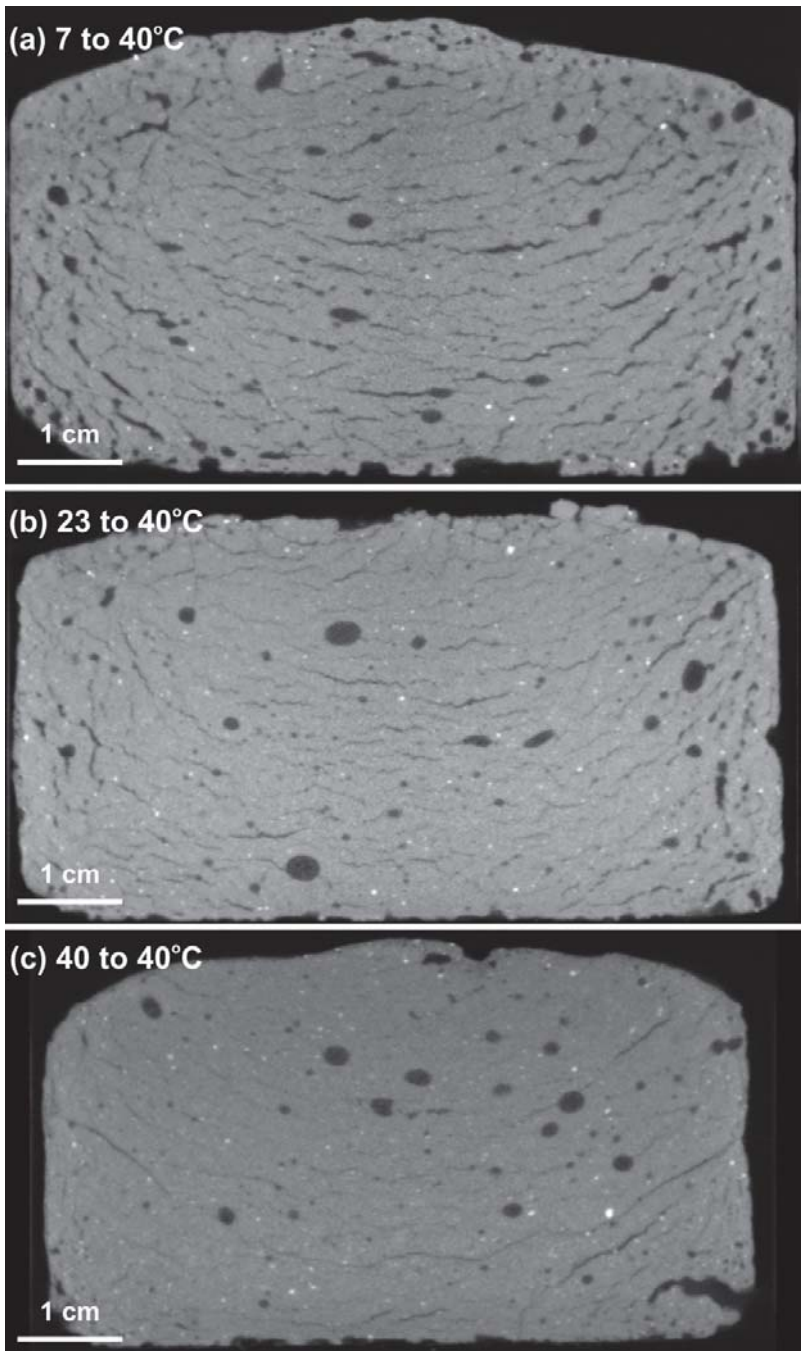

Fig. 4.6. Slices from computed tomography scans of vesicular pores created after 20 wet/dry cycles in soil exposed to different temperature increases during drying: (a) 7°C to 40°C, (b) 23°C to 40°C, and (c) 40°C to 40°C.

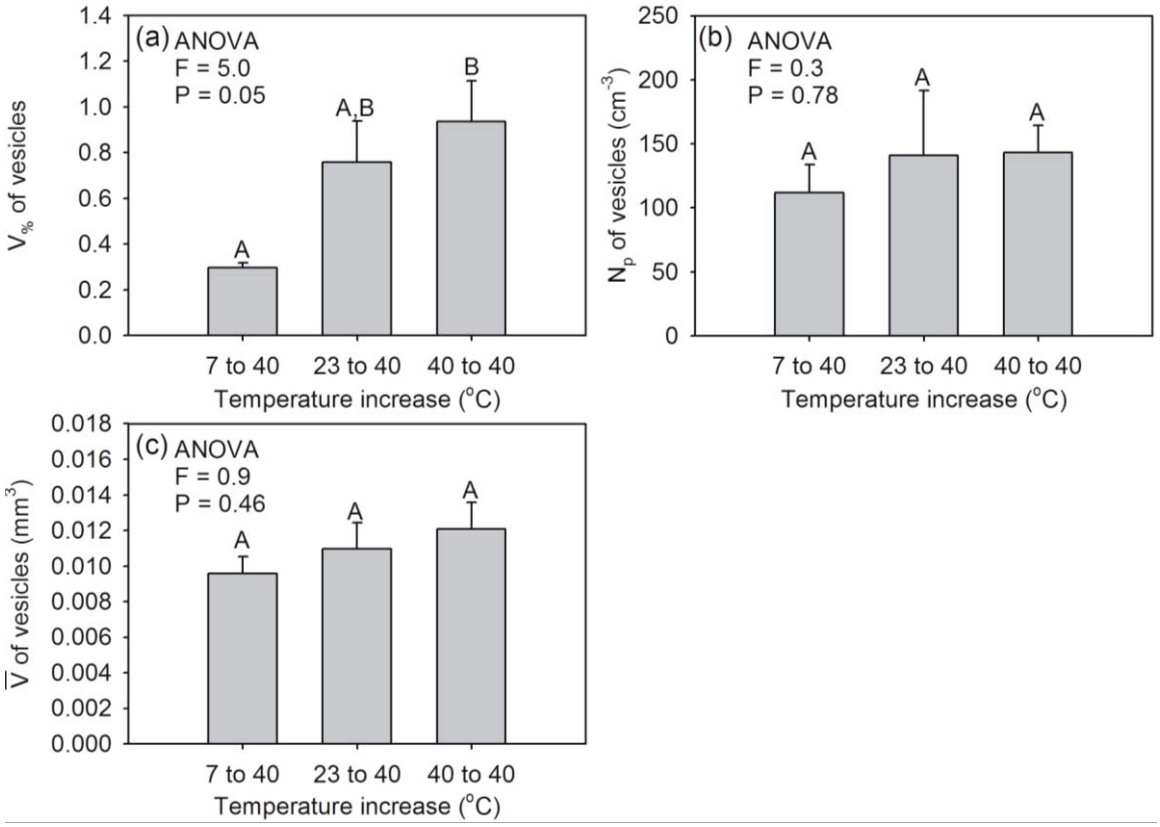

Fig. 4.7. Vesicular pore data from computed tomography scans of soils after 20 wet/dry cycles with different temperature gradients during drying: (a) percent of sample volume occupied by vesicular pores ($V_{\%}$), (b) number density of vesicular pores (N_p), and (c) average vesicular pore volume (geometric mean) ($\overline{V}$). Error bars represent 1 standard error and bars on the same graph labeled with different letters are significantly different according to Tukey's test.

amended soils to varied levels of temperature increase between wetting and drying. If the relationship between temperature and vesicular pore formation is microbially-mediated, then there would be no effect of temperature on vesicular pore growth in sterilized soils.

Past studies of vesicular pore formation under laboratory conditions have used various drying temperatures, including room temperature (Miller, 1971; Evenari et al., 1974), 45^{o}C (Figueira and Stoops, 1983), and 90^{o}C (Springer, 1958). One study compared vesicular pore formation at room temperature with formation under a heat lamp (45^{o}C), but the author observed no effect on vesicular pore formation (Miller, 1971). This is in contrast to the results of the current study, which showed greater vesicular pore formation in soils that were wet at 40^{o}C, relative to those that were wet at lower temperatures. The difference in the results of the current study and those of Miller (1971), may be explained because we controlled for the rate of soil drying, by varying the wetting temperature and keeping the drying temperature constant. Under these conditions moisture was maintained during the period when the temperature varied between treatment groups. In contrast, the heat lamp treatment described by Miller (1971), would have led to more rapid drying of the soil, thus reducing the period of time during which the soil was moist enough to support microbial activity.

The abundance of planar voids in our samples may also be influenced by the drying temperatures. The development of planar voids meant that there was no direct relationship between vesicular porosity and bulk density in our samples. However, past studies in which samples were dried at room temperature showed much more limited development of planar voids and a strong relationship between vesicular pore growth and

bulk density (Miller, 1971). We attribute the prevalence of planar voids in the oven-dried samples to more rapid drying leading to less-uniform shrinkage of the soil mass (Turk et al., 2011).

The results of this experiment suggest that extremes in temperature due to solar heating of the soil surface are unlikely to explain the distribution of soil horizons with vesicular pores (Ellis, 1990; Turk and Graham, 2011) or the depth distribution of vesicular pores within the vesicular horizons (Paletskaya et al., 1958; Hugie and Passey, 1964; Ellis, 1990; Bouza et al., 1993; McFadden et al., 1998). Other factors, including surface crusting, frequency of wetting, overburden weight, and frequency of disturbance are likely to play a more important role in the distribution and expression of vesicular horizons. Temperature may have an indirect effect on the development of vesicular pores, through the influence on microbial activity, although further analysis is required to confirm this relationship.

The first experiment demonstrated that abiotic processes play a dominant role in vesicular pores formation, since sterilization did not significantly affect formation of vesicular pores. However, formation of vesicular pores through thermal expansion of trapped gases was not supported as a possible abiotic mechanism. This means that another abiotic mechanism of vesicular pore formation must predominate. One possibility is $CaCO_3$ precipitation (Paletskaya et al., 1958; Evenari et al., 1974; Lebedeva et al., 2009); however, this is not supported by the results of this experiment, which showed the very low CO_2 emissions from the sterilized soils (Fig. 4.1a). Another possibility is the abiotic production of N-containing gases (NO, NO_y, and NH_3), which

has been demonstrated to occur in some Mojave Desert soils (McCalley and Sparks, 2009). Future studies should investigate the nature of both the abiotic and biotic mechanisms of vesicular pore formation.

SUMMARY AND CONCLUSIONS

In this study, we have tested two hypotheses about the formation of vesicular pores: 1) that biotic processes (*i.e.*, microbial respiration) influence the formation of vesicular pores and 2) that thermal expansion of gases promotes the formation of vesicular pores. We found indirect evidence for the role of biological processes in vesicular pore formation, which include: 1) increased vesicular pore formation caused by addition of a labile carbon source (*i.e.*, glucose), and 2) decreased vesicular pore formation at temperatures near biological zero. However, we also found direct evidence for abiotic production of vesicular pores, through the observation of vesicular pore formation in sterilized soils. Thermal expansion of gases was the abiotic mechanism of vesicular pore formation selected for analysis in this study, but was not supported by the results, which showed the strongest vesicular pore formation in soils that were wet and dried at uniform temperature. The results of this study support the involvement of both biotic and abiotic processes in vesicular pore formation; however, the nature of the abiotic mechanism is still unknown.

REFERENCES

Abdi, H. The Bonferroni and Šidák corrections for multiple comparisons. p. 103-106. *In* N. Salkind and K. Rasmussen (eds). Encyclopedia of Measurement and Statistics. SAGE Publications, Thousand Oaks, CA

Amit, R., and R. Gerson. 1986. The evolution of Holocene reg (gravelly) soils in deserts: an example from the Dead Sea region. Catena 13:59-79.

Amundson, R.G., O.A. Chadwick, J.M. Sowers, and H.E. Doner. 1989. Soil evolution along an altitudinal transect in the eastern Mojave Desert of Nevada, USA. Geoderma 43:349-371.

Anderson, J.P.E., and K.H. Domsch. 1978. Physiological method for quantitative measurement of microbial biomass in soils. Soil Biol. Biochem. 10:215-221.

Anderson, K., S. Wells, and R. Graham. 2002. Pedogenesis of vesicular horizons, Cima Volcanic Field, Mojave Desert, California. Soil Sci. Soc. Am. J 66:878-887.

Austin, A.T., L. Yahdjian, J.M. Stark, J. Belnap, A. Porporato, U. Norton, D.A. Ravetta, and S.M. Schaeffer. 2004. Water pulses and biogeochemical cycles in arid and semiarid ecosystems. Oecologia 141:221-235.

Beckman, W. 1962. Zur Mikromorphometrie von hohlräumen und aggregaten im boden. (in German) Zeitsh Pflazern, Düng, Bodend 99:129-139.

Blackburn, W.H. 1975. Factors influencing infiltration and sediment production of semiarid rangelands in Nevada. Water Resour. Res. 11:929-937.

Bockheim, J.G. 2010. Evolution of desert pavements and the vesicular layer in soils of the Transantarctic Mountains. Geomorphology 118:433-443.

Bouza, P., H.F. Delvalle, and P.A. Imbellone. 1993. Micromorphological, physical, and chemical characteristics of soil crust types of the central Patagonia region, Argentina. Arid Soil Res. Rehabilitation 7:355-368.

Bower, C.A., and J.T. Hatcher. 1966. Simultaneous determinations of surface area and cation exchange capacity. Soil Sci. Soc. Am. Proc. 30:525-527.

Brewer, R. 1976. Fabric and mineral analysis of soils. Robert E. Krieger, Huntington, NY.

Brown, K.J., and D.L. Dunkerley. 1996. The influence of hillslope gradient, regolith texture, stone size and stone position on the presence of a vesicular layer and

related aspects of hillslope hydrologic processes: A case study from the Australian arid zone. Catena 26:71-84.

Bunting, B.T. 1977. The occurrence of vesicular structures in arctic and subarctic soils. Z. Geomorphol. 21:87-95.

Burt, R. (ed.) 2004. Soil Survey Laborator Methods Manual. Soil Suvey Investigations Report No. 42. USDA, Washington, DC.

Caldwell, T.G., E.V. McDonald, and M.H. Young. 2006. Soil disturbance and hydrologic response at the National Training Center, Ft. Irwin, California. J. Arid Environ. 67:456-472.

Cantón, Y., A. Solé-Benet, and R. Lázaro. 2003. Soil-geomorphology relations in gypsiferous materials of the Tabernas Desert (Almeria, SE spain). Geoderma 115:193-222.

Dan, J., D.H. Yaalon, R. Moshe, and S. Nissim. 1982. Evolution of reg soils in southern Israel and Sinai. Geoderma 28:173-202.

Eckert, R.E., F.F. Peterson, M.S. Meurisse, and J.L. Stephens. 1986. Effects of soil-surface morphology on emergence and survival of seedlings in big sagebrush communities. J. Range Manage. 39:414-420.

Eckert, R.E., M.K. Wood, W.H. Blackburn, F.F. Peterson, J.L. Stephens, and M.S. Meurisse. 1978. Effects of surface-soil morphology on improvement and management of some arid and semiarid rangelands. p. 299-301. *In* D.N. Hyder (ed.) Proc. of the First Int. Rangeland Congr., Denver, CO. 14-18 Aug. 1978. Society for Range Mangement, Denver, CO.

Ellis, F. 1990. Note on soils with vesicular structure and other micromorphological features in Karoo soils. p. 326-336. *In* Proc. 16th Congress of the Soil Science Society of South Africa, Pretoria, South Africa. July 9-12 1990. Soil Science Society of South Africa, Erasmusrand, South Africa.

Evenari, M., D.H. Yaalon, and Y. Gutterman. 1974. Note on soils with vesicular structure in deserts. Z. Geomorphol. 18:162-172.

Figueira, H., and G. Stoops. 1983. Application of micromorphometric techniques to the experimental study of vesicular layer formation. Pedologie 33:77-89.

Graham, R.C., D.R. Hirmas, Y.A. Wood, and C. Amrhein. 2008. Large near-surface nitrate pools in soils capped by desert pavement in the Mojave Desert, California. Geology 36:259-262.

Hamerlynck, E.P., J.R. McAuliffe, E.V. McDonald, and S.D. Smith. 2002. Ecological responses of two Mojave Desert shrubs to soil horizon development and soil water dynamics. Ecology 83:768-779.

Henning, J.A.G., and K. Kellner. 1994. Degradation of a soil (Aridosol) and vegetation in the semiarid grasslands of southern Africa. Bot. Bull. Acad. Sin. 35:195-199.

Hillel, D. 1998. Environmental Soil Physics Academic Press, San Diego, CA.

Hugie, V.K., and H.B. Passey. 1964. Soil surface patterns of some semiarid soils in northern Utah, southern Idaho, and northeastern Nevada. Soil Sci. Soc. Am. Proc. 28:786-792.

Huxman, T.E., K.A. Snyder, D. Tissue, A.J. Leffler, K. Ogle, W.T. Pockman, D.R. Sandquist, D.L. Potts, and S. Schwinning. 2004. Precipitation pulses and carbon fluxes in semiarid and arid ecosystems. Oecologia 141:254-268.

Issa, O.M., J. Trichet, C. Defarge, A. Coute, and C. Valentin. 1999. Morphology and microstructure of microbiotic soil crusts on a tiger bush sequence (Niger, Sahel). Catena 37:175-196.

Joeckel, R.M., and B.A. Clement. 1999. Surface features of the Salt Basin of Lancaster County, Nebraska. Catena 34:243-275.

Ketcham, R.A. 2005. Computational methods for quantitative analysis of three-dimensional feature in geological specimens. Geosphere 1:32-41.

Lebedeva, M.P., D.L. Golovanov, and S.A. Inozemtsev. 2009. Microfabrics of desert soils of Mongolia. Euras. Soil Sci. 42:1204-1217.

Matmon, A., O. Simhai, R. Amit, I. Haviv, N. Porat, E. McDonald, L. Benedetti, and R. Finkel. 2009. Desert pavement-coated surfaces in extreme deserts present the longest-lived landforms on Earth. Geol. Soc. Am. Bull. 121:688-697.

McAuliffe, J.R. 1994. Landscape evolution, soil formation, and ecological patterns and processes in Sonoran Desert bajadas. Ecol. Monogr. 64:111-148.

McCalley, C.K., and J.P. Sparks. 2009. Abiotic gas formation drives nitrogen loss from a desert ecosystem. Science 326:837-840.

McDonald, E.V. 1994. The relative influences of climatic change, desert dust, and lithologic control on soil-geomorphic processes and soil hydrology of calcic soils formed on quaternary alluvial-fan deposits in the Mojave Desert, California. Ph.D. Dissertation, The University of New Mexico, Albuquerque, NM.

McDonald, E.V., L.D. McFadden, and S.G. Wells. 1995. The relative influences of climate change, desert dust, and lithologic control on soil-geomorphic processes on alluvial fans, Mojave Desert, California: Summary of results. p. 35-42. In R. E. Reynolds and J. Reynolds (ed.) Ancient surfaces of the East Mojave Desert: a volume and field trip guide prepared in conjunction with the 1995 Desert Research Symposium. Quarterly of the San Bernardino County Museum Association. San Bernardino County Museum Association, Redlands, CA.

McFadden, L.D., E.V. McDonald, S.G. Wells, K. Anderson, J. Quade, and S.L. Forman. 1998. The vesicular layer and carbonate collars of desert soils and pavements: formation, age and relation to climate change. Geomorphology 24:101-145.

McFadden, L.D., S.G. Wells, and M.J. Jercinovich. 1987. Influences of eolian and pedogenic processes on the origin and evolution of desert pavements. Geology 15:504-508.

Miller, D.E. 1971. Formation of vesicular structure in soil. Soil Sci. Soc. Am. Proc. 35:635-637.

Miller, D.M., D.R. Bedford, D.L. Hughson, E.V. McDonald, S.E. Robinson, and K.M. Schmidt. 2009. Mapping Mojave Desert ecosystem properties with surficial geology. p. 225-251. *In* R. H. Webb et al. (ed.) The Mojave Desert: Ecosystem Processes and Sustainability. University of Nevada Press, Reno, NV.

Minitab. 2010. MINITAB 16. Minitab, State College, PA.

Musick. 1975. Barrenness of desert pavement in Yuma County, Arizona. J. Arizona Acad. Sci. 10:24-28.

Noy-Meir, I. 1973. Desert ecosystems: environment and producers. Annu. Rev. Ecol. Syst. 4:25-51.

Paletskaya, L.N., A.P. Lavrov, and S.I. Kogan. 1958. Pore formation in takyr crust. Sov. Soil Sci. (Engl. Transl.) 3:245-250.

.

Peterson, F.F. 1980. Holocene desert soil formation under sodium-salt influence in a playa-margin environment. Quat. Res. 13:172-186.

Quade, J. 2001. Desert pavements and associated rock varnish in the Mojave Desert: How old can they be? Geology 29:855-858.

Rabenhorst, M.C. 2005. Biological zero: A soil temperature concept. Wetlands 25: 616-621.

Reheis, M.C., J.M. Sowers, E.M. Taylor, L.D. Mcfadden, and J.W. Harden. 1992. Morphology and genesis of carbonate soils on the Kyle Canyon fan, Nevada, USA. Geoderma 52:303-342.

Rossi, A.M., D.R. Hirmas, R.C. Graham, and P.D. Sternberg. 2008. Bulk density determination by automated three-dimensional laser scanning. Soil Sci. Soc. Am. J. 72:1591-1593.

Segal, E., P.J. Shouse, S.A. Bradford, T.H. Skaggs, and D.L. Corwin. 2009. Measuring particle size distribution using laser diffraction: implications for predicting soil hydraulic properties. Soil Sci. 174:639-645.

Smith, S.D., C.A. Herr, K.L. Leary, and J.M. Piorkowski. 1995. Soil-plant water relations in a Mojave Desert mixed shrub community: a comparison of three geomorphic surfaces. J Arid Environ 29:339-351.

Soil Survey Staff, 2012. Web Soil Survey. Available at http://websoilsurvey.nrcs.usda.gov (verified 24 Jan. 2012). USDA-NRCS, Washington, DC.

Springer, M.E. 1958. Desert pavement and vesicular layer of some soils of the desert of the Lahontan Basin, Nevada. Soil Sci. Soc. Am. Proc. 22:63-66.

Stevenson, F.J., R.M. Harrison, R. Wetselaa, and R.A. Leeper. 1970. Nitrosation of soil organic matter: III. Nature of gases produced by reaction of nitrite with lignins, humic substances, and phenolic constituents under neutral and slightly acidic conditions. Soil Sci. Soc. Am. Proc. 34:430-435.

Stoops, G. 2003. Guidelines for Analysis and Description of Soil and Regolith Thin Sections. SSSA, Madison, WI.

Sullivan, L.A., and A.J. Koppi. 1991. Morphology and genesis of silt and clay coatings in the vesicular layer of a desert loam soil. Aust. J. Soil Res. 29:579-586.

Tate, R.L. III, 2000. Soil Microbiology, 2nd ed. John Wiley and Sons, New York, NY.

Thomas, G.W. 1982. Exchangeable Cations. p. 159-165. *In* A. L. Page, (ed.) Methods of Soil Analysis. Part 2. 2nd ed. Agron. Monogr. 9. ASA and SSSA, Madison, WIl

Turk, J.K., O.A. Chadwick, and R.C. Graham. 2011. Pedogenic processes. p. 30.31-30.29. *In* P. M. Huang et al. (ed.) Handbook of Soil Sciences: Properties and Processes. 2nd ed. CRC Press, Boca Raton, FL.

Turk, J.K., and R.C. Graham. 2011. Distribution and properties of vesicular horizons in the western United States. Soil Sci. Soc. Am. J. 75:1449-1461.

Ugolini, F.C., S. Hillier, G. Certini, and M.J. Wilson. 2008. The contribution of aeolian material to an Aridisol from southern Jordan as revealed by mineralogical analysis. J. Arid Environ. 72:1431-1447.

Valentin, C. 1994. Surface sealing as affected by various rock fragment covers in West-Africa. Catena 23:87-97.

Valentine, G.A., and C.D. Harrington. 2006. Clast size controls and longevity of Pleistocene desert pavements at Lathrop Wells and Red Cone volcanoes, southern Nevada. Geology 34:533-536.

Van Vliet-Lanoë, B. 1985. Frost effects in soils. *In* J. Boardman (ed.) Soils and quaternary landscape evolution. John Wiley and Sons, Chichester, UK.

Venterea, R.T. 2007. Nitrite-driven nitrous oxide production under aerobic soil conditions: kinetics and biochemical controls. Global Change Biol. 13:1798-1809.

Williams, D.E. 1948. A rapid manometric method for determination of carbonate in soils. Soil Sci. Soc. Am. Proc. 13:127-129.

Williams, A., B. Buck, D. Soukup, and D. Merkler. 2010. Biological soil crusts and the fertile island effect: Soil-geomophic insights from the Mojave Desert, USA. *In* Abstracts, ASA-CSSA-SSSA Int. Annu. Meet., Long Beach, CA. 31 Oct.-3 Nov. 2010. ASA-CSSA-SSSA, Madison, WI.

Wood, M.K., W.H. Blackburn, R.E. Eckert, and F.F. Peterson. 1978. Interrelations of physical-properties of coppice dune and vesicular dune interspace soils with grass seedling emergence. J. Range Manage. 31:189-192.

Wood, M.K., R.E. Eckert, W.H. Blackburn, and F.F. Peterson. 1982. Influence of crusting soil surfaces on emergence and establishment of crested wheat-grass, squirreltail, thurber needlegrass, and fourwing saltbush. J. Range Manage. 35:282-287.

Wood, M.K., R.E. Eckert, W.H. Blackburn, and F.F. Peterson. 1982. Influence of crusting soil surfaces on emergence and establishment of crested wheat-grass, squirreltail, thurber needlegrass, and fourwing saltbush. J. Range Manage. 35:282-287.

Wood, Y.A., R.C. Graham, and S.G. Wells. 2005. Surface control of desert pavement pedologic process and landscape function, Cima Volcanic field, Mojave Desert, California. Catena 59:205-230.

Yonovitz, M., and P.J. Drohan. 2009. Pore morphology characteristics of vesicular horizons in undisturbed and disturbed arid soils; implications for arid land management. Soil Use Manage. 25:293-302.

Young, M.H., E.V. McDonald, T.G. Caldwell, S.G. Benner, and D.G. Meadows. 2004. Hydraulic properties of a desert soil chronosequence in the Mojave Desert, USA. Vadose Zone J. 3:956-963.

Zibilske, L.M. 1994. Carbon Mineralization. *In* R. W. Weaver (ed.) Methods of Soil Analysis Part 2. Microbiological and Biochemical Properties. ASA and SSSA, Madison, WI.

5. CONCLUSIONS

The purpose of this dissertation was to examine the distribution, properties, and pedogenic processes of vesicular horizons through soil database, field, and laboratory studies. The soil databases contained 1387 soil series with vesicular horizons, which were mostly soils classified as Aridisols, Entisols, Mollisols, Alfisols, and Inceptisols. The most common textures of the vesicular horizons were loam, sandy loam, fine sandy loam, very fine sandy loam, and silt loam. The soil series with vesicular horizons are most extensively mapped in the arid Basin and Range Province and cover a total of 156,000 km^2 of the western U.S. The strength of vesicular horizon expression can be quantified according to a field index, referred to as the vesicular horizon index (VHI). The VHI takes into account the horizon thickness, vesicular pore size class, and vesicular pore quantity class described in the field. Based on the VHI of vesicular horizons in the soil databases, vesicular horizons are better expressed in the cold desert regions (*i.e.*, central and northern Basin and Range) relative to the warm deserts (*i.e.*, Mojave and Sonoran Deserts).

In the field we examined recovery of vesicular horizons from disturbance, in artificially disturbed study plots, and also in pre-existing tire tracks and coppice dunes. These studies were conducted at 15 field areas, including sites in the Sonoran, Mojave, and central Great Basin deserts. In the artificially disturbed study plots, we found that vesicular horizon recovery was incomplete within the one-year study period. We also found that degree of recovery was dependent on the number of precipitation events that the site experienced during the recovery period. Using the relationship between

precipitation and vesicular horizon recovery, as well as the average number of precipitation events in a year, we predict recovery periods for the field sites ranging from two to 11 yrs. In tire tracks, vesicular horizons were recently disturbed (<4 to >15 yrs ago), but show little difference in pore morphology relative to undisturbed parts of the landscape. In the coppice dunes, vesicular pores, vughs, and interconnected pores of the vesicular horizons were reduced in size, and platy structure became more strongly pronounced, providing evidence for the collapse of pores that had formed in the un-buried vesicular horizon. Disturbance of the vesicular horizons resulted in only minor reduction in infiltration rates, indicating that the hydraulic properties of the vesicular horizon are not severely altered by disturbance.

The lab studies examined the effect of microbial respiration and thermal expansion of gases on vesicular pore formation. These studies found indirect evidence to support a biologically-mediated mechanism of vesicular pore growth: 1) increased vesicular pore growth in response to addition of a labile C source (*i.e.*, glucose), and 2) decreased vesicular pore growth in soils that were wet at low temperature (7^{o}C) relative to those that were wet at warmer temperature (40^{o}C). However, sterilization did not significantly inhibit vesicular pore growth, which suggests that abiotic processes are equally, or more important in driving the formation of vesicular pores. No evidence was found to support the role of thermal expansion of gases in the growth of vesicular pores, which actually formed more readily in the soils that were maintained at a constant temperature.

Together, these findings suggest a complex set of linkages between vesicular horizon formation and the climatic and biological conditions of the soil, including frequency of precipitation, soil temperature, shrub cover, and microbial respiration (Fig. 5.1). Human land use and climate change have potential to alter the balance between the variables that influence vesicular horizon formation, causing expansion or contraction of vesicular horizon extent in arid and semi-arid landscapes.

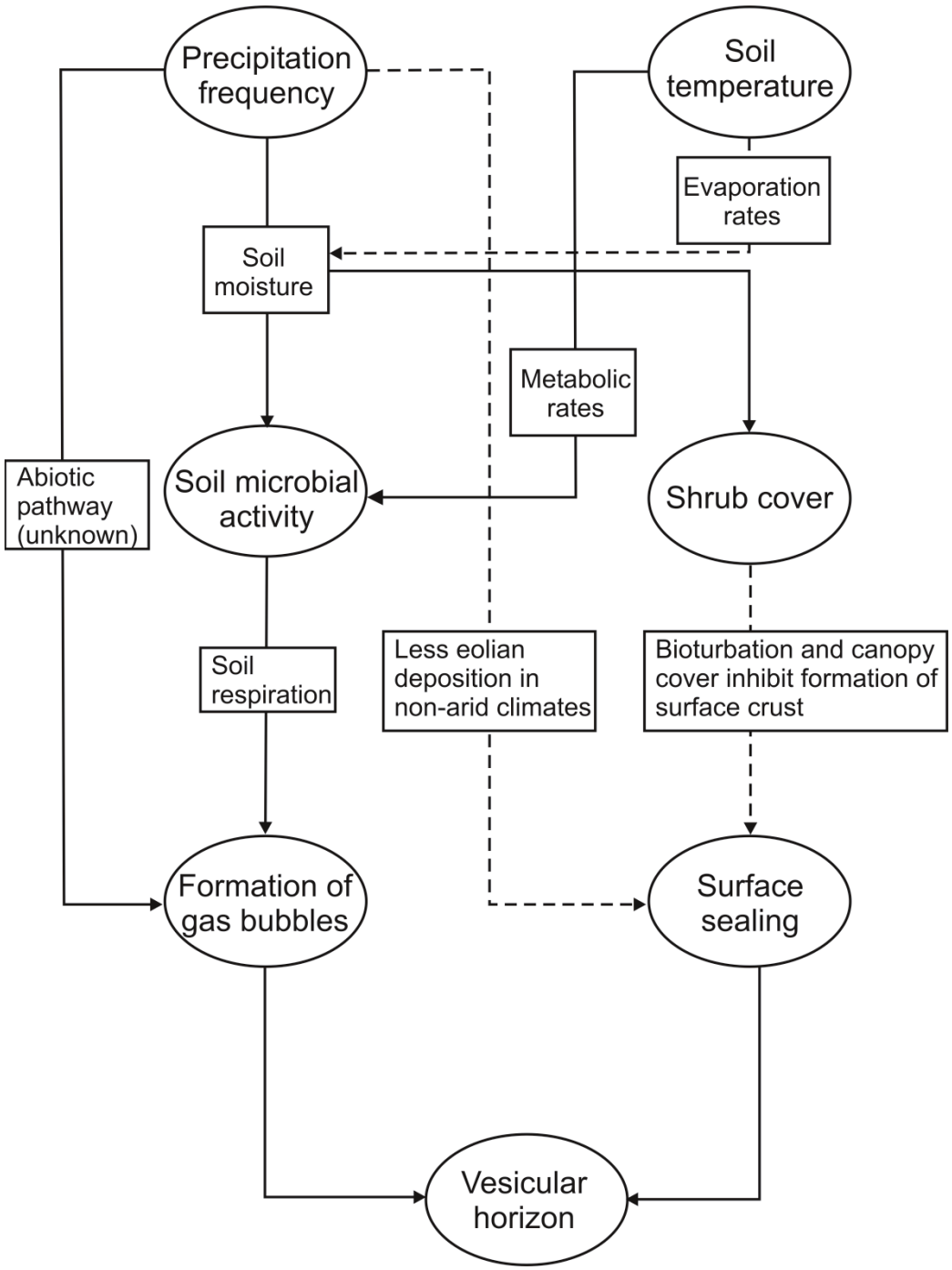

Fig. 5.1. Conceptual model of the relationship between climatic and biological variables that influence vesicular horizon development. Solid lines represent positive relationships and dashed lines represent negative relationships between nodes (ovals), text in boxes offers an explanation of the relationship represented by each line.

APPENDIX A. SOIL DESCRIPTIONS

SONORAN 1

TAXONOMIC CLASS: Petrocalcids

PEDON DESCRIPTION:

Desert Pavement—Surface; embedded gneissic and some granitic gravels, desert varnish and ventral varnish; 98% cover.

Av—0 to 4 cm; 7.5YR 4/4 moist, 10YR 6/4 dry; loam (14% gravels, 10% clay); strong medium columnar structure parting to moderate fine subangular blocky structure; hard, moderately sticky and very plastic; many very fine and many fine vesicular pores, common medium vughs; violent effervescence with 1 M HCl (ped top, sides, bottom, and interior); abrupt wavy boundary.

Bw—4 to 11 cm; 10YR 4/6 moist, 10YR 6/4 dry; gravelly loam (24% gravels; 15% clay); moderate medium subangular blocky structure; slightly hard, slightly sticky and moderately plastic; few very fine roots between peds; common very fine dendritic pores; slight effervescence with 1 M HCl; clear wavy boundary.

Bt—11 to 39 cm; 7.5YR 4/6 moist, 7.5YR 4/6 dry; very gravelly loamy sand (42% gravel, 5% weathered cobbles; 10% clay); weak fine subangular blocky structure; slightly hard, slightly sticky and moderately plastic; few very fine dendritic pores; discontinuous clay films on rock fragments and ped faces; noneffervescent with 1 M HCl; clear broken boundary.

Bkm—39 to 60+ cm; 10YR 5/6 moist, 10YR 7/3 dry; very gravelly coarse sand (52% gravel; 3% clay); structureless massive; very hard, non-sticky and non-plastic; does not slake in water, does slake in 1 N HCl; common very fine dendritic pores; violently effervescent with 1 M HCl.

PEDON LOCATION: West side of the Chuckwalla Mountains, CA on Gas Line Road, 1.3 mi south from Interstate 10; 33°39′59.2″ N, 115°31′5.4 ″ NAD83; Sec. 9 of T.6S, R.14E San Bernardino B&M; Hayfield Spring 7.5-minute topographical map quadrant.

GEOGRAPHIC SETTING: Located on erosional fan remnant of the fan piedmont. The soil is formed in mixed alluvium. Elevation is 457 meters and slope is 5 percent to the northwest. Average annual precipitation is 11.4 cm; mean annual air temperature is 20.8 degrees C, according to records from the Hayfield weather station (Fenimore, 2011).

SOIL MAPPED AS: None

USE AND VEGETATION: Land is used for utility lines and access roads. Vegetation includes: *Larrea Tridentata*, *Encelia farinose*, *Ambrosia dumosa*, *Fouquieria splendens*, *Krameria grayi*, *Cylindropuntia spp.*, *Olyneya tesota*, *Lycium andersonii*, *Simmonasia chinensis*, *Stephanomeria pacifora*, *Ditaxis lanceolata*, and *Acacia greggi*.

REMARKS:

Soil observed in a hand-dug pit on 4/16/11

Diagnostic horizons and features in this pedon:

Ochric epipedon - from 0 to 18 cm

Petrocalcic horizon – from 39-60+

The soil temperature regime is hyperthermic and the soil moisture regime is aridic.

The calcium carbonate state is III.

LAB DATA: 39-60+ cm: 10% $CaCO_3$

SONORAN 2

TAXONOMIC CLASS: Haplocambids

PEDON DESCRIPTION:

Desert Pavement—Surface; embedded tonolite, quartzite, and some gneiss gravels; desert varnish and ventral varnish; 95% cover.

Av—0 to 4 cm; 10YR 5/4 moist, 10YR 6/4 dry; silt loam (14% gravels, 20% clay); moderate medium prismatic structure; slightly hard, moderately sticky and very plastic; common very fine and common fine vesicular pores; common medium vughs; slight effervescence with 1 M HCl (ped top and sides) to strong effervescence with 1 M HCl (ped interior); abrupt smooth boundary.

Bw—4 to 17 cm; 7.5YR 4/6 moist, 7.5YR 5/6 dry; gravelly loam (20% gravels; 20% clay); weak medium and coarse subangular blocky structure; soft, moderately sticky and very plastic; few very fine roots in upper part of horizon; few very fine dendritic pores; strong effervescence with 1 M HCl; clear smooth boundary.

Bk—17 to 50+ cm; 7.5YR 4/6 moist, 7.5YR 5/6 dry; extremely gravelly sandy loam (60% gravel; 20% cobbles; 15% clay); structureless single grain; firm, slightly sticky and moderately plastic; carbonate coats on bottom surfaces of rock fragments; common medium masses of carbonates; slight effervescence with 1 M HCl.

PEDON LOCATION: East side of the Chuckwalla Mountains, CA on Corn Springs Road, 0.5 mi from Chuckwalla Valley Road; 33°40′14.2″ N, 115°14′23.9 ″ NAD83; Sec.

7 of T.6S, R.17E San Bernardino B&M; Sidewinder Well 7.5-minute topographical map quadrant.

GEOGRAPHIC SETTING: Located on the summit of an erosional fan remnant of an alluvial fan. The soil is formed in mixed alluvium. Elevation is 231 meters and slope is 3 percent to the west. Average annual precipitation is 7.9 cm; mean annual air temperature is 22.8 degrees C, according to records at Desert Center 2 NNE weather station (Fenimore, 2011).

SOIL MAPPED AS: None

USE AND VEGETATION: Recreational lands. Vegetation includes *Larrea tridentata, Ambrosia dumosa*, *Hymenoclea salsola*, *Olyneya tesota,* and *Lycium andersonii*.

REMARKS:

Soil observed in a hand-dug pit on 4/11/11

Diagnostic horizons and features in this pedon:

Ochric epipedon - from 0 to 18 cm

Cambic horizon – 4 to 50+

The soil temperature regime is hyperthermic and the soil moisture regime is aridic.

The calcium carbonate state is I+.

LAB DATA:

17-50+ cm: 4.0% $CaCO_3$

SONORAN 3

TAXONOMIC CLASS: Torriorthents

PEDON DESCRIPTION:

Desert Pavement—Surface; embedded basalt, rhyolite, and granite gravels; slight desert varnish, 95% cover.

Av—0 to 2 cm; 10YR 4/6 moist, 10YR 6/4 dry; gravelly loam (29% gravels, 20% clay); moderate medium platy structure; hard, moderately sticky and moderately plastic; few very fine roots between peds; few very fine and common fine vesicular pores; strongly effervescent with 1 M HCl on ped tops, bottoms, and interiors, slightly effervescent on ped sides; abrupt smooth boundary.

Bw—2 to 23 cm; 10YR 4/4 moist, 10YR 6/4 dry; loamy fine sand (14% gravels; 8% clay); weak coarse subangular blocky structure (krotovinas filled with loose soil); soft, slightly sticky and non-plastic; few very fine roots between peds; strongly effervescent with 1 M HCl; gradual wavy boundary.

Bk—23 to 49+ cm; 10YR 5/6 moist, 10YR 6/4 dry; extremely gravelly coarse sand (75% gravel, 2% cobbles, 0% clay); structureless single-grain; loose; discontinuous carbonate coats on the bottom of rock fragments; strongly effervescent with 1 M HCl.

PEDON LOCATION: 1.7 mi E of Vidal Junction, CA; 34^{o}11′46.3″ N, 114^{o}32′47.1 ″ NAD83; SW1/4 SE1/4 SE1/4 Sec. 3 of T.1N, R.23E San Bernardino B&M; Vidal Junction 7.5-minute topographical map quadrant.

GEOGRAPHIC SETTING: Located on an erosional fan remnant of the fan piedmont. The surface has a subdued bar and swale topography and the soil was described on the

flattened bar position. The soil is formed in mixed alluvium. Elevation is 280 meters and slope is 2 percent to the south. Average annual precipitation is 15.9 cm; mean annual air temperature is 23.3 degrees C, according to records at Parker Rsvr weather station (Fenimore, 2011).

SOIL MAPPED AS: None

USE AND VEGETATION: Recreational land. Vegetation includes: *Larrea tridentata, Ambrosia dumosa, Parkinsonia florida, Encelia farinosa, Krameria grayi, Opuntia spp., Hymenoclea salsola, Lycium andersonii, Adenophyllum porophylloides,* and *Cylindropuntia spp.*

REMARKS:

Soil observed in a hand-dug pit on 4/12/11

Diagnostic horizons and features in this pedon:

Ochric epipedon - from 0 to 18 cm

The soil temperature regime is hyperthermic and the soil moisture regime is aridic.

The calcium carbonate state is I.

LAB DATA:

23-49+ cm: 9.5% $CaCO_3$

SONORAN 4

TAXONOMIC CLASS: Haplargids

PEDON DESCRIPTION:

Desert Pavement—Surface; embedded andesite, andesitic breccia, quartzite, and quartz gravels; strong varnish, 98% cover.

Av—0 to 5 cm; 10YR 4/6 moist, 10YR 6/4 dry; silt loam (0% gravels, 20% clay); strong medium columnar structure parting to moderate very thick platy structure; hard, slightly sticky and very plastic; many very fine and common fine vesicular pores in upper 2 cm, common very fine and common collapsed vesicular pores in lower 3 cm; discontinuous clay films on ped faces; violently effervescent with 1 M HCl on ped tops and interiors, slightly effervescent on ped sides, and strongly effervescent on ped bottoms; abrupt smooth boundary.

Bk—5 to 16 cm; 7.5YR 4/6 moist, 7.5YR 5/6 dry; very gravelly loam (40% gravels; 12% clay); structureless single-grain; loose, slightly sticky and very plastic; few very fine roots throughout; carbonate coats on the bottom of rock fragments (1 mm thick), few medium carbonate masses; slightly effervescent with 1 M HCl; gradual wavy boundary.

Btk—16 to 42+ cm; 7.5YR 4/6 moist, 7.5YR 5/6 dry; extremely gravelly sandy clay loam (67% gravel, 3% cobbles, 30% clay); structureless single-grain; loose; carbonate coats on the bottom of rock fragments (2 mm thick), common coarse carbonate nodules, discontinuous clay films on nodules; strongly effervescent with 1 M HCl.

PEDON LOCATION: 2 mi NE of Quartzsite, AZ; 33°41′2.5″ N, 114°12′12.6 ″ NAD83; SE1/4 SE1/4 Sec. 15 of T.4N, R.19W Gila and Salt River B&M; Quartzsite 7.5-minute topographical map quadrant.

GEOGRAPHIC SETTING: Located on an erosional fan remnant of the fan piedmont. The soil is formed in mixed alluvium. Elevation is 273 meters and slope is 2 percent to the north. Average annual precipitation is 8.9 cm; mean annual air temperature is 22.7 degrees C, according to records at Quarzsite weather station (Fenimore, 2011).

SOIL MAPPED AS: None

USE AND VEGETATION: Recreational land. Vegetation includes: *Larrea tridentata*, *Krameria grayi*, *Parkinsonia florida*, *Olyneya tesota*, *Adenopyllum porophylloides*, *Hymenoclea salsola*, *Encelia farinosa*, *Sphaeralcea emoryi*, *Acacia greggi*, *Encelia frutescens*, *Salazaria mexicana*, *Ambrosia dumosa*, *Carnegiea gigantea*, *Stephanomeria pauciflora*

REMARKS:

Soil observed in a hand-dug pit on 4/14/11

Diagnostic horizons and features in this pedon:

Ochric epipedon - from 0 to 16 cm

Cambic horizon – from 5 to 16 cm

Argillic horizon – from 16 to 42+

The soil temperature regime is hyperthermic and the soil moisture regime is aridic.

The calcium carbonate state is I.

LAB DATA: 6-15 cm: 8.3% $CaCO_3$**,** 16-42+ cm: 9.9% $CaCO_3$

SONORAN 5

TAXONOMIC CLASS: Haplocalcids

PEDON DESCRIPTION:

Desert Pavement—Surface; embedded andesitic and granodiorite gravels; moderate varnish, 95% cover.

Av—0 to 4 cm; 10YR 4/6 moist, 10YR 6/4 dry; gravelly loam (20% gravels, 22% clay); moderate coarse columnar structure; hard, moderately sticky and moderately plastic; common very fine, common fine, and common medium vesicular pores; discontinuous clay films on bottom of peds; very slightly effervescent with 1 M HCl on ped tops, non-effervescent on ped sides, and violently effervescent on ped bottoms and interiors; clear smooth boundary.

Btk—4 to 19 cm; 7.5YR 4/4 moist, 7.5YR 5/4 dry; very gravelly sandy loam (42% gravels; 8% clay); weak medium and coarse subangular blocky structure; hard, slightly sticky and non-plastic; few very fine roots throughout; few very fine tubular pores; patchy carbonate coats on the bottom of rock fragments, discontinuous clay films on the top of rock fragments; slightly effervescent with 1 M HCl; gradual smooth boundary.

Bk—19 to 50+ cm; 7.5YR 4/6 moist, 7.5YR 4/6 dry; extremely gravelly sandy loam (75% gravel, 5% clay); structureless single-grain; loose, slightly sticky and very plastic; continuous carbonate coats on the bottom of rock fragments (2 mm thick); strongly effervescent with 1 M HCl.

PEDON LOCATION: 0.3 mi NW of Vicksburg, AZ; 33°44′52.4″ N, 113°44′52.0 ″ NAD83; SW1/4 NW1/4 Sec. 29 of T.5N, R.14W Gila and Salt River B&M; Hope 7.5-minute topographical map quadrant.

GEOGRAPHIC SETTING: Located on an erosional fan remnant of an alluvial fan. The soil is formed in mixed alluvium. Elevation is 431 meters and slope is 2 percent to the south. Average annual precipitation is 15.6 cm; mean annual air temperature is 21.2 degrees C, according to data recorded at Bouse weather stations (Fenimore, 2011).

SOIL MAPPED AS: None

USE AND VEGETATION: Mining access roads. Vegetation includes: *Larrea tridentata, Fouquieria splendens, Carnegiea gigantea, Parkinsonia florida, Ambrosia dumosa, Lycium andersonii, Krameria grayi, Encelia farinosa, Cylindropuntia spp.*, and *Olyneya tesota*

REMARKS:

Soil observed in a hand-dug pit on 4/15/11

Diagnostic horizons and features in this pedon:

Ochric epipedon - from 0 to 18 cm

Cambic horizon – from 4 to 19 cm

Calcic horizon – from 19 to 50+ cm

The soil temperature regime is hyperthermic and the soil moisture regime is aridic.

The calcium carbonate state is II.

LAB DATA: 4-19 cm: 6.1% $CaCO_3$

19-50+ cm: 11.4% $CaCO_3$

MOJAVE 2

TAXONOMIC CLASS: Haplosalids

PEDON DESCRIPTION:

Desert Pavement—Surface; embedded quartzite and quartz monzonite gravels with strong desert and ventral varnish; 98% cover.

Avt—0 to 3 cm; 10YR 5/6 moist, 10YR 6/4 dry; loam (10% gravels, 15% clay); strong medium columnar structure parting to moderate medium and thick platy structure; hard, slightly sticky and moderately plastic; few very fine roots between peds; common very fine and common fine vesicular pores, few medium vughs; continuous clay films on the bottom face of columnar peds; non-effervescent with 1 M HCl on top, sides, and interior of peds, strongly effervescent on the bottom of peds; abrupt smooth boundary.

Bw—3 to 12 cm; 10YR 4/6 moist, 10YR 6/4 dry; very gravelly loamy sand (40% gravels; 4% clay); single grain; loose, non-sticky and non-plastic; few very fine roots matted around rock fragments; slightly effervescent with 1 M HCl; clear smooth boundary.

Btz1—12 to 19 cm; 7.5YR 4/6 moist, 10YR 6/6 dry; very gravelly loamy sand (55% gravel; 10% clay); weak fine and medium subangular blocky structure; slightly hard, slightly sticky and non-plastic; few very fine dendritic pores; common soluble salt masses with purple stains beneath rock fragments; discontinuous clay films on ped faces and the top of rock fragments; non-effervescent with 1 M HCl; clear smooth boundary.

Btzy2—19 to 45+ cm; 7.5YR 4/6 moist, 10YR 7/6 dry; very gravelly sandy loam (45% gravel; 15% clay); moderate very fine, fine, medium, and coarse subangular blocky

structure; hard, slightly sticky and slightly plastic; few very fine dendritic pores; few fine gypsum nests (snowballs) on faces of peds and around rock fragments; continuous clay films on ped faces; non-effervescent with 1 M HCl.

PEDON LOCATION: South of Nellie Bly Mountain along northern boundary of Johnson Valley OHV area; 34°36′31.4″ N, 116°37′11.7 ″ W NAD83; Sec. 13 of T.6N, R.3E San Bernardino B&M; Iron Ridge 7.5-minute topographical map.

GEOGRAPHIC SETTING: Erosional fan remnant of the fan piedmont. The soil is formed in mixed alluvium. Elevation is 1061 meters and slope is 5 percent to the south. Average annual precipitation is 7.6 cm; mean annual air temperature is 18.5 degrees C, according to records at Means Lake RAWS (Western Regional Climate Cent., 2011).

SOIL MAPPED AS: Oldwoman series: Loamy-skeletal, mixed, superactive, thermic Typic Calciargids

USE AND VEGETATION: Recreational land (OHV area). Vegetation includes *Larrea tridentata*, *Yucca spp.*, *Ambrosia dumosa*, *Sphaeralcea ambuigua*, *Xylorhiza tortifolia*, *Krascheninnikovia lanata*, *Adenophyllum cooperi*, *Salazaria mexicana*, *Senna armata*, *Echinocactus polycephalus*

REMARKS:

Soil observed in a hand-dug pit on 4/19/11

Diagnostic horizons and features in this pedon:

Ochric epipedon – 0 to 12 cm

Argillic horizon – 12 to 45+ cm

Salic horizon – 12 to 45+ cm

The soil temperature regime is thermic and the soil moisture regime is aridic.

LAB DATA:

12-19 cm: 32.2 dS m^{-1} EC_e, <1% gypsum

19-45 cm: 48.3 dS m^{-1} EC_e, 1% gypsum

MOJAVE 3

TAXONOMIC CLASS: Haplocambids

PEDON DESCRIPTION:

Desert Pavement—Surface; embedded andesite and volcanic fanglomerate gravels; ventral varnish; 80% cover.

Av—0 to 6 cm; 10YR 5/4 moist, 10YR 6/4 dry; gravelly loam (25% gravels, 25% clay); strong coarse columnar structure parting to moderate thick and very thick platy structure; slightly hard, moderately sticky and very plastic; few very fine roots between peds; common very fine, common fine, and many medium vesicular pores (medium pores in upper 2 cm only); sandy layer on tops and sides of peds; very slightly effervescent with 1 M HCl on top and interior of peds, strongly effervescent in the bottom of peds, and non-effervescent on sides of peds; clear smooth boundary.

Btk—6 to 28 cm; 7.5YR 4/4 moist, 7.5YR 4/4 dry; gravelly sandy loam (20% gravels; 18% clay); weak fine and medium subangular blocky structure; soft, slightly sticky and very plastic; common very fine roots throughout; common very fine dendritic pores; common medium and coarse irregular carbonate masses and threads; discontinuous carbonate coats on rock fragments (<1 mm thick), discontinuous clay films on rock fragments; very slightly effervescent with 1 M HCl; gradual wavy boundary.

Bk—28 to 50+ cm; 10YR 4/4 moist, 10YR 4/6 dry; gravelly loamy sand (22% gravel; 10% clay); moderate medium and coarse subangular blocky structure; slightly hard, slightly sticky and slightly plastic; few very fine tubular pores; common medium and

coarse irregular carbonate masses; discontinuous carbonate coats on the bottom of rock fragments (1 mm thick); non-effervescent with 1 M HCl.

PEDON LOCATION: 8 km northwest of Afton Canyon Campground (along Arrowhead trail); 35°5′2.4″ N, 116°26′50.5 ″ W NAD83; Sec. 33 of T.12S, R.5E San Bernardino B&M; Dunn 7.5-minute topographical map.

GEOGRAPHIC SETTING: Erosional fan remnant of the fan piedmont. The soil is formed in mixed alluvium. Elevation is 574 meters and slope is 4 percent to the northeast. Average annual precipitation is 10.6 cm; mean annual air temperature is 19.4 degrees C, according to records at Barstow Daggett Airport weather station (Fenimore, 2011).

SOIL MAPPED AS: Not mapped

USE AND VEGETATION: Mine access road. Vegetation includes *Larrea tridentate*, *Ambrosia dumosa, Krameria erecta, Malacothrix glabrata*, and *Eschscholzia glyptosperma*

REMARKS:

Soil observed in a hand-dug pit on 4/21/11

Diagnostic horizons and features in this pedon:

Ochric epipedon - from 0 to 18 cm

Cambic horizon – from 6 to 28 cm

The soil temperature regime is thermic and the soil moisture regime is aridic.

Calcium carbonate stage is I+.

LAB DATA: 6-28 cm: 7.2% $CaCO_3$

28-50+ cm: 4.4% $CaCO_3$

MOJAVE 5

TAXONOMIC CLASS: Haplargids

PEDON DESCRIPTION:

Desert Pavement—Surface; embedded quartzite and quartzitic sandstone gravels with ventral varnish and some desert varnish; 98% cover.

Avt—0 to 4 cm; 10YR 4/6 moist, 10YR 6/4 dry; silt loam (0% gravels, 23% clay); strong medium columnar structure parting to weak very thick platy structure; hard, slightly sticky and slightly plastic; few very fine, common fine, and common medium vesicular pores; patchy clay films on the bottom faces of peds; very slightly effervescent with 1 M HCl on top and sides of peds, strongly effervescent in the ped interior, and violently effervescent on bottom of peds; abrupt smooth boundary.

Bk—4 to 16 cm; 7.5YR 4/6 moist, 7.5YR 6/4 dry; loam (14% gravels; 15% clay); moderate coarse subangular blocky structure; soft, moderately sticky and very plastic; common very fine and few fine roots throughout; few very fine tubular pores; common fine carbonate threads and common medium irregular carbonate masses, patchy carbonate coats on rock fragments; violently effervescent with 1 M HCl; clear smooth boundary.

Btk—16 to 32 cm; 7.5YR 4/6 moist, 7.5YR 5/6 dry; very gravelly loam (42% gravel; 24% clay); moderate very fine, fine, and medium subangular blocky structure; slightly hard, moderately sticky and very plastic; few very fine and few fine tubular pores; discontinuous clay films on ped faces, common fine carbonate threads, and patchy

carbonate coats on the bottom of rock fragments; non-effervescent with 1 M HCl; gradual smooth boundary.

Bt—32 to 50+ cm; 7.5YR 4/6 moist, 7.5YR 6/6 dry; extremely gravelly sandy clay loam (60% gravel; 27% clay); moderate very fine, fine, and medium subangular blocky structure; slightly hard, moderately sticky and very plastic; few very fine tubular pores; discontinuous clay films on ped faces; non-effervescent with 1 M HCl.

PEDON LOCATION: 4 miles southeast of Crystal, NV; 36°27′8.1″ N, 116°6′29.9 ″ W NAD83; Sec. 27 of T.17S, R.52E Mt. Diablo B&M; Mt. Schader 7.5-minute topographical map.

GEOGRAPHIC SETTING: Erosional fan remnant of the alluvial fan. The soil is formed in mixed alluvium. Elevation is 863 meters and slope is 3 percent to the south. Average annual precipitation is 13.2 cm; mean annual air temperature is 16.6 degrees C, according to records from Pahrump weather stations (Fenimore, 2011).

SOIL MAPPED AS: Ashmed series: Loamy-skeletal, mixed, superactive, thermic Typic Haplargids (Soil Survey Staff, 2011), Surficial geology: 40-100 ka alluviul deposits with cambic B horizon and stage I-II carbonates or argillic B horizon and Stage III-IV carbonates (Slate et al., 2009)

USE AND VEGETATION: Land used for grazing. Vegetation includes: *Yucca shidigera*, *Larrea tridentata*, *Ambrosia dumosa*, *Lycium shockleyi*, *Krascheninnikovia lanata*, *Ephedra nevadensis*, *Opuntia basilaris*, *Krameria erecta*, *Cylindropuntia spp.*, *Echinocereus engelmanni*, *stephanomeria parryi*, *Encelia actoni*, and *Xylorhiza tortifolia*

REMARKS:

Soil observed in a hand-dug pit on 4/23/11.

Diagnostic horizons and features in this pedon:

Ochric epipedon - from 0 to 16 cm

Argillic horizon – from 16 to 50+

The soil temperature regime is thermic and the soil moisture regime is aridic.

Calcium carbonate stage is I+.

LAB DATA:

4-16 cm: 10.2% $CaCO_3$

16-32 cm: 1.0% $CaCO_3$

32-50+ cm: 1.4% $CaCO_3$

GREAT BASIN 1

TAXONOMIC CLASS: Haplocamids

PEDON DESCRIPTION:

Desert Pavement—Surface; mixture of embedded and non-embedded gravels of andesite, basalt, and amphibolite with some ventral varnish; 90% cover.

Av—0 to 2 cm; 10YR 4/4 moist, 10YR 6/3 dry; loamy fine sand (18% gravels, 8% clay); moderate coarse columnar structure; slightly hard, non-sticky and non-plastic; common very fine, common fine, and many medium vesicular pores (fine and medium concentrated in upper 1 cm); strongly effervescent with 1 M HCl on all ped surfaces and ped interior; abrupt smooth boundary.

Bkq1—2 to 14 cm; 10YR 4/4 moist, 10YR 6/3 dry; gravelly loamy fine sand (29% gravels; 8% clay); moderate coarse subangular blocky structure; slightly hard, non-sticky and non-plastic; few very fine and few fine roots throughout; few fine tubular pores; patchy carbonate coats on rock fragments; patchy opaline silica coats on bottom surfaces of rock fragments; slightly effervescent with 1 M HCl; clear smooth boundary.

Bkq2—14 to 50 cm; 10YR 4/4 moist, 10YR 6/3 dry; very gravelly fine sandy loam (45% gravel; 12% clay); moderate medium and coarse subangular blocky structure; slightly hard, non-sticky and non-plastic; few very fine, few fine, and few medium roots throughout; few fine tubular pores; discontinuous carbonate coats on all surfaces of rock fragments; continuous carbonate coats and patchy opaline silica coats on bottom surfaces of rock fragments; strongly effervescent with 1 M HCl, diffuse smooth boundary.

Bkq3—50 to 80+ cm; 10YR 4/4 moist, 10YR 6/3 dry; gravelly loamy fine sand (34% gravel; 10% clay); moderate medium and coarse subangular blocky structure; soft, non-sticky and non-plastic; few very fine and few fine roots throughout; few very fine tubular poress; patchy carbonate coats and opaline silica coats on bottom surfaces of rock fragments; strongly effervescent with 1 M HCl.

PEDON LOCATION: 5.8 miles east of Lida, NV on HWY 266; 37°26′40.4″ N, 117°23′54.3 ″ W NAD83; Sec. 2 of T.6S, R.41E Mt. Diablo B&M; Lida 7.5-minute topographical map.

GEOGRAPHIC SETTING: Inset fan on the fan piedmont. The soil is formed in alluvium derived from mixed volcanic rocks. Elevation is 1561 meters and slope is 2 percent to the southeast. Average annual precipitation is 17.1 cm; mean annual air temperature is 10.7 degrees C, according to records at Goldfield weather station (Fenimore, 2011).

SOIL MAPPED AS: Izo series: Sandy-skeletal, mixed, mesic Typic Torriorthents (Soil Survey Staff, 2011)

USE AND VEGETATION: Land used for grazing. The vegetation includes *Lycium shockleyi*, *Artemisa spinescens*, *Ephedra nevadensis*, *Atriplex confertifolia*, *Yucca brevifolia*, and *Ceratoides lanata*.

REMARKS:

Soil observed in a pit found at the site (unknown original use) on 4/26/11

Diagnostic horizons and features in this pedon:

Ochric epipedon - from 0 to 18 cm

Cambic horizon – from 14-50 cm

The soil temperature regime is mesic and the soil moisture regime is aridic.

Calcium carbonate stage is I.

LAB DATA:

2-14 cm: 7.6% $CaCO_3$

14-50 cm: 8.0% $CaCO_3$

50-80+ cm: 8.4% $CaCO_3$

GREAT BASIN 2

TAXONOMIC CLASS: Torriorthents

PEDON DESCRIPTION:

Desert Pavement—Surface; embedded tuff, andesite, and basalt gravels; some ventral varnish; 98% cover.

Av—0 to 7 cm; 10YR 4/4 moist, 10YR 7/3 dry; loam (10% gravels, 20% clay); moderate coarse columnar structure; hard, moderately sticky and slightly plastic; few very fine, common fine, and many medium vesicular pores; strongly effervescent with 1 M HCl on top surface of peds, very slightly effervescent on sides of peds, and violently effervescent on bottom and interior of peds; abrupt smooth boundary.

Bw—7 to 21 cm; 10YR 5/6 moist, 10YR 6/4 dry; very gravelly loamy sand (40% gravels; 9% clay); strong very coarse prismatic structure; very hard, non-sticky and non-plastic; few very fine tubular pores; non-effervescent with 1 M HCl; clear wavy boundary.

Bk—21 to 60+ cm; 7.5YR 5/6 moist, 10YR 6/3 dry; very gravelly loamy sand (53% gravel; 11% clay); structure-less single grain; loose, non-sticky and non-plastic; few very fine roots throughout; discontinuous carbonate coats on rock fragments; discontinuous carbonate coats on all surfaces of rock fragments and continuous 3-mm thick carbonate coats on bottom surfaces of rock fragments; slightly effervescent with 1 M HCl.

PEDON LOCATION: 3.1 miles southeast of Alkali Lake, NV; 37°49′54.4″ N, 117°19′35.5 ″ W NAD83; Sec. 25 of T.1S, R.41E Mt. Diablo B&M; Alkali 7.5-minute topographical map.

GEOGRAPHIC SETTING: Erosional fan remnant of the fan piedmont. The soil is formed in alluvium derived from mixed volcanic rocks. Elevation is 1512 meters and slope is 2 percent to the northwest. Average annual precipitation is 14.8 cm; mean annual air temperature is 11.0 degrees C, according to records at Tonopah weather station (Fenimore, 2011).

SOIL MAPPED AS: Unsel benchmark series: Fine-loamy, mixed, superactive, mesic Durinodic Haplargids (Soil Survey Staff, 2011)

USE AND VEGETATION: Land used for grazing. Vegetation includes *Sacrobatus vermiculatus*, *Lycium shockleyi*, *Artemisa spinescens*, *Atriplex confertifolia*, *Ceratoides lanata*, *Sacrobatus baileyi*, *Ephedra nevadensis*, and *Tetradymia glabrata.*

REMARKS:

Soil observed in a hand-dug pit on 4/26/11

Diagnostic horizons and features in this pedon:

Ochric epipedon - from 0 to 18 cm

The soil temperature regime is mesic and the soil moisture regime is aridic.

Calcium carbonate stage is I.

LAB DATA:

21-60+ cm: 4.4% $CaCO_3$

GREAT BASIN 3

TAXONOMIC CLASS: Haplocambids

PEDON DESCRIPTION:

Desert Pavement—Surface; embedded tuff, andesite, and rhyolite gravels; ventral varnish and desert varnish; 95% cover.

Av—0 to 6 cm; 10YR 6/4 moist, 10YR 7/3 dry; clay loam (3% gravels, 30% clay); moderate medium columnar structure; hard, slightly sticky and moderately plastic; few very fine, common fine, and few medium vesicular pores and many medium vughs; collapsed vesicles in the bottom 2 cm of the horizon; patchy clay films on the bottom faces of peds; violently effervescent with 1 M HCl on top and sides of peds, strongly effervescent in the ped interior, and slightly effervescent on bottom of peds; abrupt smooth boundary.

Bq—6 to 21 cm; 10YR 5/6 moist, 10YR 6/4 dry; gravelly sandy loam (31% gravels; 18% clay); moderate fine, medium, and coarse subangular blocky structure; slightly hard, slightly sticky and moderately plastic; few very fine, few fine, and common medium roots throughout; few very fine tubular pores; few coarse spherical durinodes; slightly effervescent with 1 M HCl; gradual wavy boundary.

Bk—21 to 58+ cm; 10YR 5/6 moist, 10YR 7/3 dry; very gravelly loamy sand (41% gravel; 4% clay); weak fine and medium subangular blocky structure; soft, non-sticky and non-plastic; few very fine and few fine roots throughout; few very fine tubular pores; few medium spherical carbonate nodules; discontinuous carbonate coats on bottom surfaces of rock fragments; violently effervescent with 1 M HCl.

PEDON LOCATION: 6.8 miles southwest of Tonopah, NV along powerline road; 37°58′32.1″ N, 117°16′43.4 ″ W NAD83; Sec. 32 of T.2N, R.42E Mt. Diablo B&M; Klondike 7.5-minute topographical map.

GEOGRAPHIC SETTING: Erosional fan remnant of the fan piedmont. The soil is formed in alluvium derived from mixed volcanic rocks. Elevation is 1626 meters and slope is 4 percent to the southwest. Average annual precipitation is 14.8 cm; mean annual air temperature is 11.0 degrees C, according to records form Tonopah weather station (Fenimore, 2011).

SOIL MAPPED AS: Unsel benchmark series: Fine-loamy, mixed, superactive, mesic Durinodic Haplargids (Soil Survey Staff, 2011).

USE AND VEGETATION: Land used for grazing. Vegetation includes *Ephedra nevadensis, Artemisa spinescens, Sacrobatus vermiculatus, Lycium shockleyi, Sacrobatus baileyi*.

REMARKS:

Soil observed in a hand-dug pit on 4/24/11

Diagnostic horizons and features in this pedon:

Ochric epipedon - from 0 to 18 cm

Cambic horizon – from 6 to 21 cm

The soil temperature regime is mesic and the soil moisture regime is aridic.

Calcium carbonate stage is II.

LAB DATA:

21-58+ cm: 12.9% $CaCO_3$

GREAT BASIN 4

TAXONOMIC CLASS: Haplargids

PEDON DESCRIPTION:

Desert Pavement—Surface; embedded gravels of andesite, tuff, and basalt with desert varnish and ventral varnish; 98% cover.

Av—0 to 3 cm; 10YR 5/4 moist, 10YR 7/3 dry; silt loam (5% gravels, 20% clay); strong medium prismatic structure parting to moderate thick platy and weak medium platy structure; hard, moderately sticky and moderately plastic; common very fine, common fine, and many medium vesicular pores; many medium vughs; non-effervescent with 1 M HCl (ped sides) to slightly effervescent with 1 M HCl (ped top and interior); abrupt smooth boundary.

Avq—3 to 7 cm; 10YR 5/4 moist, 10YR 6/3 dry; silty clay loam (10% gravels; 35% clay); strong medium prismatic structure parting to moderate thick platy and weak medium platy structure; very hard, moderately sticky and moderately plastic; common very fine and few fine vesicular pores; continuous opaline silica coats on ped faces; strongly effervescent with 1 M HCl (ped bottoms); abrupt smooth boundary.

Bzyq/Bt—7 to 22 cm; 7.5YR 4/4 moist, 10YR 6/4 dry; gravelly fine sandy loam (22% gravel; 10% clay); moderate very fine, fine, medium, and coarse subangular blocky structure; slightly hard, slightly sticky and slightly plastic; common very fine and few fine roots throughout; discontinuous opaline silica coats on ped faces; common coarse gypsum or soluble salt masses beneath rock fragments; continuous clay films on ped

faces beneath large rock fragment; non-effervescent with 1 M HCl, clear smooth boundary.

Btq—22 to 36 cm; 10YR 4/6 moist, 10YR 6/4 dry; gravelly clay loam (23% gravel; 5% cobbles; 30% clay); moderate very fine, fine, and medium subangular blocky structure; hard, slightly sticky and very plastic; few very fine and few fine roots throughout; discontinuous clay films on ped faces and discontinuous opaline silica coats on ped faces; slightly effervescent with 1 M HCl; gradual smooth boundary.

Btk—36 to 57+ cm; 7.5YR 4/4 moist, 10YR 5/4 dry; gravelly clay (33% gravel; 42% clay); moderate very fine, fine, and medium subangular blocky structure; very hard, slightly sticky and very plastic; continuous clay films on ped faces and discontinuous carbonate coats on ped faces; few coarse irregular carbonate nodules; slightly effervescent with 1 M HCl.

PEDON LOCATION: Southwest of Mina, NV; 38°22′45.9″ N, 118°6′51.8 ″ NAD83; SE1/4 of NE1/4 of Sec. 18 of T.6N, R.35E Mt. Diablo B&M; Mina 7.5-minute topographical map.

GEOGRAPHIC SETTING: Summit of late Pleistocene (22-25 ka) (Bell, 1995) erosional fan remnant of an alluvial fan. The soil is formed in mixed volcanic alluvium. Elevation is 1429 meters and slope is 4 percent to the northeast. Average annual precipitation is 15.4 cm; mean annual air temperature is 12.7 degrees C, according to records at Mina weather station (Fenimore, 2011).

SOIL MAPPED AS: Candelaria Series: Sandy-skeletal, mixed, mesic Durinodic Haplocalcids (Soil Survey Staff, 2011), Surficial geology: Haplargids (Bell, 1995)

USE AND VEGETATION: Recreational land. Vegetation includes: *Lycium Shockleyi*, *Artemisia spinescens*, *Forsellesia nevadensis*, *Ephedra nevadensis*, *Sacrobatus baileyi*, *Atriplex confertifolia*, *Sacrobatus vermiculatus*, *Gutierrezia sarothrae*, and *Chrysothamnus nauseosus*.

REMARKS:

Soil observed in a hand-dug pit on 4/27/11

Diagnostic horizons and features in this pedon:

Ochric epipedon - from 0 to 22 cm

Argillic horizon – from 22 to 57+ cm

The soil temperature regime is mesic and the soil moisture regime is aridic.

The calcium carbonate state is II.

LAB DATA:

7-22 cm: 50.4 dS m^{-1} EC_e, 4% gypsum

36-57+ cm: 10.5% $CaCO_3$

GREAT BASIN 5

TAXONOMIC CLASS: Haplosalids

PEDON DESCRIPTION:

Desert Pavement—Surface; embedded rhyolitic gravels with ventral varnish; 98% cover.

Av—0 to 4 cm; 2.5Y 4/4 moist, 10YR 7/2 dry; loam (3% gravels, 15% clay); moderate medium and coarse columnar structure parting to strong medium and thick platy structure; hard, slightly sticky and moderately plastic; common very fine and common fine vesicular pores; non-effervescent with 1 M HCl (top and sides of peds) to strongly effervescent with 1 M HCl (bottom of peds) and violently effervescent with 1 M HCl (ped interiors); abrupt smooth boundary.

Bq—4 to 10 cm; 10YR 4/6 moist, 10YR 5/4 dry; loamy fine sand (9% gravels; 6% clay); moderate very fine, fine, and medium subangular blocky structure; soft, slightly sticky and slightly plastic; few very fine tubular pores; patchy opaline silica coats on ped faces; slightly effervescent with 1 M HCl; clear smooth boundary.

Bz—10 to 30 cm; 10YR 5/6 moist, 2.5Y 5/4 dry; gravelly loamy fine sand (20% gravel; 4% clay); moderate fine, medium, and coarse subangular blocky structure; soft, non-sticky and non-plastic; common very fine roots throughout; few very fine dendritic pores; common fine irregular salt masses; very slightly effervescent with 1 M HCl, clear wavy boundary.

Bq′—30 to 70+ cm; 2.5Y 4/4 moist, 2.5Y 6/4 dry; gravelly fine sand (23% gravel; 2% clay); moderate medium and coarse subangular blocky structure; hard, non-sticky and

non-plastic; few very fine tubular pores and few very fine interstitial pores; discontinuous opaline silica coats on ped faces; non-effervescent with 1 M HCl.

PEDON LOCATION: Southern Dixie Valley, NV on Eleven Mile Canyon Road (0.14 mi from HWY 121); 39°24′25.8″ N, 118°9′50.7 ″ W NAD83; Sec. 21 of T.18N, R.34E Mt. Diablo B&M; Pirouette Mountain 7.5-minute topographical map.

GEOGRAPHIC SETTING: Inset fan on the fan piedmont. The soil is formed in alluvium derived from rhyolite, tuff, and metamorphic rocks (phylite, metasandstone, and metasiltstone). Elevation is 1246 meters and slope is 3 percent to the east. Average annual precipitation is 13.7 cm; mean annual air temperature is 10.2 degrees C; according to records form Dixie Valley Anderson and Middlegate-Clifford weather stations (averaged) (Fenimore, 2011).

SOIL MAPPED AS: Trocken benchmark series: Loamy-skeletal, mixed, superactive, calcareous, mesic Typic Torriorthents/Bluewing benchmark series: Sandy-skeletal, mixed, mesic Typic Torriorthents (Soil Survey Staff, 2011).

USE AND VEGETATION: Land used for grazing. Vegetation includes: Annual grasses, *Lycium shockleyi*, *Artemisa spinescens*, *Ephedra nevadensis*, *Atriplex confertifolia*. Moss crust is prevalent around shrubs and on scarps.

REMARKS:

Soil observed in a hand-dug pit on 4/28/11

Diagnostic horizons and features in this pedon:

Ochric epipedon - from 0 to 18 cm

Salic horizon – form 10 to 30 cm

The soil temperature regime is mesic and the soil moisture regime is aridic.

LAB DATA:

10-30 cm: 79.2 dS m^{-1} EC_e, <1% gypsum

REFERENCES

Bell, 1995. Quaternary geologic map of the Mina quadrangle, NV. Nevada Bureau of Mines and Geology, Reno, NV.

Fenimore, C. 2011. NCDC: Locate Weather Observation Station Record. Available at http://www.ncdc.noaa.gov/oa/climate/stationlocator.html (verified 15 Jan. 2012). Natl. Oceanic and Atmospheric Administration, Natl. Climatic Data Cent., Ashville, NC.

Slate, J.L., M.E. Berry, and C.M. Menges. 2009. Surficial geologic map of the Death Valley Junction 30' x 60' quadrangle, California and Nevada. USGS, Reston, VA.

Soil Survey Staff, 2011. Web Soil Survey. Available at http://websoilsurvey.nrcs.usda.gov (verified 24 Sept. 2011). USDA-NRCS, Washington, DC.

Western Regional Climate Cent. 2011. RAWS USA climate archive. Available at <http://www.raws.dri.edu/> (accessed 15 Jan. 2012). Desert Research Institute, Reno, NV.

APPENDIX B. DERIVATION OF VOLUMETRIC LOBATION RATIO FORMULA (EQ. 3.1)

The volumetric lobation ratio (LR_v) is defined as the ratio between the surface area of a sphere, with a volume equal to the measured volume of the pore, and the measured surface area. The formula can be derived starting with:

(1) The volume of a sphere (V_s):

$$V_s = \frac{4}{3}\pi r^3 \qquad (\text{eq. A2. 1})$$

(2) The surface area of a sphere (S_s):

$$S_s = 4\pi r^2 \qquad (\text{eq. A2.2})$$

First, solve both equations for radius (r) and set them equal to each other:

$$r = \sqrt[3]{\frac{3V_s}{4\pi}} = \sqrt{\frac{S_s}{4\pi}}$$

Second, solve for S_s:

$$S_s = \left(\sqrt[3]{\frac{3V_s}{4\pi}} * \sqrt{4\pi}\right)^2 = \frac{(3V_s)^{2/3}}{(4\pi)^{2/3}} * 4\pi = 3^{2/3} * (4\pi)^{1/3} * {V_s}^{2/3} = 4.836 * {V_s}^{2/3}$$

Finally, calculate LR_v by dividing the $S_{s,}$ calculated using the measured volume (V), by measured surface area (S):

$$LR_v = \frac{S_s}{S} = \frac{4.836V^{(2/3)}}{S}$$